

**Dynamic of Polymers in Solution:
From the Macroscopic View
to the
Single Molecule Approach**

DISSERTATION

zur Erlangung des akademischen Grades eines
Doktors der Naturwissenschaften

- Dr. rer. nat. -

der Fakultät Biologie, Chemie und Geowissenschaften
der Universität Bayreuth

vorgelegt von
Ute Annegret Zettl,
geborene Lippert
Bayreuth, 2015

Die vorliegende Arbeit wurde in der Zeit von Oktober 2004 bis Juni 2006 am Lehrstuhl für Physikalische Chemie II unter der Betreuung von Prof. Dr. Georg Krausch und von Januar 2007 bis August 2009 am Lehrstuhl für Physikalische Chemie I unter der Betreuung von Prof. Dr. Matthias Ballauff sowie zuletzt unter der Betreuung von Prof. Dr. Andreas Fery angefertigt.

Vollständiger Abdruck der von der Fakultät für Biologie, Chemie und Geowissenschaften der Universität Bayreuth genehmigten Dissertation zur Erlangung des akademischen Grades eines Doktors der Naturwissenschaften (Dr. rer. nat.).

Dissertation eingereicht am: 04.03.2015

Zulassung durch die Prüfungskommission: 26.03.2015

Wissenschaftliches Kolloquium: 14.07.2015

Amtierender Dekan: Prof. Dr. Rhett Kempe

Prüfungsausschuss:

Prof. Dr. Andreas Fery (Erstgutachter)

Prof. Dr. Mathias Weiss (Zweitgutachter)

Prof. Dr. Hans-Werner Schmidt (Vorsitzender)

JProf. Dr. Matthias Karg

Für meine Familie

*Anyone who has never made a mistake
has never tried anything new.*

Albert Einstein

Contents

1	Introduction	1
1.1	Theory and Status of the Field	2
1.1.1	Theory of Polymer Diffusion in Solution	5
1.1.2	Measurements of Diffusion in Polymer Solution	8
1.1.3	Block Copolymers	12
1.1.4	Diffusion in Thin Polymer Films	14
1.2	Experimental Methods	16
1.2.1	Dynamic Light Scattering (DLS)	16
1.2.2	Fluorescence Correlation Spectroscopy (FCS)	18
1.2.3	FCS in Polymer Science	21
1.2.4	Ellipsometry	25
1.2.5	Atomic Force Microscopy (AFM)	28
1.3	Overview of the Thesis	30
1.3.1	Synopsis	30
1.3.2	Individual Contributions to each Publication	35
2	Swelling Dynamic of Thin Films	39
2.1	Abstract	40
2.2	Introduction	40
2.3	Experimental Section	44
2.3.1	Polymer	44
2.3.2	Sample Preparation	44
2.3.3	Swelling Experiments	45
2.3.4	Scanning Force Microscopy (SFM)	46
2.3.5	Optical microscopy	46
2.4	Results and Discussion	46
2.4.1	Swelling Experiments	46
2.4.2	Ellipsometric compared to SFM Thickness Measurements	52
2.4.3	Phase Behavior of Solvent-Annealed Films	54
2.4.4	Mesoscale Swelling Inhomogeneity in Block Copolymer Films	60

2.5	Conclusions	62
3	Collective Diffusion obtained by FCS	67
3.1	Abstract	68
3.2	Introduction	68
3.3	Experimental Section	70
3.3.1	Dye Labeled Polystyrene	70
3.3.2	Methods	70
3.3.3	Evaluation of Data	71
3.4	Diffusion Coefficients Measured by FCS	74
3.5	Scaling Theory and Langevin Equation Approach	78
3.5.1	Scaling Theory and Reptation Model	79
3.5.2	Internal Motions of Chains	80
3.5.3	Cooperative Diffusion	82
3.5.4	Langevin and Ornstein-Zernike Equation	83
3.5.5	Cooperative Fluctuations and Single Polymer Chain Motion	87
3.5.6	Onset of Glassy Dynamics	93
3.6	Comparison with Production of Nanofibers	95
3.7	Conclusion	97
4	Tracer Diffusion in Polymer Solutions	106
4.1	Abstract	107
4.2	Introduction	107
4.3	Dye Labeled Tracer Polystyrene Chains	108
4.4	Fluorescence Correlation Spectroscopy	110
4.5	Autocorrelation Functions Measured by FCS	111
4.6	Langevin and Integral Equation Theory	113
4.7	Conclusions	118
5	Summary / Zusammenfassung	121
6	List of All Publications	124
A	Direct Calculation of FCS Functions	125
A.1	Autocorrelation Function	125
A.2	Number Density Autocorrelation	126
A.3	Derivation of Autocorrelation Function	130
A.4	Autocorrelation Methods	134

Chapter 1

Introduction

A lot of things in our daily life are made of polymers instead of wood or steel, as in former times. Just to mention a few reasons, the lower density results in less weight and reduces energy costs. Common polymers are isolative and are used to build the housing of electrical appliances. Hydrophobic polymers are useful to keep water in a bottle or to leave water out of the raincoat. Amphiphilic polymers can be used as additives to improve the properties, e. g. for the use of tixotropic agents of dispersion colour for a proper viscosity.

The field of use of polymers is broad, but in most cases the key is the same: diffusion, meaning the mobility of polymers, in the product as in the colour or during the production process for example the extrusion of a bottle. The first is the diffusion of polymers in solution, the latter is diffusion in melt. Therefore it is necessary to investigate the physical behavior of the polymers and hence fundamental research has to be done.

This work is focused on diffusion of polymers in so called "good" solvents. The mobility of polymers in solution for all concentration regimes needs to be understood to explain the rheological and viscoelastic behaviour. The comprehension is important for fundamental research in the complex system of block copolymers as well as for processing of polymer solutions in industry, for example print colours, surface coating by spreading and fibre spinning from solution.

1.1 Theory and Status of the Field

Diffusion in polymer solutions is among the oldest subjects of polymer physics. [1, 2, 3, 4] Polymer solutions can be described by the change of the coil dimensions, de Gennes used the root-mean-square end-to-end distance $\langle R^2 \rangle$. [1] In melt where the polymer is surrounded by itself, the coil dimension is $\langle R_\theta^2 \rangle$. Adding a good solvent, the solvent molecules interpenetrate the polymer coils due to the attractive interaction forces between the molecules. The polymer coils swell and get larger with $\langle R^2 \rangle > \langle R_\theta^2 \rangle$. A bad solvent has repulsive interaction forces between the polymer and solvent molecules. Here the interpenetration is not possible, the polymer coil shrinks to $\langle R^2 \rangle < \langle R_\theta^2 \rangle$ and the polymer precipitates. The status of zero interaction forces is the θ -condition, the so called θ -solution is stable and the polymer coil dimension is the same as in melt $\langle R^2 \rangle = \langle R_\theta^2 \rangle$

Polymer solutions of good solvents are divided in three different concentration regimes, the dilute, semi dilute and concentrated regime, see fig. 1.1. At infinite dilution the coil size is $\langle R_0^2 \rangle \geq \langle R_\theta^2 \rangle$. In dilute solution the polymer coils are still separated from each other. With increasing concentration the distance between the coils decreases until they touch each other comparable to a dense package of coils. This concentration is called overlap concentration c^* . Adding more polymer to the solution is just possible with shrinking of the swollen dimensions of the polymer coils, the solution is called semi dilute. The shrinkage is limited to the coil size at θ -conditions. Passing this second cross over concentration c^\pm the solution enters the concentrated concentration regime, here the coil size is constant. [1, 3]

Taking the molecular conformations into account, five concentration regimes are obtained, see fig. 1.2. In the semidilute and concentrated regimes polymer molecules interpenetrate each other. When the polymer chain molecules are long enough the chains are entangled. This molecular size is called entanglement molecular weight M_e . So the semidilute and the concentrated regime is split in an entangled and a not entangled region.

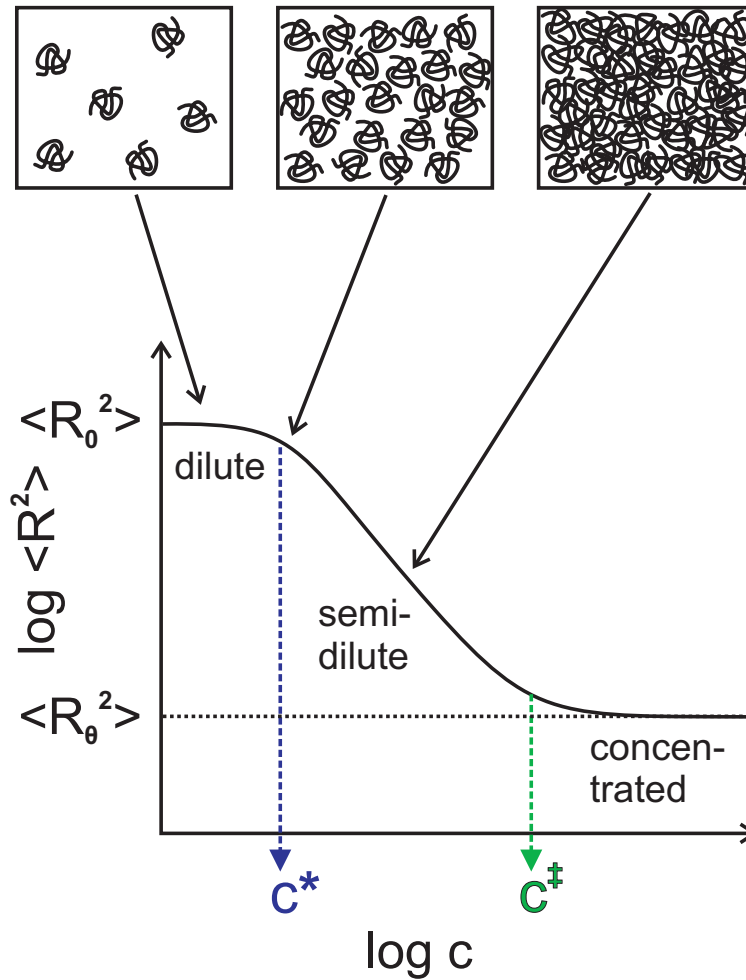


Figure 1.1: Polymer coils in a good solvent solution according to De Gennes: The coil dimension expressed in the "root-mean-square-end-to-end-distance" $\langle R^2 \rangle$ shrinks with increasing concentration. In the dilute system the coils are swollen by the good solvent molecules and the coils are separated. With increasing concentration the coils come nearer until the overlap concentration c^* , here the coils touch each other. Adding more polymer in the so called semi-dilute solution gives less room for each single coil and $\langle R^2 \rangle$ decreases. The decrease of $\langle R^2 \rangle$ is finished in the concentrated regime while reaching the coil dimension at θ -conditions $\langle R_\theta^2 \rangle$ [1, 4]

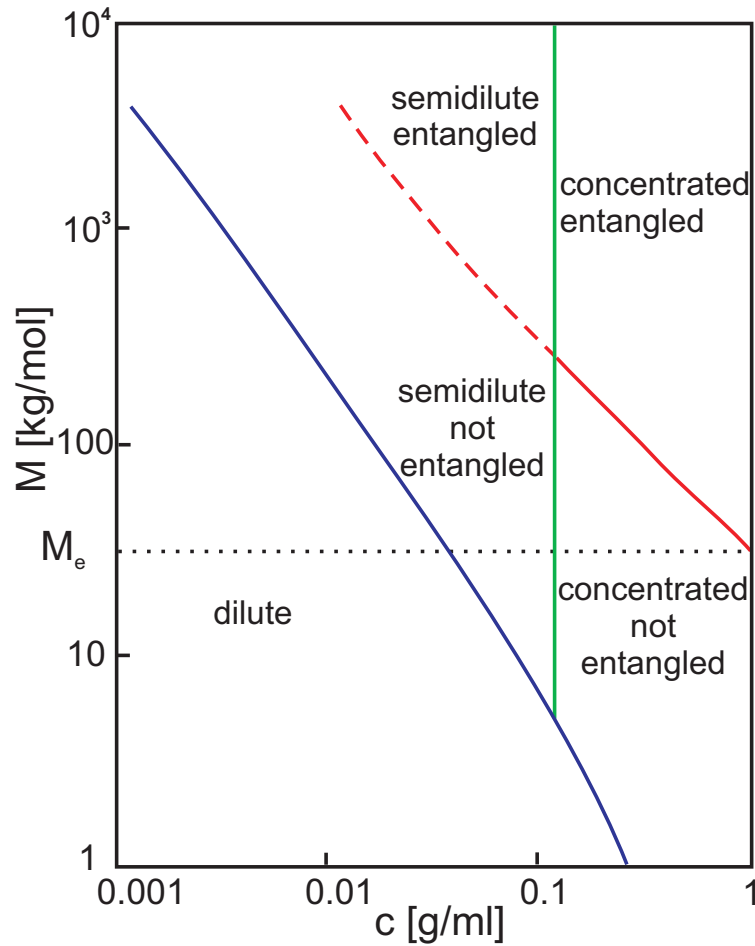


Figure 1.2: The concentration regimes for polymers in a good solvent dependent on the molecular weight and on the concentration. The lines are calculated by Graessley for polystyrene on the base of the viscoelastic information. [4] The blue line is the overlap concentration c^* and at higher molecular weights c^* is smaller because there are less molecules needed to get a "dense package of coils". The green line separates the semidilute and the concentrated regime. The red line indicates the border between entangled and not entangled polymer molecules.

1.1.1 Theory of Polymer Diffusion in Solution

Polymer particles in dilute solution at temperature $T > 0$ K are not static but they move around. The driving force is the thermal energy for an undisturbed solution. The movement is in all directions and so disordered. When polymer particles touch each other, both particles change the direction.

The first diffusion equation presents the diffusion coefficient D as constant of proportionality between the flux of the particles $\partial N/\partial t$ and the concentration gradient $\partial c/\partial x$ to [5]

$$\frac{\partial N}{\partial t} = -D \frac{\partial c}{\partial x} \quad (1.1)$$

with the concentration of particles c , the time t and the space x . For infinite dilution of particles, the diffusion coefficient can be expressed by the Stokes-Einstein diffusion equation

$$D_0 = \frac{k_B T}{6\pi\eta R_h} \quad (1.2)$$

Here the thermal energy $k_B T$ is weighted with the friction coefficient $f_0 = 6\pi\eta R_h$ depending on the viscosity of the solvent η and the hydrodynamic radius R_h of the particle. Equ. 1.2 is modeled for spherical particles in solution, the infinite dilution is indicated by the index 0. This model is valid for polymer coils dissolved in a good solvent. For increasing concentration the inter polymer distances increase and interactions between the molecules needs to be taken into account.

In general there are two diffusion coefficients due to different views on the same system. [6] The self diffusion coefficient D_s describes the relative movement of a single, well defined tracer particle in the environment of other soluted particles and solvent particles. The collective diffusion coefficient D_c describes the motion of an ensemble of polymer molecules due to local concentration fluctuations. The particles moves from higher concentration to lower concentration regions, as described in equ. 1.1. Fig. 1.3 presents the characteristic differences in these two diffusion coefficients.

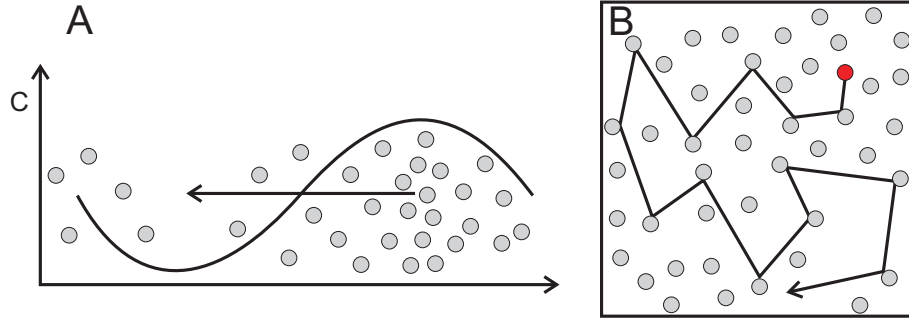


Figure 1.3: Scheme of collective diffusion (A) and self diffusion (B). The selfdiffusion follows the movement of a single particle whereas the collective diffusion describes the ensemble behaviour.

The self diffusion is given by

$$D_s = \frac{k_B T}{f}. \quad (1.3)$$

With increasing concentration c the friction f increases and so D_s decreases.

The concentration dependence of D_c depends additionally on the osmotic pressure $d\pi/dc$ which is a driving force and accelerates the molecules [3, 7]

$$D_c = \frac{k_B T}{f} (1 - c\bar{v})^2 \left(\frac{d\pi}{dc} \right) \quad (1.4)$$

\bar{v} is the specific volume of the polymer in solution. The equations 1.3 and 1.4 are derived by Vink [6] using friction formalism.

The concentration dependencies of both diffusion coefficients are presented in fig. 1.4. At infinite dilution both diffusion coefficients starts at the same value $D_s = D_c = D_0$. With increasing concentration D_s decreases because of the increasing friction. D_c increases with the concentration due to the dominance of the osmotic pressure at low concentrations. The more the concentration increases the more the friction increases and becomes the dominant part. So D_c reaches a maximum and decreases strongly with higher concentration.

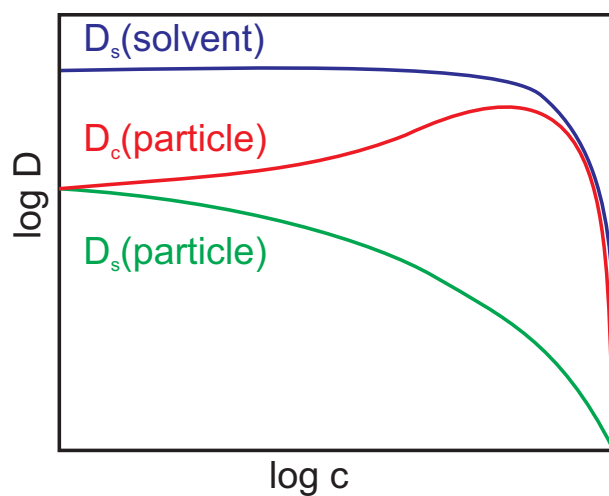


Figure 1.4: Concentration dependency of self- and collective diffusion coefficient of the polymer and the diffusion coefficient of the solvent. At infinite dilution both diffusion coefficients starts at the same value $D_s = D_c = D_0$. With increasing concentration D_s decreases because of the increasing friction. D_c increases with the concentration due to the dominance of the osmotic pressure at low concentrations. The more the concentration increases the more the friction increases and becomes the dominant part. So D_c reaches a maximum and decreases strongly with higher concentration.

1.1.2 Measurements of Diffusion in Polymer Solution

There are several possibilities to measure diffusion coefficients. Here are presented some examples:

The most common method to evaluate collective diffusion is dynamic light scattering (DLS), also known as photon correlation spectroscopy (PCS) and quasi-elastic light scattering (QELS). [8, 9, 10] The density fluctuations of the sample causes a scatter of incident laser light. At a fixed angle the scattered intensity fluctuations are detected by a fast photon detector. The correlation of the time dependend signal leads to the collective diffusion. The theory of DLS is presented in section 1.2.1

The self diffusion is typically obtained by label techniques. Forced Rayleigh scattering (FRS) was developed by Hervet and Leger. [11, 12] The positive interference of two lasers produces a holographic grating in the sample which causes the selective photobleaching of statistically spread dyes. The selfdiffusion of the non-bleached dyes can be followed via disappearance of the grating. The diffusion of free dye molecules in a polymer solution can be seen as the diffusivity of the solvent in the system. To measure the diffusion coefficient of the polymer, it is thus necessary to label it. The FRS is a good technique to follow slower dynamics, e. g. in semidilute and concentrated polymer solutions or in polymer melt. For Diffusion measurements in solutions with lower polymer concentration the polymer molecular weight needs to be high enough to reach a high enough viscosity.

A further label technique, fluorescence correlation spectroscopy (FCS) was developed for biological systems in water and recently adapted for measurements in organic solvents. [13, 14, 15, 16] In contrary to FRS, FCS is a single molecule technique. Single dye molecules diffuse into and out off a small detection volume. The fluorescence light is detected time resolved by a fast photon detector. The correlation of the intensity fluctuations gives the decay time, meaning the average time of the dye in the detection volume. With the knowledge of the size and the shape of the detection volume, the self diffusion coefficient is obtained. The theory of FCS is explained in section 1.2.2. The advantage of FCS is the small amount of the sample. FCS

was developed for dilute concentrations. With increasing the concentration the solution changes the refractive index. This change needs to be adjusted optically, e.g. by the correction ring of the objective. The slower dynamic at higher concentration or at high molecular weight leads to a longer time of the dye labeled polymer molecule in the focus. When the maximum excitation cycles until photodestruction is reached during the pass of the dye through the excitation volume, the result of the measurement is the photostability of the dye and not the diffusivity of the polymersystem. In general the photophysical properties of the dye influences the quality of diffusion measurements using label techniques. [17]

The self diffusion coefficient is also obtained by pulsed field gradient nuclear magnetic resonance (PFG NMR). [18, 19] The spin echo in a field gradient gives the information in space of the nucleus, typically protons. Pulsed signals lead to a better intensity of the echo and a better resolution in time. As advantage the PFG NMR is a non destructive technique and it is no label necessary. Whereas diffusion regards molecules or particles, so the information of the nuclei or protons have to be recalculated for the molecules. This leads to a limitation of this technique on small molecular weight polymers. Measurements of higher molecular weight gives more the information of segmental dynamics than of self diffusion.

The amount of experimental measurements on diffusion coefficients are rather large. Whereas there are just some comparisons of self- and cooperative diffusion coefficients. These comparisons are presented in the following and in fig. 1.5:

Kim et al. [7] presents the system polystyrene ($M= 900$ kg/Mol) in toluene measured with FRS and DLS in a rather large concentration range, see fig. 1.5 D. At dilute concentrations the self diffusion coefficient D_s and the collective diffusion coefficient D_c come together. The point on the x-axis is a literature value for the diffusion coefficient at infinite dilution D_0 . The different concentration dependences are nicely presented. The high molecular weight with $M= 900$ kg/Mol was necessary to measure with FRS in the dilute system, where the molecules are fast, to be able to follow the destruction of

the grating. But in the concentration dependence of the collective diffusion coefficient D_c the maximum was not reached. Probably because the sample preparation for the DLS measurements at high concentrations gets more and more difficult. Usually the solutions are filtered to get rid of the dust. The higher the concentration and the higher the molecular weight, the higher gets the viscosity, until it is nearly impossible to bring the solution through the filter.

Branca et al. [18] measured poly(ethylene glycol) ($M = 8 \text{ kg/Mol}$) in water at different temperatures with NMR and DLS, see fig. 1.5 C. For first, the data is not presented in the double logarithmic scale as usual. At infinite dilution the two diffusion coefficients are interpolated to the same, as expected. The principle increase of the collective diffusion coefficient and the maximum is visible. The decrease of the selfdiffusion coefficient is hidden in the linear scale. As mentioned above, the NMR measurements are limited to small polymers. The used molecular weight of $M = 8 \text{ kg/Mol}$ is quite short and in polymer science this is an oligomere.

Kanematsu et al. [19] evaluated cellulose tris(phenyl carbamate) with five molecular weights (M from 40, 62, 103, 150 to 232 kg/Mol) in THF measured with PFG-NMR and DLS. Kanematsu presents a huge amount of DLS measurements with a clear dependence of the collective diffusion coefficient D_c on the molecular weight. The maximum of D_c in the semidilute concentration regime was not reached, see fig. 1.5 B. The datapoints of DLS measurements were used for a calculation of the selfdiffusion coefficient, named \tilde{D} in the paper. Figure 1.5 A presents the selfdiffusion coefficients: the huge amount of calculated values \tilde{D} (open symbols) fits quite nicely to some measured values of D_s (closed symbols). Kanematsu presents the self- and collective diffusion coefficients in two different figures.

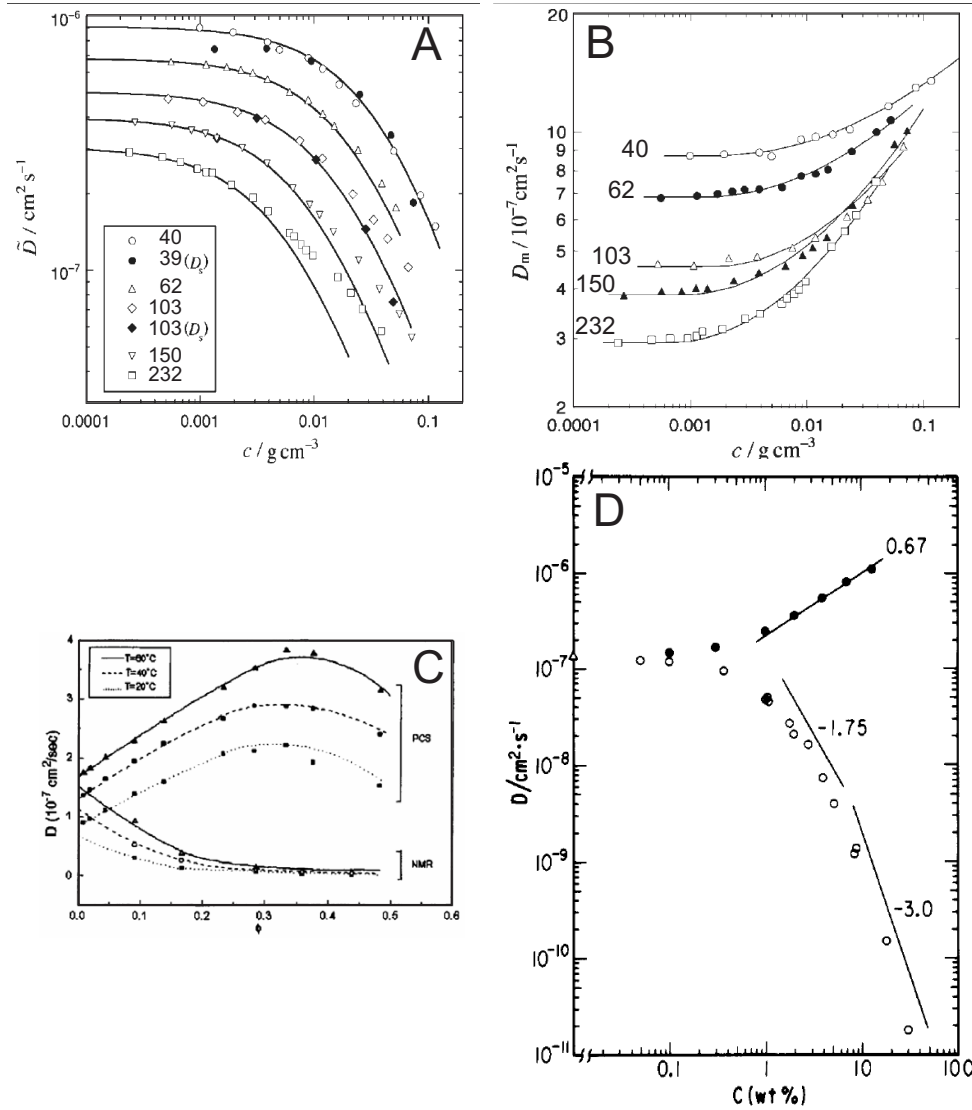


Figure 1.5: Comparison of self and cooperative diffusion coefficients in the systems: cellulose tris(phenyl carbamate) in THF measured with (B) DLS (open and closed symbols) and (A) PFG NMR (just the closed symbols, open symbols are calculated of the DLS-measurements), [19] (C) poly(ethylene glycol) (M=8kg/Mol) in water measured at different temperatures with NMR and DLS [18] and (D) polystyrene (M=900kg/Mol) in toluene measured with FRS and DLS. [7]

1.1.3 Block Copolymers

The former sections describe diffusion of homopolymers in solution. This section gives a small introduction to Block Copolymers in solution. Block copolymers have a covalent bond between two (A-B) or more homopolymer blocks (e.g. A-B-A or A-B-C). Linear block copolymers are synthesised by living polymerisation with a time shift in addition of the monomers for the next block.

Microphase Separation

In general, the thermodynamic stability of a mixture is given by the Gibbs free energy $\Delta G_{mix} = \Delta H_{mix} - T\Delta S_{mix}$ with the enthalpy ΔH_{mix} and the entropy ΔS_{mix} of mixing. A stable mixture has a negative ΔG_{mix} whereas the phase separation is indicated by a positive ΔG_{mix} .

A mixture of two homopolymers A and B is usually very poorly mixable with $\Delta G_{mix} > 0$. The enthalpy of mixing polymers is typically positive. According to the model of Flory $\Delta H_{mix} \propto \chi_{AB}$ with the Flory-Huggins interaction parameter χ_{AB} between monomer A and monomer B. This interaction parameter is in most cases $0 < \chi_{AB} < 1$. The entropy is a value of disorder and decreases with increasing degree of polymerisation N . When the polymer chain is long enough, $\Delta H_{mix} > T\Delta S_{mix}$ and the polymer blend is phase separated.

The properties of the microdomain phases of a A-B block copolymer are calculated by Matsen and Schick using the self-consistent mean field theory (SCFT). [20] Here, the microdomain structure is given by three parameters: the polymer volume fraction f_A of the block A and the degree of polymerisation N multiplied with the Flory-Huggins interaction parameter χ_{AB} .

The resulting phase diagram is valid for polymer melts at constant temperature. Different points in the phase diagram are just reachable with a variation in the molecular structure of the polymers. The microphase separation occurs where $\chi_{AB}N$ is large enough. The repulsive interaction leads to a loss of translational and configurational entropy and so the polymer coils are stretched.

This phase diagram was first verified experimentally by Khandpur et al. in the system of polystyrene-polyisoprene. [21] The distance in the structures depends on the degree of polymerisation and is in a length scale of $10\text{ nm} - 100\text{ nm}$.

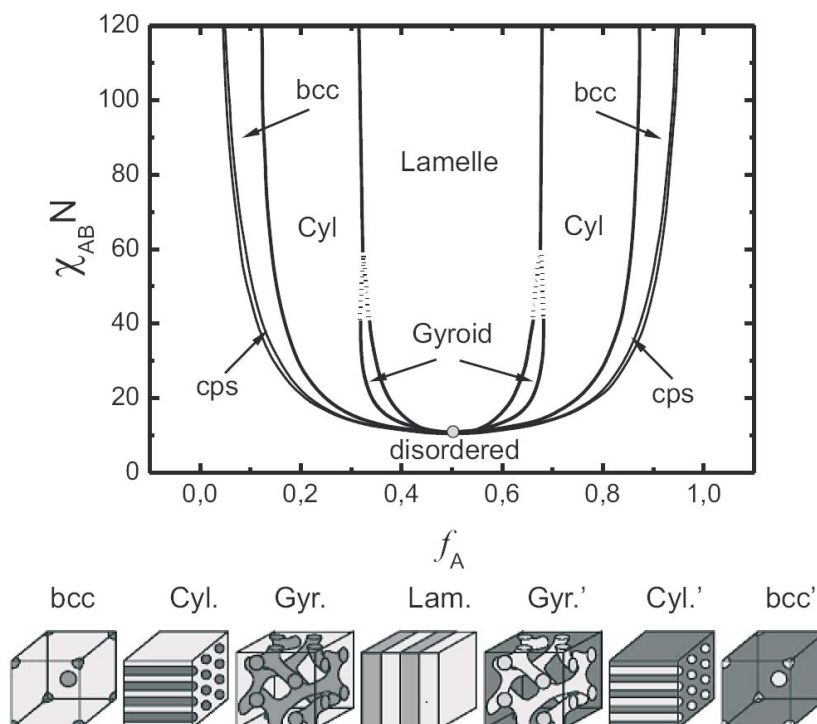


Figure 1.6: Phase diagram of self-assembled structures in AB diblock copolymer melt predicted by self-consistent mean field theory (SCFT) calculations. [20] With increasing polymer volume fraction f_A of the minor component the corresponding microdomain structures varies from closed packed spheres (CPS), cubic packed spheres (bcc), hexagonal packed cylinders (Cyl) via a double gyroid (Gyr) to a lamella structure (Lam) at $f_A = 0.5$.

Diffusion of Block Copolymers

Usually the Flory-Huggins interaction parameter χ_{AB} is inverely proportional to the temperature of the system. In typical systems χ_{AB} is positive and smaller than unity. If the temperature increases and χ_{AB} decreases, the entropic factor dominates and the system becomes disordered. The change is

called order-disorder transition (*ODT*) and the corresponding temperature is the order-disorder transition temperature (T_{ODT}).

A higher entropy means a higher mobility of the polymer molecules. Alternatively the higher mobility can be reached with the addition of a non selective solvent. Here the solvent molecules increase the distance between monomer A and monomer B leading also to a decrease in the interaction forces. In general the mobility can be quantified by the diffusion of the system.

1.1.4 Diffusion in Thin Polymer Films

The diffusion of small molecules into a surface layer was described first by Crank et al.[22, 23] The system can be described as follows: A dry film with an initial film thickness is exposed to an atmosphere saturated with good solvent molecules. The molecules adsorb on top of the surface and an initial concentration gradient is observed. The diffusion of the small molecules into the surface layer is a Fickian process, this means the diffusion coefficient D is constant. During this diffusion process the concentration gradient decreases until the solvent molecules reach the basis ground of the film. Due to the solvents the film swells and its thickness increases until an equilibrium swollen film thickness is obtained. The time-resolved increase of mass of a film on an impermeable substrate can be written as

$$\frac{M_t}{M_\infty} = \frac{2}{h_0} \sqrt{Dt} \left(\frac{1}{\sqrt{\pi}} + 2 \sum_{n=1}^{\infty} (-1)^n \operatorname{ierfc} \frac{nh_0}{2\sqrt{Dt}} \right) \quad (1.5)$$

with the mass M_t at any time t , in the swollen equilibrium state M_∞ and the initial film thickness h_0 . ierfc is the inverse complex error function and $n \in \mathbb{N}$. Using the simplified expression for short times

$$\frac{M_t}{M_\infty} = 2\sqrt{\frac{D}{\pi}} \cdot \frac{\sqrt{t}}{h_0} \quad (1.6)$$

the diffusion coefficient can be determined from the initial slope of the swelling curves plotted as $\frac{M_t}{M_\infty}$ versus $\frac{\sqrt{t}}{h_0}$. The diffusion coefficients increase with in-

creasing film thickness.

The diffusion of solvent molecules into a swelling polymer film is reported by Vogt et al.[24, 25] The absorption process of water into ultrathin poly(vinyl pyrrolidone) films was followed by using X-ray reflectivity and quartz crystal microbalance measurements.

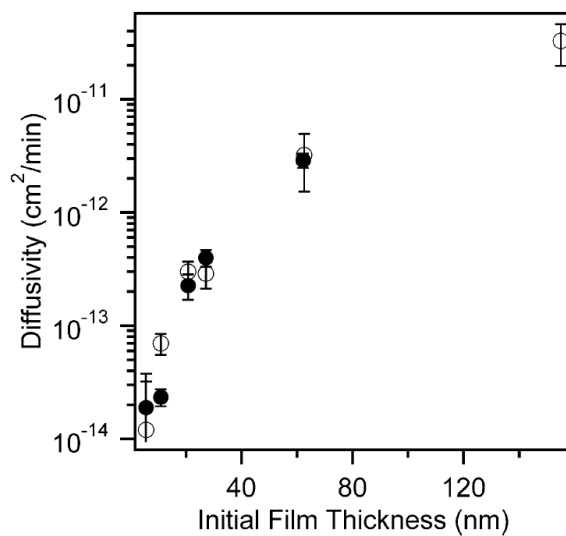


Figure 1.7: Diffusion coefficients of water into poly(vinyl pyrrolidone) films increases with increasing polymer film thickness, as reported by Vogt [25]. The absorption process was followed by using X-ray reflectivity and quartz crystal microbalance measurements.

1.2 Experimental Methods

1.2.1 Dynamic Light Scattering (DLS)

The dynamic light scattering (DLS) became important in the 1960ies with the development of the laser and the photo multiplier. In the setup of a DLS experiment the linear polarized light passes the sample. Brownian motion in the sample causes small density fluctuations. The light is scattered on these fluctuations in all directions with interference of the electric field $E(\mathbf{q}, t)$. The scattering vector \mathbf{q} describes the difference between the incident wave vector \mathbf{k}_0 and the scattered wave vector \mathbf{k} meaning $\mathbf{q} = \mathbf{k}_0 - \mathbf{k}$. The interfered light is detected by a photo multiplier at several fixed angles Θ to the incident light between 30° and 150° . A typical setup is presented in fig. 1.8 The time resolved signal is autocorrelated and evaluated.

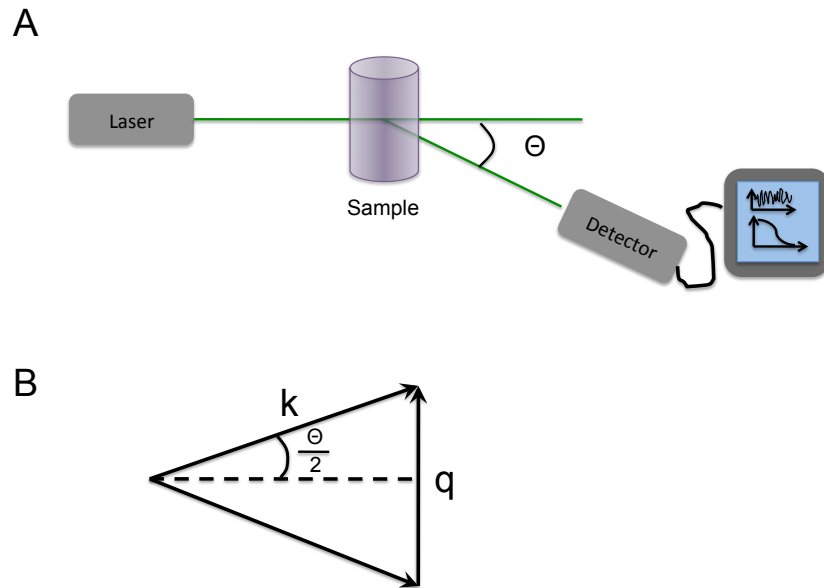


Figure 1.8: (A) Scheme of a setup for Dynamic Light Scattering: The incident laser light is scattered at small density fluctuations in the sample. The interference of the scattered light is detected by time resolved at fixed angles Θ between 30° and 150° . (B) The scattering vector \mathbf{q} is the difference between the incident \mathbf{k}_0 and the scattered wave vector \mathbf{k} .

The theory of DLS is presented by Pecora. [8] The normalised field-field autocorrelation function of the incident and the scattered electromagnetic wave is defined as

$$g^{(1)}(\mathbf{q}, t) = \frac{\langle E(\mathbf{q}, t) \cdot E^*(\mathbf{q}, t + \tau) \rangle}{\langle E(\mathbf{q}, t) \cdot E^*(\mathbf{q}, t) \rangle}. \quad (1.7)$$

The electric field $E(\mathbf{q}, t) = E_0 \exp(i\mathbf{q} \cdot \mathbf{r}(t))$ at time t is correlated with conjugate complex one after a lag time τ . The brackets $\langle \rangle$ symbolise integration and normalisation $\langle E(\mathbf{q}, t) \cdot E^*(\mathbf{q}, t + \tau) \rangle = 1/T \int_0^T E(\mathbf{q}, t) \cdot E^*(\mathbf{q}, t + \tau) dt$. The absolute value of the scattering vector \mathbf{q} is given by

$$q = |\mathbf{q}| = \left(\frac{4\pi n}{\lambda} \right) \sin \left(\frac{\theta}{2} \right). \quad (1.8)$$

Here n is the refractive index of the medium, λ is the incident wavelength and θ is the scattering angle. For mono disperse particles the field-field autocorrelation function can be calculated [8] to

$$g^{(1)}(q, t) = \exp(-q^2 D_c \tau) \quad (1.9)$$

with the collective diffusion coefficient D_c .

The experimentally accessible quantity in DLS is the normalised intensity autocorrelation function

$$g^{(2)}(\mathbf{q}, t) = \frac{\langle I(\mathbf{q}, t) \cdot I(\mathbf{q}, t + \tau) \rangle}{\langle I(\mathbf{q}, \mathbf{0}) \rangle^2}. \quad (1.10)$$

The scattered intensity can be described as $I(\mathbf{q}, \tau) \propto E_0^2 \sum e^{i\mathbf{q} \cdot \mathbf{r}}$. The Siegert relation

$$g^{(2)}(q, t) = B + \beta |g^{(1)}(\mathbf{q}, t)|^2 \quad (1.11)$$

combines the measured with the calculated autocorrelation function. Eq. 1.11 is necessary for the evaluation of data.

1.2.2 Fluorescence Correlation Spectroscopy (FCS)

E. Elson, D. Magde and W. W. Webb developed the theoretical background fluorescence correlation spectroscopy (FCS) in the early 1970ies on the basis of dynamic light scattering (DLS) [26, 27, 28]. In 1993 R. Rigler et al. combined this fluorescence technique with a confocal setup [29]. A scheme of

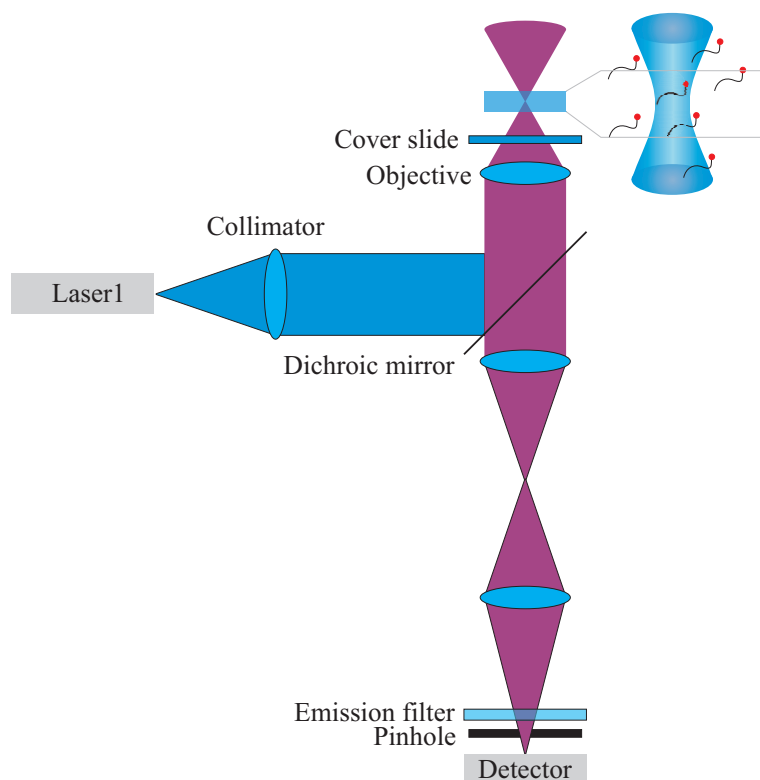


Figure 1.9: Scheme of a confocal set up for Fluorescence Correlation Spectroscopy [30].

the confocal setup is presented in fig. 1.9. The incoming laser light is strongly focused by a objective with high numerical aperture (ideally $NA > 0.9$) to a diffraction limited spot. Usually solutions with a dye concentration of about 1 nM are used, so that just a few molecules are excited in the illuminated region. The emitted light is collected by the same objective and passes a dichroic mirror. To limit the detection volume a pinhole is placed in the image plane, which blocks all light not coming from the focal point.

Theoretical Basis of FCS

The normalised autocorrelation function is defined as

$$G(\tau) = \frac{\langle F(t) \cdot F(t + \tau) \rangle}{\langle F \rangle^2}. \quad (1.12)$$

The fluctuations in fluorescence intensity $F(t)$ depend on the concentration fluctuations $C(\mathbf{r}, t)$ of dyes in the observation volume.

$$F(t) = b \int W(\mathbf{r}) C(\mathbf{r}, t) d^3\mathbf{r} \quad (1.13)$$

The specific brightness b of the fluorescent molecule is assumed to be independent of time and depends on the absorption cross section and the quantum yield of fluorescence. The molecule detection function $W(\mathbf{r})$ is independent of time and contains the profile of the laser and the geometry of detection. Using confocal detection the shape is assumed to be a Gauss'ian ellipsoid with the radius w_{xy} in the focus plane and the expansion of w_z along the optical axis.

$$W(\mathbf{r}) = W_0 e^{-\frac{2(x^2+y^2)}{w_{xy}^2}} e^{-\frac{2z^2}{w_z^2}} \quad (1.14)$$

The prefactor W_0 contains the intensity of excitation including the detector efficiency and the loss of filters.

As the system is stationary the average properties (in angle brackets) are independent of time. The autocorrelation function depends on the time interval τ but not on the absolute time t . Using equ. (A.1) leads to

$$G(\tau) = \frac{\langle \delta F(0) \cdot \delta F(\tau) \rangle}{\langle F \rangle^2} + 1 \quad (1.15)$$

$$G(\tau) = \frac{b^2 \int \int W(\mathbf{r}) W(\mathbf{r}') \langle \delta C(\mathbf{r}, 0) \cdot \delta C(\mathbf{r}', \tau) \rangle d^3\mathbf{r} d^3\mathbf{r}'}{b^2 (\int W(\mathbf{r}) \langle C \rangle d^3\mathbf{r})^2} + 1 \quad (1.16)$$

Assuming ideal diluted solutions the fluorescent molecules moves Brown'ian like in three dimensions with the (self-)diffusion constant D . The number density autocorrelation term is calculated on the base of 2. Fick's law (see

appendix A.2) to

$$\langle \delta C(\mathbf{r}, 0) \cdot \delta C(\mathbf{r}', \tau) \rangle = \frac{\langle C \rangle}{(4\pi D\tau)^{3/2}} \cdot e^{-\frac{(\mathbf{r}-\mathbf{r}')^2}{4D\tau}} \quad (1.17)$$

Integration of the molecule detection function $\int W(\mathbf{r})d^3\mathbf{r} = \pi^{3/2}w_{xy}^2w_z = V_{\text{eff}}$ results in the effective detection volume V_{eff} . With the average concentration we obtain the average number of fluorescent molecules in the detection volume $\langle N \rangle = \langle C \rangle V_{\text{eff}}$. Further integration (see appendix A.3) results in

$$G(\tau) = \frac{1}{\langle N \rangle} \cdot \frac{1}{1 + \frac{\tau}{\tau_d}} \cdot \frac{1}{\sqrt{1 + \frac{w_{xy}^2}{w_z^2} \frac{\tau}{\tau_d}}} + 1 \quad (1.18)$$

This geometrical decay function is the basic equation for fluorescence correlation spectroscopy. It depends on the average diffusion time of the fluorescent molecule τ_d through the effective volume.

Include Triplett Dynamic

Photo physic causes also intensity fluctuations. [17] Most important for FCS is the triplett state dynamic $G_{\text{triplett}}(\tau) = 1 - T + T \cdot \exp(-\frac{\tau}{\tau_{tr}})$ with the fraction of dyes T switching to the triplet t state and the triplet lifetime τ_{tr} . Regarding l different kinds of particles the autocorrelation function is obtained to [31, 32]

$$G(\tau) = (1 - T + T \cdot e^{-\tau/\tau_{tr}}) \cdot \left(1 + \frac{1}{\langle N \rangle} \sum_{j=1}^l \frac{\Phi_j}{1 + \frac{\tau}{\tau_{d,j}}} \frac{1}{\sqrt{1 + \frac{w_{xy}^2}{w_z^2} \frac{\tau}{\tau_{d,j}}}} \right) \quad (1.19)$$

with the fraction Φ_j of particle j .

1.2.3 FCS in Polymer Science

Fluorescence correlation spectroscopy was developed for the use in biophysics and medicine science. Recently the FCS was propagated for the use in polymer science. [13, 14, 30] To use this method for the investigation in polymer science are two points need to be mentioned. The next section describes the importance of a mono-disperse sample. As second the FCS technique is commonly used in aqueous systems. The adjustment of an commercial FCS setup for the use with organic solvents is presented in section 1.2.3

Request on the Samples

For FCS research the material needs to carry fluorescent dyes. In general there are two possibilities to label chemically via bonds or physically, e.g. via ionic interaction. This thesis contains results with both label versions. The ideal material has the same amount of dyes on each investigated molecule. So the physical labeling is easier because of the very low amount of dyes ($10^{-8}M$) in comparison of the investigated material. But for neutral synthetic polymers well defined labeling is not easy. A polymer analog reaction with reactivity to each repeating unit results in statistically labeled polymers [33]. Another possibility is living polymerisation with a small block of dye containing monomers [34]. This way is more defined, because the dyes are at a definite position of the polymer. But still there are more than one dye attached to one molecule. The best way to get just one dye to one polymer molecule was found by Zettl et al. via a polymeranaloge reaction of the end of the chain with the dye molecules. [13]

A further problem of FCS at polymeric systems is the molecular weight distribution. This FCS technique detects single molecules and the self similarity of the signal gives the diffusion time τ_d . This diffusion time is related to the diffusion coefficient D via the relation $\tau_d = w_{xy}^2/(4D)$. According to the Stokes-Einstein law (1.2) the diffusion coefficient depends on the hydrodynamic radius R_h . The polymer coil can be seen as a sphere with the volume $V = \frac{4\pi}{3}R_h^3$. With the density $\rho = m/V$ the hydrodynamic radius R_h depends on the mass of the polymer coil m . Finally the diffusion time τ_d depends on

the mass of the polymer coil m as

$$\tau_d = \frac{w_{xy}^2}{4} \cdot \frac{6\pi\eta}{k_bT} \cdot \sqrt[3]{\frac{3}{4\pi} \cdot \frac{m}{\rho}} \propto \sqrt[3]{m}$$

So the molecular weight distribution causes a range of diffusion times. The influence of different polydispersity indices PDI on FCS measurements was investigated by Starchev et al. [35]. With $\text{PDI} < 1.06$ the autocorrelation function does not change and in the range of $1.06 < \text{PDI} < 1.2$ the influence is still small enough.

Request on the Setup

The most important problem to solve is the solvent of synthetic polymer solutions. Commercial fluorescence correlations spectrometers are developed for water systems. But water is a bad solvent for most synthetic polymers. This means that the polymers precipitate. To investigate diffusion properties of synthetic polymers in solution it is necessary to measure in organic solvents. Most organic solvents have a much higher refractive index in comparison to water ($n = 1.33$). With change in the refractive index the corrections of the spherical and chromatic aberrations are not valid any more. Finally using a water immersion objective for measurements in organic solvents the excitation volume is not congruent with the detection volume any more. The difference of the detection volumes are shown in fig. 1.10. The misalignment causes a decrease of the counts per molecule and thus a decrease of the signal to noise ratio.

This problem was recently solved by using different immersion objectives. [13, 30, 14] In general the immersion medium should have the same refractive index as the sample. So an oil immersion objective is ideal for solutions with a refractive index of $n \approx 1.5$. Whereas for samples with intermediate refractive index a multi immersion objective can be used. This multi immersion objective allows to work with different immersion media because it has a correction ring to adjust. The detection volume of the multi immersion objective used with multi immersion oil to measure in toluene is compared

with a Gaussian intensity distribution in fig. 1.11.

Last but not least the sample chambers needed to be sealed to avoid evaporation of the organic solvent. The walls of the sample chambers are made of stainless steel. The cover slides has been fixed on bottom of the chamber by an epoxid hardener. The top was closed by a screw formed cap also made of stainless steel and sealed by indium wire. The soft indium wire was deformed after reopening the chamber and had to be recycled. Using new Indium wire lead to noise signals in the FCS trace. The geometry of the sample chamber is described in detail by [30].

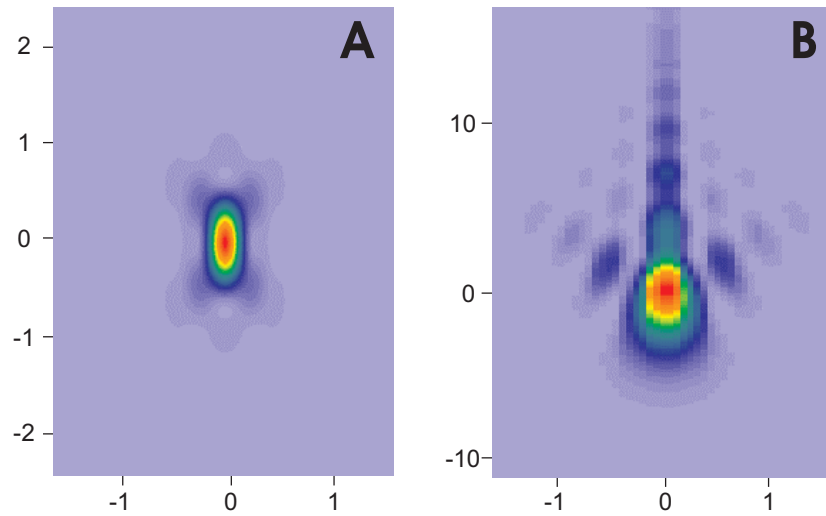


Figure 1.10: Molecule detection function of a water immersion objective with a numerical aperture of 1.2. The focus was chosen $200 \mu\text{m}$ above the cover slide. Figure A and B show the calculation with a refractive index of 1.333 (water) and 1.49 (toluene) respectively. Note the different y-scales for figure A and B [30].

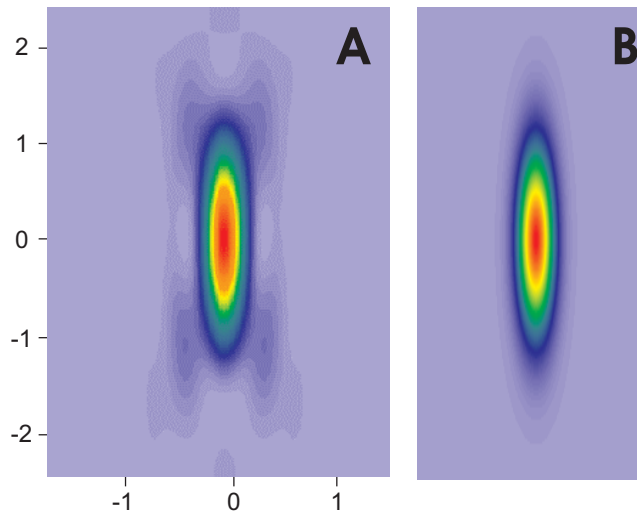


Figure 1.11: Figure A shows the calculated intensity distribution for a multi-immersion objective. This objective has a magnification of $40\times$ and a numerical aperture of 0.9. The dye was dissolved in toluene. The volume has a size of $1.2 fL$. Figure B represents the intensity distribution approximated by a Gaussian distribution in all directions [30].

1.2.4 Ellipsometry

The Ellipsometry gives information about the thickness of surface layers and their refractive index. The theory is presented by Azzam and Bashara and an introduction is given by Tompkins. [36, 37]

The principle setup of an Ellipsometer experiment is shown in fig. 1.12. The incident light passes a polariser (for linear polarisation) and a compensator (for circular polarisation), is reflected on the sample and passes the analyser to reach the detector. The change of polarisation from the incident beam to the reflected beam is expressed in the amplitude ratio Ψ and the phase shift Δ .

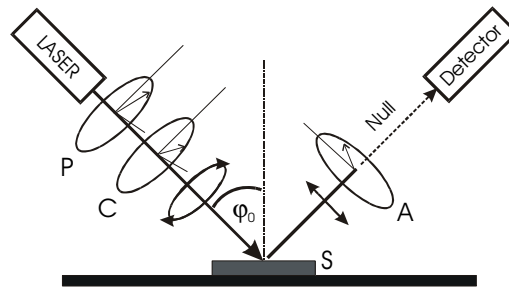


Figure 1.12: Scheme of a setup for Ellipsometry: The incident light passes a polariser (for linear polarisation) and a compensator (for circular polarisation), is reflected on the sample and passes the analyser to reach the detector. [38]

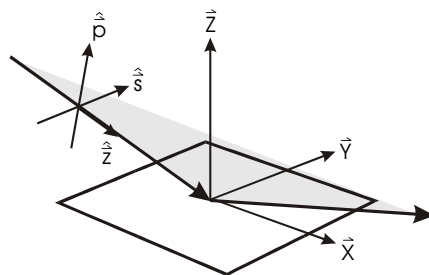


Figure 1.13: System of coordinates in the experiment, the plane of reflection is light grey. [38]

The electric field of a linear polarised light is given by $\mathbf{E}(\mathbf{z}, t) = \mathbf{E}_0 \exp(i(\omega t - \mathbf{kz} + \delta))$ with the wave vector $|\mathbf{k}| = k = 2\pi/\lambda$, the field amplitude \mathbf{E}_0 and the phase δ . The overlay of two linear polarised waves results in a wave

$$\mathbf{E}(\mathbf{z}, t) = \begin{pmatrix} E_p^E \\ E_s^E \end{pmatrix} = \begin{pmatrix} \mathbf{E}_0 \cos(\omega t - \mathbf{kz} + \delta_p) \\ \mathbf{E}_0 \cos(\omega t - \mathbf{kz} + \delta_s) \end{pmatrix} \quad (1.20)$$

with index p for the electric field in plane of reflection and with index s for the electric field perpendicular to the plane of reflection, see fig. 1.13.

The changes of polarisation between the incident wave \mathbf{E}^E and the reflected wave \mathbf{E}^R is indicated by the so called ellipsometric angles Ψ and Δ

$$\tan \Psi = \frac{|E_{0p}^R| / |E_{0p}^E|}{|E_{0s}^R| / |E_{0s}^E|} \quad (1.21)$$

$$\Delta = (\delta_p^R - \delta_s^R) - (\delta_p^E - \delta_s^E) \quad (1.22)$$

With the definition of the complex reflection coefficients R_p and R_s for p - and s -polarised light

$$R_p = \frac{|E_{0p}^R|}{|E_{0p}^E|} \exp i(\delta_p^R - \delta_p^E) \text{ and } R_s = \frac{|E_{0s}^R|}{|E_{0s}^E|} \exp i(\delta_s^R - \delta_s^E) \quad (1.23)$$

equ.1.21 becomes the ellipsometric equation:

$$\tan \Psi e^{i\Delta} = \frac{R_p}{R_s} \quad (1.24)$$

The change of the polarisation for each optical component is calculated using the Jones Matrices \mathbf{T} for the polarisator \mathbf{T}_P , compensator \mathbf{T}_C , sample \mathbf{T}_S and analyser \mathbf{T}_A . Additionally the transformation matrix $\mathbf{D}(\alpha) = \begin{pmatrix} \cos \alpha & \sin \alpha \\ -\sin \alpha & \cos \alpha \end{pmatrix}$ is necessary between the components. Now the electric field on the detector \mathbf{E}^{det} is calculated to

$$\mathbf{E}^{det} = \mathbf{D}(-A)\mathbf{T}_A\mathbf{D}(A)\mathbf{T}_S\mathbf{D}(-C)\mathbf{T}_C\mathbf{D}(C)\mathbf{D}(-P)\mathbf{T}_P\mathbf{D}(P)\mathbf{E}^E \quad (1.25)$$

Working with zero order reflection the last rotation of the analyser $\mathbf{D}(-A)$ is negligible. The detector measures the intensity which is proportional to the

energy of the light $I \propto E E^*$.

$$\mathbf{E}^{det} = \mathbf{T}_A(\Omega_1 + \Omega_2)(E_s^E \cos P + E_s^E \sin P) \quad (1.26)$$

with

$$\Omega_1 = R_p \cos A (\cos C \cos(C - P) - i \sin C \sin(C - P)) \quad (1.27)$$

$$\Omega_2 = R_s \sin A (\sin C \cos(C - P) + i \cos C \sin(C - P)) \quad (1.28)$$

The zero order reflection is reached when the intensity at the detector disappears, with $\mathbf{E}^{det} = 0$ or $(\Omega_1 + \Omega_2) = 0$. Leading to

$$\frac{R_p}{R_s} = -\tan A \frac{\tan C + i \tan(C - P)}{1 - i \tan C \tan(C - P)} \quad (1.29)$$

Now two of the three angles P , C and A are fixed. One can be chosen by free, this is commonly the compensator to $C = \pm 45^\circ$. With equ. 1.21 and 1.29 we obtain

$$\tan \Psi e^{i\Delta} = \tan A e^{i(2P + \pi/2)} \text{ for } C = -45^\circ \quad (1.30)$$

$$\tan \Psi e^{i\Delta} = -\tan A e^{i(\pi/2 - 2P)} \text{ for } C = 45^\circ \quad (1.31)$$

Finally the ellipsometric angles Ψ and Δ are obtained to

$$\Psi = |A| \text{ and } \Delta = 2P \pm 90^\circ \text{ for } C = -45^\circ \quad (1.32)$$

$$\Psi = |A| \text{ and } \Delta = -2P \pm 90^\circ \text{ for } C = 45^\circ \quad (1.33)$$

The measurements are done at several different incident angles. The refractive index and the thickness of the material layer are obtained by fitting a model, typically the Cauchy model $n_p(\lambda) = n_0 + n_1 \cdot \frac{100}{(\lambda/\text{nm})^2}$ is used.

1.2.5 Atomic Force Microscopy (AFM)

Atomic force microscopy (AFM) is a very good method to investigate the topography of thin films. There are no special requirements of the sample like electrical conductivity which is needed for scanning tunneling microscopy. Like with all other scanning probe microscopies, the sample is scanned. Therefore a small tip at the end of a cantilever scans the surface line by line. A setup of an AFM is shown in Fig. 1.14.

Using TappingModeTM the cantilever is forced to a vertical oscillation towards the surface normal by a piezoelectric element. The excitation frequency is close to the resonance frequency of the AFM cantilever tip, which is typical about 250-350 kHz. The free amplitude is about 20 nm. If the tip comes closer to the surface the oscillation of the tip is influenced by the air layer between sample surface and the tip. Moving the tip further to the surface leads to an attraction leading to a lower amplitude of the cantilever. At a distance of about 100 pm the repulsive force between tip and sample dominates.

This behavior can be described in approximation by the Lennard-Jones potential $U(r) = \frac{A}{r^{12}} - \frac{B}{r^6}$. A and B are material constants of the tip and the sample and r describes the distance between both. The repulsive forces are given by A/r^{12} and is caused by repulsion of the electron clouds. The term B/r^6 describes the attractive forces which are mainly caused by dipol-dipol interaction between sample and tip.

In the TappingModeTM the average distance between tip and surface is kept constant. A laser is adjusted to the end of the cantilever to detect the deviation which gives information about the conditions particular the topography of the sample. The laser is reflected at the cantilever and is detected at a segmented photodiode. The information of the adjusted signal of the amplitude is directly given to a computer which converts the signal to an image.

In general there are further modes for AFM measurements. Just to mention one, in the Contact Mode the sample surface is scanned with a constant distance between surface and tip without oscillation of the cantilever. Here

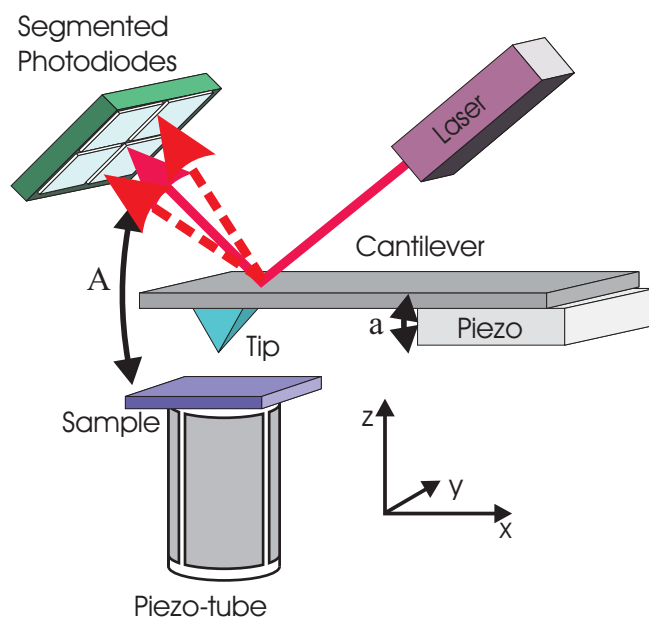


Figure 1.14: Scheme of a setup for Atomic Force Microscopy. [39]

the signal can be converted directly to a height image. The disadvantage of this mode is the force on the sample, so that soft surfaces like proteins or soft polymers can be damaged by the tip.

1.3 Overview of the Thesis

1.3.1 Synopsis

This thesis starts with the analysis of the swelling behaviour and the microphase separation of block copolymers in thin films. The results of these measurements are diffusion informations of solvent in thin block copolymer films. For a detailed understanding of the behaviour of blockcopolymers during the microphase separation the diffusion behaviour of polymer molecules has to be investigated. Therefore a model system of homopolymers was used to study the diffusion of single polymer chains in solution.

Chapter 2 presents the dynamic behavior and the resulting structure of block copolymers in thin films. The dry block copolymer thin films are swollen by a defined solvent vapour pressure. The change in the film thickness was followed by in-situ ellipsometry. Evaluation of the initial change of thickness results in the diffusion coefficient of concentrated solutions.

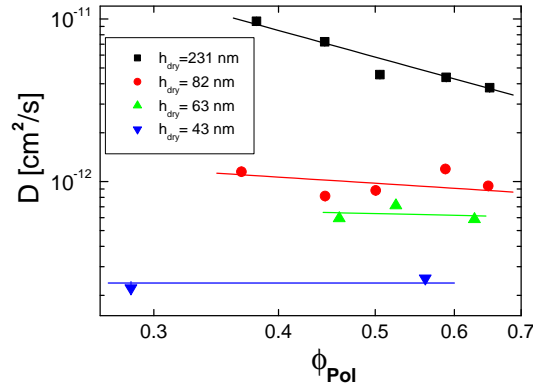


Figure 1.15: Diffusion coefficients D in thin films as a function of the concentration, here the polymer volume fraction ϕ_{Pol} , and increasing thickness of the dry thin film h_{dry} from bottom to top.

Fig. 1.15 shows the diffusion coefficients depending on the film thickness and minor on the concentration, expressed in the polymer volume fraction ϕ_{Pol} . The diffusion is independent of the concentration in thin films with a thickness less than three times of characteristic spacings. The diffusion in

thicker films depends moderately on the concentration.

Chapter 2 presents also the corresponding morphology of the microphase separated diblock copolymers. Annealing with the same solvent vapor pressure, films with one cylinder layer have a higher uptake of solvent. This higher uptake can be seen at annealing conditions near the order-disorder transition. Here the second terrace has a long range order in the aligned cylinders whereas the cylinders in the first layer have no long range order. This effect was presented in the same sample with both terraces coexisting next to each other.

Chapter 3 presents diffusion coefficients of a homopolymer in a good solvent, polystyrene in toluene. The FCS technique yields the selfdiffusion coefficient D_s in dilute solutions, as expected. In the semidilute entangled concentration regime a second decay appears in the FCS measurements. With increasing concentration, the decay time increases moderately. Typical explanations for the second decay like free dye or the triplett state can clearly be eliminated. Free dye should be present also in the diluted solutions. Moreover the absence of free dyes in the diluted solution was shown already earlier by [13]. In the case of the molecular weight near $M_{w,e}$ the second decay is between free dye and a triplett state decay. But the triplett state of the dye can't either give the explanation, because the change to the triplett state of the dye molecule needs the interaction with a triplett state molecule like e.g. physically dissolved oxygene in water. The presence of triplett decay times in FCS in aqueous solutions can be suppressed by bubbling nitrogen gas through the solution to get rid of the oxygen. But in this case the unpolar solvent toluene has no dissolved oxygen. And the triplett decay time is not a function of the concentration, as shown here for the higher molecular weight polymers. Some of the polymer solutions are measured also with a different setup to get rid of artefacts. However the second decay time in semidiluted entangled polymer solutions were no artefact.

Comparison with DLS measurements leads to the finding that the collective diffusion coefficient D_c is overlaid by the corresponding diffusion coefficient, calculated from this second decay time in FCS. Fig. 1.16 presents the diffusion coefficients measured with both techniques.

We were able to show, that the second decay in the FCS measurements is based on effective long-range interaction of the labeled chains in the transient entanglement network of the semi diluted solution. Meaning the second decay in the FCS measurements represents the collective diffusion. The measurements verify the basic scaling and reptation theory for semidilute entangled polymer solutions. A quantitative basis for the modelling of the cooperative diffusion coefficient is given by a Langevin and generalized Ornstein-Zernike equation. The so calculated cooperative diffusion coefficients agree with the measured results both in the dilute and semidilute regimes. In particular the features of the crossover region between the dilute and the semidilute regimes are captured correctly by the underlying integral equation theory.

Chapter 4 presents diffusion coefficients of long tracer molecules in shorter polymer matrixes. Depending on the concentration and the molecular weight of the matrix polymer chains two different types of macromolecular tracer diffusion behavior were obtained. Autocorrelation functions of measurements with the matrix polymer molecular weight M_w shorter than the $M_{w,e}$ shows a single self diffusion process for arbitrary concentrations. Whereas autocorrelation functions of measurements with $M_w > M_{w,e}$ turns from a single decay to a two diffusion phenomenon, comparable to chapter 3. The long time decay gives the self diffusion coefficient and the short time decay correspondes to the collective diffusion coefficient of the matrix polymer weight measured by DLS, see figure 1.16, in bottom.

We called the minimum concentration at which the cooperative diffusion appears in the FCS measurements as c^+ . Having a constant M_w for the tracer molecules, c^+ increases with the M_w of the matrix. On the other hand a variation of M_w of the tracer molecules in the same M_w of the matrix does not influences c^+ . Moreover tracer molecules with $M_w > M_{w,e}$ in a matrix with $M_w < M_{w,e}$ shows just the self diffusion behavior, even in the high semidilute concentration solutions. This means the fast diffusion process in FCS is a characteristic property of the matrix polymer chains. This concentration c^+ corresponds to the cross over concentration to the entangled regime as presented by Graessley, see fig. 1.17.

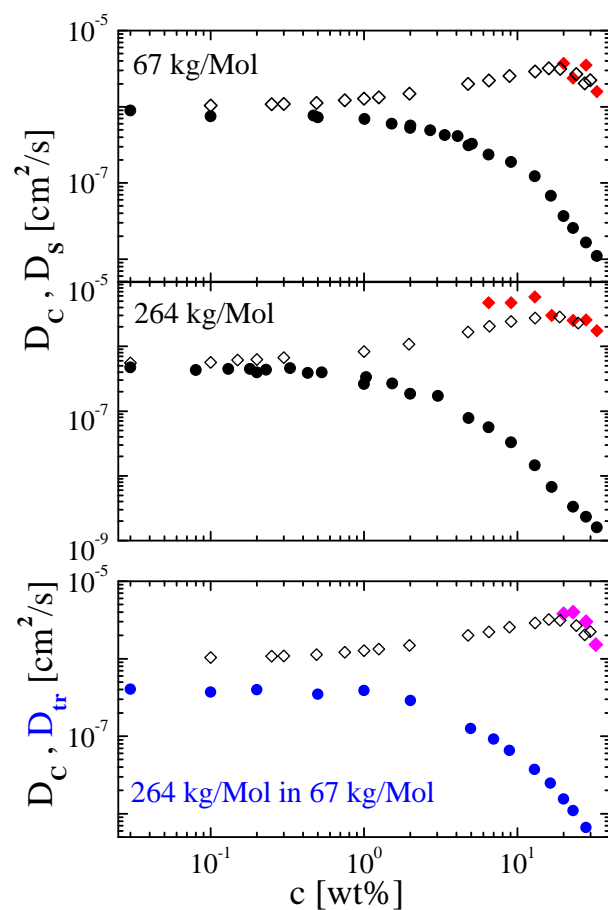


Figure 1.16: Diffusion coefficients of polystyrene in toluene: closed symbols present the measurements with fluorescence correlation spectroscopy (FCS) and open symbols the dynamic light scattering (DLS) measurements. In the top and in the middle tracer and matrix polymers have the same molecular weight (presented in chapter 3). In the bottom the molecular weight of the tracer is higher, than that of the matrix (presented in chapter 4).

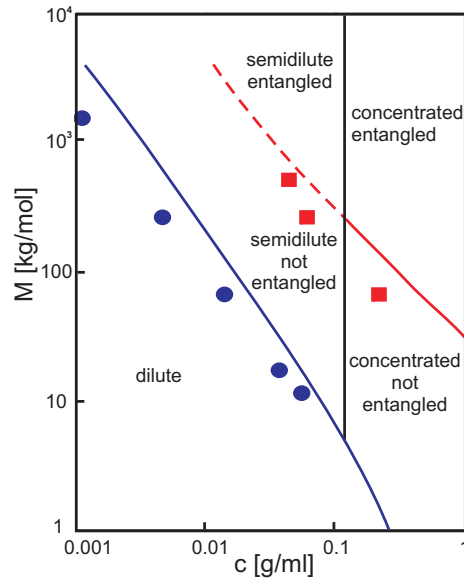


Figure 1.17: Viscoelastic regimes dependent on molecular weight M and concentration c of polystyrene in a good solvent, the lines are calculated by Graessley [4]. The symbols are measured data with fluorescence correlation spectroscopy for polystyrene in toluene: \bullet indicates the overlap concentration measured by Zettl et al [14] and \blacksquare marks the cross over concentration c^+ to the entangled regime as presented in chapter 4. [16]

In general the fluorescence correlation spectroscopy was used for the investigation of polymer dynamic in solution in the dilute, semidilute and for molecular weights near the entanglement molecular weight even in slightly concentrated solutions.

Fig. 1.17 presents the five viscoelastic regimes of polystyrene in a good solvent depending on the molecular weight M and concentration c . The lines are calculated by Graessley [4]. The symbols are measured data for polystyrene in toluene: \bullet indicates the overlap concentration [14] and \blacksquare marks the cross over concentration c^+ to the entangled regime. [16]. The investigated molecular weights M_w range from 11 kg/mol to 1.550 kg/mol.

1.3.2 Individual Contributions to each Publication

In the following part my own contribution to each publication is listed. The corresponding author is marked by *.

Chapter 2 is published in *Langmuir* (2010, 26, 6610) with the title **Effect of Confinement on the Mesoscale and Macroscopic Swelling of Thin Block Copolymer Films** by Ute Zettl, Armin Knoll and Larisa Tsarkova *

I planned and conducted all experiments, evaluated the data and wrote the publication. Armin Knoll and Larisa Tsarkova were involved in the scientific discussion.

Chapter 3 is published in *Macromolecules* (2009, 42, 9537) with the title **Selfdiffusion and Cooperative Diffusion in Semidilute Polymer Solutions as measured by Fluorescence Correlation Spectroscopy** by Ute Zettl, Sebastian T. Hoffmann, Felix Koberling, Georg Krausch, Joerg Enderlein, Ludger Harnau and Matthias Ballauff *

I planned all experiments, evaluated the data and wrote the publication except the theoretical descriptions in section 3.5. Sebastian T. Hoffmann conducted the experiments and evaluated the data for his diploma thesis, Felix Koberling conducted the measurements at the company PicoQuant. Ludger Harnau performed the theoretical analysis and wrote the theoretical descriptions in section 3.5. Georg Krausch, Joerg Enderlein and Matthias Ballauff were involved in the scientific discussion.

Chapter 4 is published in *Journal of Physics: Condensed Matter*, (2010, 22, 49) with the title **A Fluorescence Correlation Spectroscopy Study of Macromolecular Tracer Diffusion in Polymer Solutions** by Ute Zettl, Matthias Ballauff, Ludger Harnau *

I planned and conducted all experiments, evaluated the data and wrote the publication except the theoretical descriptions in section 4.6. Matthias Ballauff was involved in the scientific discussion and Ludger Harnau performed the theoretical analysis and wrote the theoretical descriptions in section 4.6.

Bibliography

- [1] P.-G. De Gennes, *Scaling Concepts in Polymer Physics*, Cornell University Press, 1979.
- [2] M. Doi and S. F. Edwards, *The Theory of Polymer Dynamics*, Clarendon Press, 1986.
- [3] H. Fujita, *Polymer solutions*, Studies in polymer science ; 9, Elsevier, Amsterdam, 1990.
- [4] W. W. Graessley, *Polymer*, 1980, **21**(3), 258.
- [5] A. Fick, *Poggendorff's Annalen der Physik*, 1855, **94**, 59–86.
- [6] H. Vink, *J. Chem. Soc., Farad. Transact.*, 1984, **81**, 1725.
- [7] H. D. Kim, T. Y. Chang, J. M. Yohanan, L. Wang, and H. Yu, *Macromolecules*, 1986, **19**(11), 2737–2744.
- [8] R. Pecora, *Dynamic light scattering : applications of photon correlation spectroscopy*, Plenum Press, New York, 1985.
- [9] E. J. Amis and C. C. Han, *Polymer*, 1982, **23**(10), 1403 – 1406.
- [10] W. Brown, *Polymer*, 1984, **25**(5), 680 – 685.
- [11] H. Hervet, L. Léger, and F. Rondelez, Jun , 1979, **42**(25), 1681–1684.
- [12] L. Léger, H. Hervet, and F. Rondelez, *Macromolecules*, 1981, **14**(6), 1732.
- [13] H. Zettl, W. Häfner, A. Böker, H. Schmalz, M. Lanzendörfer, A. H. E. Müller, and G. Krausch, *Macromolecules*, 2004, **37**(5), 1917.
- [14] H. Zettl, U. Zettl, G. Krausch, J. Enderlein, and M. Ballauff, *Physical Review E*, 2007, **75**(6), 061804.
- [15] *Polymer*, 2008, **49**(19), 4115.

- [16] U. Zettl, S. T. Hoffmann, F. Koberling, G. Krausch, J. Enderlein, L. Harnau, and M. Ballauff, *Macromolecules*, 2009, **42**(24), 9537–9547.
- [17] M. Boehmer and J. Enderlein, *Chem. Phys. Chem.*, 2003, **4**, 729.
- [18] C. Branca, A. Faraone, T. Lokotosh, S. Magazu, G. Maisano, N. P. Malomuzh, P. Migliardo, and V. Villari, *Journal of Molecular Liquids*, 2001, **93**(1), 139.
- [19] T. Kanematsu, T. Sato, Y. Imai, K. Ute, and T. Kitayama, *Polymer Journal*, 2005, **37**(2), 65.
- [20] M. W. Matsen and M. Schick, *Physical Review Letters*, 1994, **72**, 2660.
- [21] A. K. Khandpur, S. Foerster, F. S. Bates, A. J. Hamley, I. W. and Ryan, W. Bras, K. Almdal, and K. Mortensen, *Macromolecules*, 1995, **28**, 8796.
- [22] J. Crank and G. S. Park, *Diffusion in polymers*, Academic Press, London, 1968.
- [23] J. Crank, *The Mathematics of Diffusion*, Oxford Univ. Press, Oxford, 2005.
- [24] B. D. Vogt, C. L. Soles, R. L. Jones, C.-Y. Wang, E. K. Lin, W.-l. Wu, S. K. Satija, D. L. Goldfarb, and M. Angelopoulos, *Langmuir*, 2004, **20**(13), 5285.
- [25] B. D. Vogt, C. L. Soles, H. J. Lee, E. K. Lin, and W. Wu, *Polymer*, 2005, **46**(5), 1635.
- [26] D. Magde, W. W. Webb, and E. Elson, *Phys. Rev. Lett.*, 1972, **29**(11), 705.
- [27] E. L. Elson and D. Magde, *Biopolymers*, 1974, **13**(1), 1–27.
- [28] D. Magde, E. L. Elson, and W. W. Webb, *Biopolymers*, 1974, **13**(1), 29–61.

- [29] R. Rigler, U. Mets, and P. Widengren, J. Kask, *Euro. Biophys. J.*, 1993, **22**, 169.
- [30] H. Zettl *New Applications of Fluorescence Correlation Spectroscopy in Materials Science* PhD thesis, Universität Bayreuth, 2006.
- [31] *Fluorescence Correlation Spectroscopy*, R. Rigler and E. S. Elson, 2000.
- [32] P. Schwille, *Cell Biochem. Biophys.*, 2001, **34**(3), 383–408.
- [33] R. G. Liu, X. Gao, J. Adams, and W. Oppermann, *Macromolecules*, 2005, **38**(21), 8845.
- [34] T. Cherdhirankorn, A. Best, K. Koynov, K. Peneva, K. Muellen, and G. Fytas, *J. Phys. Chem. B*, 2009, **113**(11), 3355.
- [35] K. Starchev, J. Buffle, and E. Perez, *Journal of Colloid and Interface Science*, 1999, **213**(2), 479–487.
- [36] R. M. Azzam and N. M. Bashara, *Ellipsometry and Polarized Light*, Elsevier Science Pub., 1987.
- [37] H. G. Tompkins, *A User's Guide to Ellipsometry*, Dover Publications Inc., Mineola, 2006.
- [38] Ellipsometrie. Institut für Physik, www.uni-potsdam.de/u/physik/fprakti/ANLEIF9.pdf, 2002.
- [39] A. Knoll *Equilibrium and Dynamic Phase Behavior in Thin Films of Cylinder-Forming Block Copolymers* PhD thesis, Universität Bayreuth, 2003.

Chapter 2

Effect of Confinement on the Mesoscale and Macroscopic Swelling of Thin Block Copolymer Films

Ute Zettl¹, Armin Knoll² and Larisa Tsarkova¹ *

¹Physikalische Chemie II, Universitaet Bayreuth, 95440 Bayreuth, Germany.

²Present address: IBM Research - Zurich, Saeumerstrasse 4, CH-8803
Rueschlikon, Switzerland.

Published in *Langmuir*, **2010**, *26* (9), pp 6610-6617.

2.1 Abstract

We report on the swelling behavior and the corresponding morphological behavior of cylinder-forming polystyrene-*b*-polybutadiene diblock copolymers which are confined to several layers of structures. The equilibration of thin films has been done under controlled atmosphere of a non-selective solvent. *In-situ* spectroscopic ellipsometry measurements revealed more than 10% increase of the solvent up-take with decreasing film thickness. With the scanning force microscopy of the microphase separated patterns in quenched films the correlation between the degree of the long-range order of cylinder domains and the degree of the macroscopic swelling has been established. In the case of spontaneously formed micrometer-sized topographic features with discrete film thickness (terraces) the increased solvent uptake by thinner films holds true even for isolated terraces on the mesoscale. The observation of non-homogeneous swelling of the films on the micrometer scale brings novel insights into the properties of confined soft matter, and suggest new approaches towards the fabrication of polymer-based nano-structured responsive materials.

2.2 Introduction

In recent years the focus of research has been shifted towards miniaturization of structures and devices. The related topical question concerns the effect of confinement on the fundamental physical properties and functioning of polymer materials.[1] Rapid development of novel sensor and lab-on-chip technologies,[2] and of polymer-based stimuli-responsive materials, raises the question of changes in solvent - polymer interactions under confinement. Both, organo- and water-soluble polymers have been subjected to studies of the swelling dynamics and equilibrium swelling behavior using different experimental techniques including spectroscopic ellipsometry (SE),[3, 4] optical reflectometry, X-ray or neutron reflectivity,[5, 6, 7] grazing incidence small angle X-ray scattering (GISAXS),[8] quartz crystal microbalance (QCM),[9] and other complementary techniques. Special technologically

approved interest triggered the study of moisture sorption by polymeric films, with materials ranging from commercial linear chain homopolymers such as polyacrylamide,[10, 6] polyimides,[7] poly(vinyl pyrrolidone),[9] poly(methyl methacrylate)[11], common polyelectrolytes [12] to photoresists,[5] thermoresponsive gelling polymers,[8] and more complex water-soluble chains with hydrophobic moieties.[3]

Among mentioned above measuring techniques, neutron reflectivity has an advantage of providing information regarding the distribution of the solvent within swollen films as well as of the distribution of the electron density along the depth of dried films.[5, 6, 7]. Recent research established a decisive contribution of the affinity of the solvent molecules towards the substrate on the swelling behavior of hydrophilic polymers with water vapor. Vogt et al have demonstrated that the concentration of water near an interface is influenced by the chemistry of the substrate. [13, 14, 9] A hydrophilic substrate accumulates water at the substrate/polymer interface which leads to a gradient in water concentration along the depth of the film.[5] The enhanced absolute swelling with decreasing thickness of photoresist films was attributed to an interfacial excess of solvent which dominates the swelling.[5] The same phenomena was also reported for other kinds of hydrophilic polymers.[8, 10] In contrast, depletion of water from a hydrophobic substrate creates a gradient in water concentration through the film, and leads to a strong reduction in the equilibrium uptake with decreasing film thickness.[9]

At the same time, several groups did not confirm the effect of the film thickness on the equilibrium degree of swelling of thin polymer films with water vapor [11, 9] and with the vapor of organic solvents.[15, 16] The obvious discrepancy in the reported results suggests that the thickness dependent swelling, the distribution of the solvent in the depth of the film and the accumulation/depletion of a solvent at the polymer/substrate interface should be considered not only in terms of the solvent-substrate interactions, but rather in terms of "surface fields", i.e. of the difference between the solvent-substrate and solvent-polymer interactions, with the latter being quite sensitive to the particular swelling conditions and to the sample preparation.

Another factor affecting the swelling behavior of thin polymer films is

associated with conformational changes of the polymer chains which are imposed by the confined geometry and by the film preparation.[10, 17, 18] The most significant confinement effects are expected when the film thickness approaches the radius of gyration (R_g). Several authors noticed, that the swelling behavior of ultrathin polymer films can be correlated to a similar behavior of the glass transition temperature, T_g , of the same polymer.[11] Very recently, as-cast films were reported to have a substantially reduced effective viscosity compared to annealed films. The reduced viscosity was explained in terms of nonequilibrium chain conformations giving rise to a reduced entanglement density caused by the rapid quenching of the film during spin coating.[17]

In block copolymer research, swelling of thin films is routinely used to increase chain flexibility and to promote their self-assembly into regular patterns. Solvent processing has been proved to be a simple and effective approach to control the size [19, 20, 21, 22, 23, 24] and the shape of microdomains [25, 26, 27, 24] as well as their orientation and order in thin films [28, 29, 30] by choosing selective solvents, [28, 31] by utilizing directional solidification/quenching [30, 31, 32, 33] or by varying the ambient conditions. [34] In order to get full understanding of the solvent processing of block copolymers it is indispensable to have a precise control over the procedure parameters, such as the temperature of the substrate and of the solvent vapor, the values of the total and partial vapor pressures, the quality and the selectivity of the solvent towards the block copolymer components. Even dynamic characteristics of the annealing procedure such as the total gas flow through the chamber, the volume and the geometry of the annealing chamber, the velocity of the final quench, etc, all crucially affect the resulting microstructure and hence the reproducibility of the results.

Block copolymers offer an additional possibility to study the effect of confinement on the polymer-solvent interactions due to the well-established sensitivity of the microphase separated structures towards the film thickness, the surface interactions, [35] and towards the solvent concentration in the film. [36, 37] In contrast to swollen homopolymer films, only a limited number of studies on thin films of block copolymers have been reported where

the degree of film swelling has been directly accessed. *In-situ* SE has been used before to evaluate polymer-solvent interaction parameters, [38] to construct phase diagrams of surface structures [36, 37], to explore the mechanism of lamella reorientation in thick swollen films, [39, 40] and to study the microphase separation of donor-acceptor block copolymers for polymer electronics. [41] Spectroscopic reflectometry combined with real-time grazing incidence small angle X-ray scattering (GISAXS) allowed to follow structural instabilities in swollen lamella films.[42] Recently was demonstrated that swelling of diblock copolymer films in organic selective solvents follows the same physical principles as that observed for thin films of homopolymers. In particular, a clear thickness-dependent degree of equilibrium swelling has been found with *in-situ* SE.[43]

Here we report on the equilibrium swelling behavior, swelling dynamics and on the corresponding changes of the morphological behavior of cylinder-forming polystyrene-*b*-polybutadiene diblock copolymers (denoted as SB1 and SB2) confined to several layers of structures. *In-situ* spectroscopic ellipsometry measurements revealed more than 10% decrease in the solvent vapor up-take with increasing film thickness upon long-term equilibration under controlled atmosphere of chloroform, a non-selective solvent. Moreover, the microstructure within neighboring terraces, i.e. within the regions of spontaneously quantized film thickness, points to a non-homogenous swelling of the films on a mesoscale. The cylinder domains within the first layer exhibit a low degree of a long-range order due to the vicinity to the order-disorder transition (ODT), in contrast to well-ordered cylinder domains in the neighboring terrace with two layers of structures. These results disclose newly observed nanoscale confinement effects on the chain conformations and on the polymer-solvent interactions in thin films.

2.3 Experimental Section

2.3.1 Polymer

Diblock copolymers polystyrene(PS)-*block*-polybutadiene(PB) with total molecular weights of $M_w = 47.3 \text{ kg/mol}$ (denoted as SB1), and $M_w = 70.0 \text{ kg/mol}$ (SB2) were purchased from (Polymer Source Inc). Important physical parameters of the polymer samples are listed in Table 2.1 In bulk they form glassy PS which are embedded in a soft PB matrix. The glass transition temperature of the PB is $T_{g,PB} = -60^\circ\text{C}$, while that of PS depends on the molecular weight, and is in the range of $T_{g,PS} = 80 - 100^\circ\text{C}$. [44] The surface tension of PB $\gamma_{PB} = 31 \text{ mN/m}$ is considerably smaller than the surface tension of PS, $\gamma_{PS} = 41 \text{ mN/m}$, [44] which drives PB to segregate to the free surface.

Table 2.1: Diblock copolymers

Label	Structure ^a	M_w , kg/mol	$f_{PS, \text{wt}\%}$	a_0, nm^b	χN
SB1	$S_{13}B_{34}$	47.3	26.1	30	30
SB2	$S_{26}B_{70}$	96	24.5	70	60

^a Subscripted indexes indicate the molecular weight (in kg/mol) of respective blocks. ^b a_0 is the characteristic cylinder spacing in melts determined by SAXS measurements. [35]

2.3.2 Sample Preparation

Block copolymer films were spun cast onto silicon substrates from toluene solution. The initial film thickness was controlled by the concentration of the spread solution (0.5, 1 and 2 wt%) and by the spinning rate (1000 – 2000 rpm) resulting in films with an initial dry thickness h_{dry} in the range of 40 – 200 nm. Silicon substrates were cut from the same silicon wafer (<100> orientation, Wacker Siltronic AG), cleaned in fresh 1:1 H_2SO_4 (conc.)/ H_2O_2 (30%) solution, thoroughly rinsed in hot and then cold Millipore water and then dried.

2.3.3 Swelling Experiments

As-spuncoated films were annealed under controlled atmosphere of chloroform vapor pressure. The swelling behavior in the presence of a given $CHCl_3$ vapor pressure was followed by *in-situ* spectroscopic ellipsometry (SENTECH SE 850) as described elsewhere.[39]

All measurements were done at 65° incidence angle within a spectral range from 400 to 800 nm in a home-made thermostated cell which allowed ellipsometric measurements under full control over the solvent vapor atmosphere p/p_0 where p_0 is the chloroform vapor pressure at saturation and p is the actual pressure adjusted by a combination of the saturated $CHCl_3$ vapor flow and by dry nitrogen flow (2.1). Before and when possible after swelling in a solvent vapor, the thickness h_{dry} of the samples was measured. The temperature of the sample and the temperature of a solvent reservoir were controlled to within 0.1 K . The block copolymer film is modeled as a homogeneous material with an effective refractive index $n(\lambda) = n_0 + n_1 \frac{100}{(\lambda/nm)^2}$ where λ is the wavelength and n_0 , n_1 , and n_2 are fitting parameters (Cauchy model); the absorption in the film was assumed to be negligible.

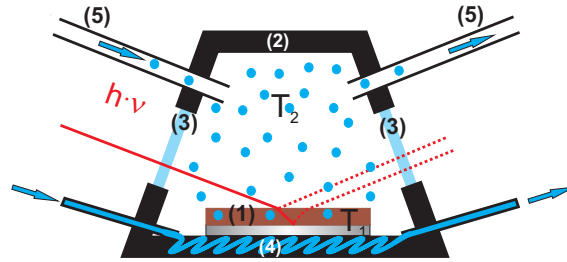


Figure 2.1: Schematic of the annealing chamber: (1) substrate-supported polymer film; (2) sealed stainless steel chamber; (3) glass windows which are perpendicular to the incident light; (4) temperature control of the substrate (T_1); (5) input and output for the temperature and flow controlled solvent vapor (T_2).

2.3.4 Scanning Force Microscopy (SFM)

The microdomain morphology, the terrace heights, and the absolute film thickness were measured with a Dimension 3100 SFM (Digital Instruments, Veeco Metrology Group) operated in a TappingModeTM using silicon tips with a spring constant ca. 40 N/m , and the resonance frequency ranging from 200 to 300 kHz . The measurements of the surface morphology (phase images) were performed at free amplitudes of about 30–50 nm and a relative setpoint of ≈ 0.95 . The phase contrast is well resolved at room temperature at a scale of 10–20 degrees due to the different mechanical properties of the PS (glassy) and PB (soft) components.

For precise determination of the cylinder spacings, of the absolute films thickness and of relative terrace heights imaging has been done with a Dimension 3100 Metrology SFM which is based on a hardware linearized piezo-scanner. The signal distortions are compensated in the x, y and z-directions; therefore the measurements of distances and heights are possible with sub-nanometer resolution.[45]

2.3.5 Optical microscopy

Optical microscopy was used to investigate the characteristic surface topography in equilibrated films (Axiotech microscope from Carl Zeiss AG combined with a digital camera having a resolution of 752×582 pixels).

2.4 Results and Discussion

2.4.1 Swelling Experiments

2.2 presents the time-resolved swelling and deswelling behavior of a SB2 film when the partial vapor pressure p/p_0 in the chamber was varied by a stepwise adjustment of the solvent reservoir temperature while keeping the temperature of the sample at a constant level of $20 \pm 0 C$. The resulting p/p_0

can be calculated according to Clausius–Clapeyron relation:

$$\frac{p}{p_0} = \exp\left(-\frac{\Delta H_{vap}}{R} \left(\frac{1}{T_2} - \frac{1}{T_1}\right)\right) \quad (2.1)$$

Here R is the ideal gas constant, ΔH_{vap} is the enthalpy of evaporation for the solvent, T_2 is the temperature of the solvent reservoir and T_1 is the temperature of the polymer film (always higher than that of the vapor) (2.1).

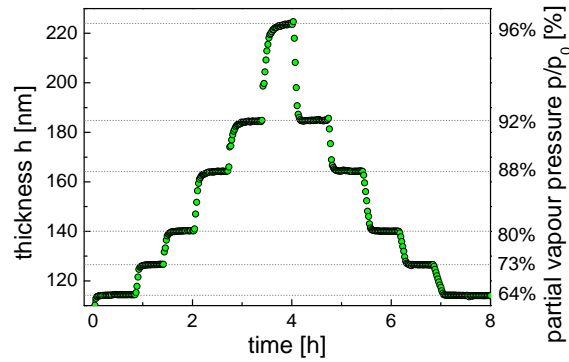


Figure 2.2: Kinetics of the stepwise swelling and deswelling of a 82 nm (h_{dry}) thick SB2 film. The temperature of the substrate was maintained at a constant level of $20 \pm 0.1^\circ C$, and the temperature of the reservoir with the solvent was varied (from bottom to top): 10, 13, 15, 17, 18 and $19^\circ C$. The resulting partial vapor pressure of chloroform p/p_0 (right hand axis) was calculated according to equation (2.3).

After an ordinary adjustment of the solvent temperature, the next equilibrium degree of swelling is achieved in about 10 minutes. The swelling cycle is free of hysteresis within the resolution of the thickness measurements. A similar reversible swelling and deswelling behavior has been measured for SB1 (not shown here).

The data as in 2.2 was used to evaluate the diffusion coefficient of solvent molecules into the swollen film according to the procedure reported earlier by Vogt et al.[5, 9] The uptake of small solvent molecules is described as a Fickian process where the time-resolved increase of the thickness of a film on

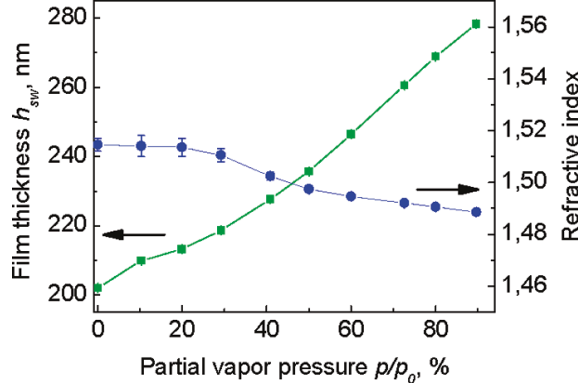


Figure 2.3: Swollen film thickness h_{sw} (left-hand-axis) and refractive index of SB2 film as a function of the partial vapor pressure of chloroform p/p_o .

an impermeable substrate can be written as [46]

$$\frac{h_t - h_0}{h_{sw} - h_0} = \frac{2}{h_0} \sqrt{Dt} \left(\pi^{-1/2} + 2 \sum_{n=1}^{\infty} (-1)^n \operatorname{ierfc} \frac{nh_0}{2\sqrt{Dt}} \right) \quad (2.2)$$

with the film thickness h_t at any time t , in the swollen equilibrium state h_{sw} and the initial film thickness h_0 . ierfc is the inverse complex error function and $n \in \mathbb{N}$. At short times this expression can be simplified to

$$\frac{h_t - h_0}{h_{sw} - h_0} = 2\sqrt{\frac{D}{\pi}} \cdot \frac{\sqrt{t}}{h_0} \quad (2.3)$$

which results in a simple expression for the diffusion coefficient.

$$D = \frac{\pi}{4} \left(\frac{\Delta \frac{h_t - h_0}{h_{sw} - h_0}}{\Delta \frac{\sqrt{t}}{h_0}} \right)^2. \quad (2.4)$$

Diffusion coefficients were determined from the initial slopes of the swelling curves plotted as $(h_t - h_0)/(h_{sw} - h_0)$ versus \sqrt{t}/h_0 (2.4). The curves are well represented by the Fickian model. Figure 2.5 displays the diffusivity of the solvent molecules as a function of the partial vapor pressure for a set of SB1 and SB2 films with varied thicknesses. At a given vapor pressure the diffusivity increases by an order of magnitude as the thickness of SB2 films

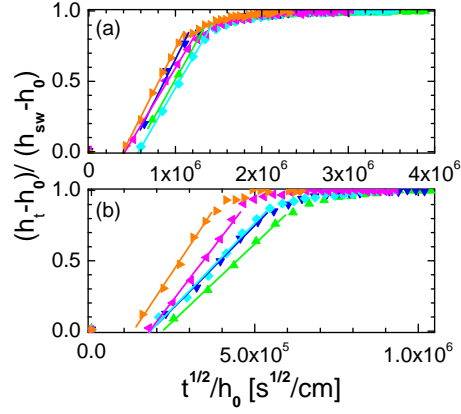


Figure 2.4: Adsorption kinetic of solvent for different film thickness h_0 : (a) 57 nm; (b) 82 nm and 231 nm. Same symbols refer to the same partial vapor pressure p/p_0 , \bullet 64; \blacktriangle 73; \blacktriangledown 80; \blacklozenge 88; \blacktriangleleft 92 and \blacktriangleright 96%.

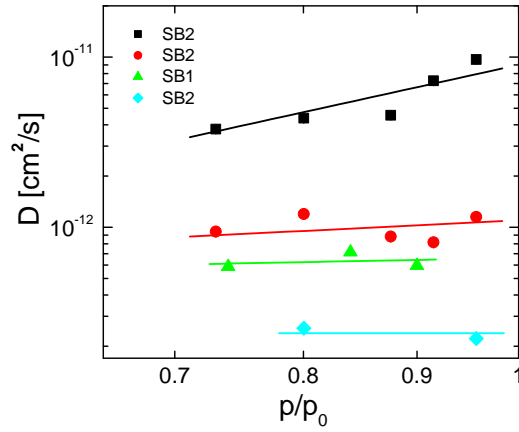


Figure 2.5: Effective solvent diffusion coefficients in SB films as a function of the partial solvent vapor pressure p/p_0 and film thicknesses from bottom to top: 43, 57, 63, 82 and 231 nm.

increases from 40 to 230 nm (lower and upper set of points in 2.5). Another important observation concerns the dependence of the solvent diffusivity on p/p_0 for the 230 nm-thick film ($h_{dry} \geq 2.5a_0$) while thinner films seem not to show such dependence within the data scatter. In a simple approximation, the diffusion coefficient should depend primarily on the initial uptake, which emphasizes transport near the free interface. Therefore, one would expect the dependence of the diffusivity on the solvent vapor concentration. On the other hand, at high polymer concentration, the diffusion of solvent in swollen films can be used as a probe of the segmental polymer dynamics.[9] This view is supported by the observation of decreased transport rates of small molecules in ultrathin polyvinylpyridine films even with large amounts of absorbed water.[9]

The swelling cycles as in 2.2 have been used to evaluate the dependence of the equilibrium degree of swelling on the partial vapor pressure p/p_0 of the solvent. Assuming that the partial volumes of the polymer and of the solvent in the film are additive, the polymer fraction in a swollen film is straightforward to estimate as: $\phi_{pol} = h_{dr}/h_{sw}$, where h_{dr} and h_{sw} are the thicknesses of a dried film and of the respective film in a swollen state, respectively. 2.6 displays ϕ_{pol} (which is reversely proportional to the degree of swelling) versus p/p_0 for SB1 (2.6a) and SB2 (2.6b) films with different starting dry thickness h_{dr} . For both polymers the equilibrium polymer volume fraction in a film at a given vapor pressure becomes smaller as the film thickness h_{dr} decreases. This effect is summarized in 2.7, where ϕ_{pol} at $p/p_0 = 50\%$ is plotted versus film thicknesses h_{dr} reduced by the characteristic period of the structure in bulk. The data indicates that solvent uptake by several layers-thick block copolymer films decreases as the film thickness increases. We note that similar effect has been recently reported for the swelling behavior in a selective solvent of relatively thick films (up to 1 μm thick) of lamella-forming diblock copolymers;[39, 43] and this work excluded a substantial contribution of an excess solvent layer at the polymer-substrate interface to an enhanced swelling of ultrathin films.

The uptake of solvents for a given film thickness is remarkably different for the two polymers under study, although the chemical structure of the blocks

is the same. For example an 146 nm thick SB1 film takes up less solvent than an 170 nm thick film of SB2. Since the chemical nature of the blocks is the same, this indicates that the amount of segregation plays an important role and the stronger segregated SB2 polymer takes up more solvent. In strongly segregated block copolymers the polymer chains are highly stretched, which favors the incorporation of the solvent molecules both by stretched chains and by A-B interface. In this case the increased uptake of solvent would be a specific feature of block copolymers films. On the other side, a similar line of arguments could be held for the geometric constraints at the hard substrate boundary.

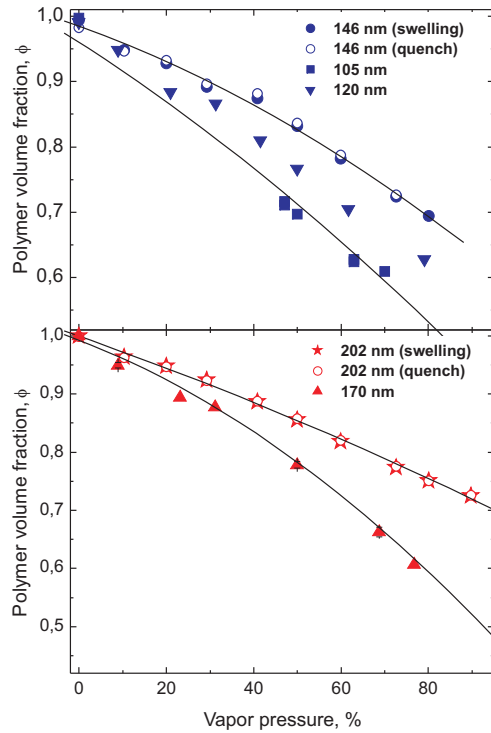


Figure 2.6: Polymer volume fraction $\phi = h_{dry}/h_{sw}$, in swollen SB1 (a) and SB2 (b) films with the indicated h_{dry} as a function of the partial chloroform vapor pressure p/p_0 .

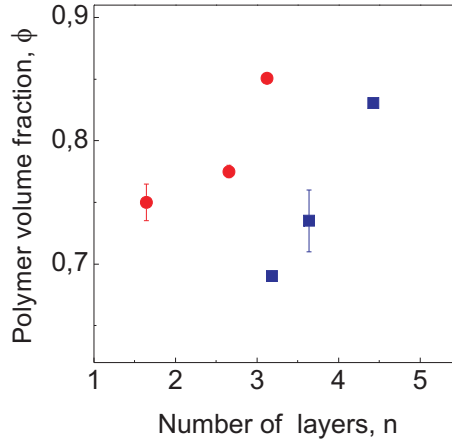


Figure 2.7: Polymer volume fraction $\phi = h_{dry}/h_{sw}$, in SB1 (squares) and SB2 (circles) films which have been equilibrated at 50% of the partial chloroform vapor pressure p/p_0 versus the number of layers (film thickness normalized by the respective a_0 in bulk).

2.4.2 Comparison of the Ellipsometric and SFM Thickness Measurements

Long-term equilibration of block copolymer films under solvent vapor is aimed at achieving thermal equilibrium of the microphase separated structures, and is typically accompanied by the development of the topographic features at the substrate (terrace formation). The lateral dimensions of the terraces range from several to tens of μm , both in the swollen [36] and in the dry state (2.8). We note that terrace formation is most pronounced at high vapor pressure conditions and for low molecular weight sample, i.e. strongly depend on the chain mobility. For SB1(SB2) films thicker than 200(100)nm we did not observe surface relief structures even upon long-term equilibration.

The absolute and relative terrace heights are determined with SFM, while the thickness of the swollen film is typically accessed with large-space averaging techniques, such as ellipsometry. We took special care to evaluate a possible influence of the terracing-related surface roughness on the height determination with *in-situ* ellipsometry. The strategy was to quantify the areal coverage of the terraces in quenched samples with optical microscopy, then

to measure the relative height difference between the terraces with Metrology SFM, and finally to compare ellipsometric heights with those evaluated by the combined SFM-optical microscopy analysis.

2.8 displays an optical micrograph of solvent-annealed SB1 film supported by reflective substrate. Two distinct colors in the optical image correspond to the coexistence of terraces with i and $(i+1)$ number of layers and hence with a well defined local film thickness. [35] In order to determine the *fraction of the higher terrace* $i + 1$, denoted as β_{i+1} , an optical image was analyzed with the software KS 100 3.0 which counts the intensity of red, green and blue colors in gray scale of the optical micrograph (with 0 representing the darkest(highest) and 255 corresponding to the brightest(lowest) color(thickness)). In the case of two terraces, two distinct maxima appear on the resulting curve (2.8, bottom). The maximum at lower values corresponds to darker color in optical micrograph and hence to the higher terrace ($i + 1$). The relative area of the maxima represents the relative terrace distribution. Next, the cumulative sum $\beta_{i+1} + \beta_i$ was normalized to 100% for the hole range of the grayscale. The value of the cumulative sum at the minimum between the two maxima gives the β_{i+1} .

Ellipsometric data for swollen thickness of SB films with both macroscopically smooth and topographically structured (due to terrace formation) surfaces can be precisely fitted with the Cauchy model (2.9). We recall that ellipsometry measures the ratio of the p and s components of the zero-order reflection coefficient $\rho = R_{p0}/R_{s0} = \text{Tan}\psi \cdot e^{j\Delta}$. In so-called scalar approach, [47] the reflections from adjacent areas of topographically structured surfaces sum coherently. The total reflection coefficients are given by

$$R_{i0} = f_m r_{im} + f_e r_{ie} e^{-j2\gamma_0}$$

where $\gamma_0 = 2\pi \left(\frac{h_{sw}}{\lambda_0} \right) \cos\varphi$; r_{im}, r_{ie} are the reflection coefficients for each area, φ - angle of the incidence. Diffraction effects are completely ignored since the pattern dimensions are significantly larger than the optical wavelength. We note that the scalar analysis of ellipsometric data has been successfully used to determine in real time the etch depth in patterned semiconductor substrates. [47]

The above assumption that ellipsometric measurements provide a geomet-

ric average over the topographic features at the film surface, has been supported by the comparison of the ellipsometry and AFM height measurements. 2.10 displays a diagram of the equilibrium thicknesses (terrace heights) in a swollen state h_{sw_i} versus the volume fraction of SB1 in a film. Each set of data at a particular ϕ_{pol} belongs to different samples and represents direct ellipsometric data (circles) and the result of the fit of SFM measurements (dry thickness) with the volume fraction ϕ_{pol} .

The SFM heights of adjacent terraces h_{sw_i} and $h_{sw_{(i+1)}}$, together with the evaluated terrace ($i + 1$) fraction β was fitted in the swollen state was determined from the *in situ* ellipsometry measurements of the average swollen thickness h_{sw} and from the SFM-measured step height Δh_{SFM} between terraces h_i and h_{i+1} of the same sample in a quenched (dry) state. The following relation has been utilized: $h_{sw_{(i+1)}} = h_{sw} + \Delta h_{SFM} / \phi_{pol} \cdot \beta$.

2.10 displays a diagram of the equilibrium thicknesses (terraces) in a swollen state h_{sw_i} versus the volume fraction of SB1 in a film. Each set of data at a particular ϕ_{pol} belongs to different samples and represents the result of the comparison of the ellipsometric and SFM measurements. The data strongly suggests that ellipsometric measurements provide a geometric average over the topographic features at the film surface, and hence the formation of terraces does not affect the precision of the macroscopic thickness measurement by *in situ* ellipsometry.

2.4.3 Phase Behavior of Solvent-Annealed Films

Along with the topographic features, the morphological behavior in SB1 and SB2 films upon solvent annealing has been analyzed. A non-selective solvent acts as a plasticizer and effectively lowers the glass-transition temperature of the glassy components. As a result, the chain mobility in swollen films is considerably enhanced without a significant increase in the processing temperature. Additionally, the solvent affects polymer-polymer and polymer-surface interactions, thereby allowing the strength of the molecular interactions to be varied in a controlled way. Therefore, variation of the solvent amount in a film allows to tune the phase behavior of a block copolymer.

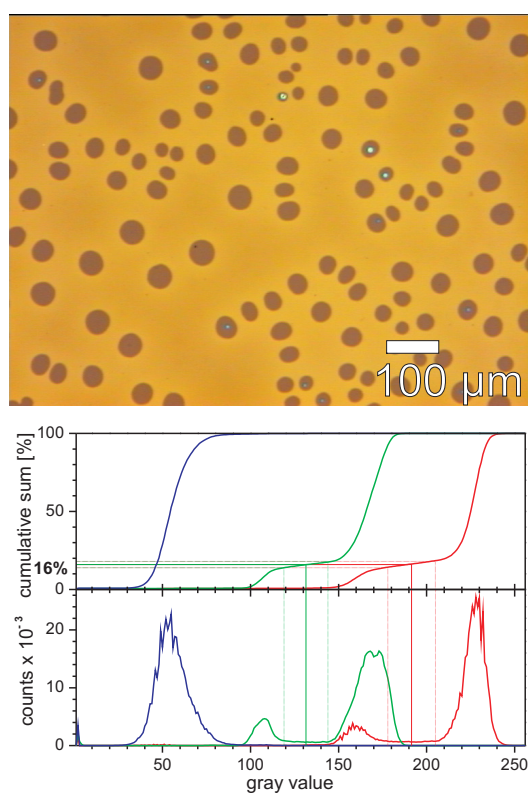


Figure 2.8: Top: Optical image of 64 *nm* thick SB1 film presenting terrace formation during the solvent annealing. Darker areas correspond to a higher terrace with two layers of cylinders. Bottom: Evaluation of the areal fraction of terraces using Zeiss-software.

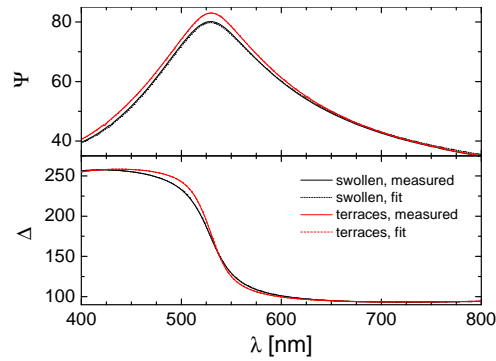


Figure 2.9: Ellipsometric spectral data for swollen smooth (black) and for topographically structured (red) films with corresponding fitting curves which confirm the validity of the Cauchy model in evaluation the thickness of topographically structured films.

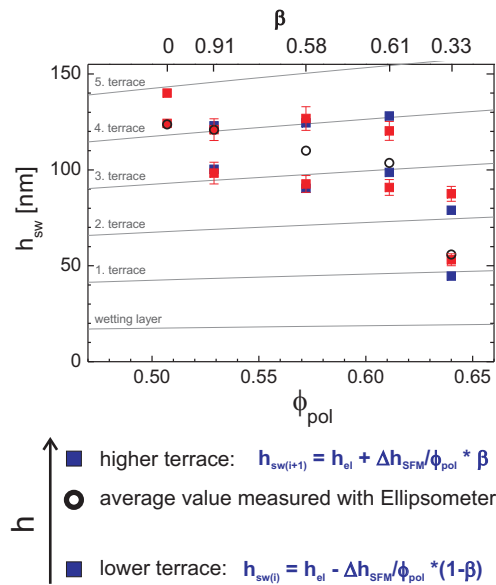


Figure 2.10: Diagram of the equilibrium thicknesses (terraces) in a swollen state h_{sw_i} versus the volume fraction of SB1 ϕ_{Pol} in a film. Each set of data at a particular ϕ_{pol} belongs to different samples with a volume fractions β of the higher terrace shown in the upper axis. The blue squares correspond to the values which have been evaluated according to the relations in the sketch below the figure. The red squares represent absolute terrace heights (measured with Metrology SFM) and divided by the polymer volume fraction ϕ_{pol} . The circles are the measured ellipsometric data. The gray lines

The morphology of swollen microphase separated structures was imaged by conventional SFM measurements of fast-quenched films. In our experiments, the quench to the glassy state of the polystyrene block has been achieved within tens of seconds, and has been shown not to alter the phase separation in a swollen state.[36]

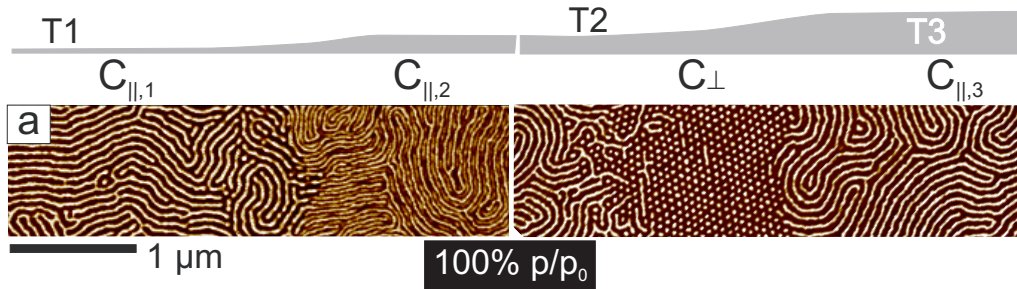


Figure 2.11: SFM phase images of the SB2 films swollen at p/p_0 of 100%. Surface structures show ordered microdomains with a thickness-dependent morphological behavior as the film thickness increases: within flat terraces the cylinders are aligned parallel to the film plane (C_{\parallel}) with vertical cylinders at transition regions between the terraces (C_{\perp}). Schematic of the crosssection introduces the mesoscale surface topography at imaged parts of the film.

Shown in 2.11 is a sequence of surface structures in SB2 films as a function of film thickness upon annealing in an atmosphere of 100% partial pressure of chloroform vapor p/p_0 . The sketch above the images illustrates the profile of the film thickness, increasing from left to right. At an equilibrated thickness, i.e. within flat terraces, the cylinders (white stripes) are aligned parallel to the film plane. Starting from the second layer, at transition thicknesses between the terraces a vertical orientation of cylinders is stabilized (hexagonally packed white dots). Such thickness-dependent phase behavior in block copolymer films is well-established experimentally and has been confirmed by computer simulations [48].

2.12a presents the surface structures in films of SB1 which have been exposed to a relative vapor pressure $p/p_0=72\%$. In this case, vertically oriented cylinders are absent at the free surface. Instead, the border between neighboring terraces is marked by an increased defect density within the ly-

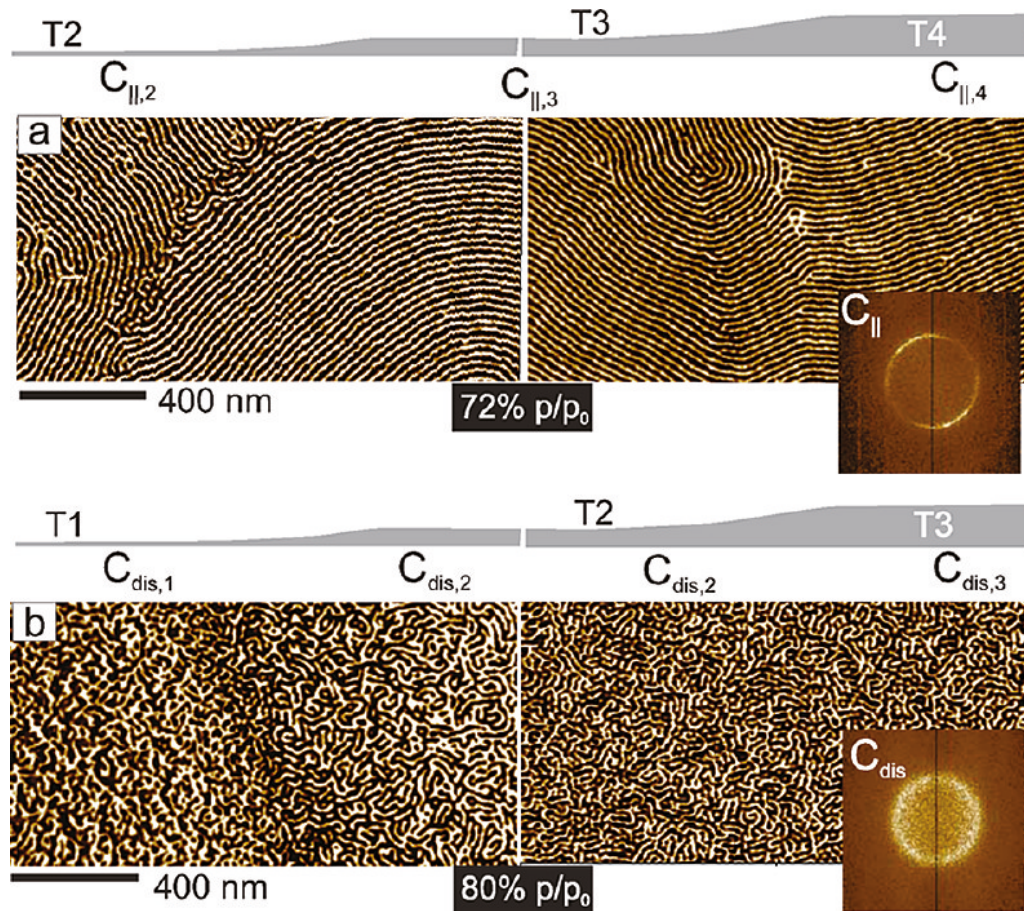


Figure 2.12: SFM phase images of the SB1 films swollen (a) at $p/p_0=72\%$ showing lying cylinders with a high degree of a long-range order, and (b) at $p/p_0=80\%$ presenting a phase-separated pattern with a low long-range order (a disordered cylinder phase). The insets below the SFM images are FFT of the respective surface patterns.

ing cylinders. [49] In comparison to the behavior of SB2 films at $p/p_0=100\%$ (2.11), the amount of long range order is significantly higher, although the polymer is equilibrated at much lower solvent vapor pressure. Despite the greater solvent content in SB2 films, the SB2 still has stronger segregation and lower chain mobility as compared to highly swollen SB1 films in 2.12a which causes the difference in the phase behavior and the degree of ordering of cylinder domains.

Shown in 2.12b are the surface structures in SB1 film after exposure to $p/p_0=80\%$. Although the surface topography clearly reveals macroscopic features (terraces), the in-plane order of the microdomains is dramatically reduced. The reduced order indicates the vicinity of the system to the ODT, meaning that the interface between two blocks in the swollen film is subjected to strong composition fluctuations. The intriguing observation is the development of terraces (i.e. layering of microdomains) in the swollen films which are very close to (if not above) the ODT. This observation presumably implicate a difference in ODT of the lateral and of the in-plane ordering of microdomains. We note that possible indications to this result have been reported on sphere-forming block copolymers [50].

The increase of solvent concentration in SB1 films upon raising the partial pressure of chloroform vapor and the related loss of the long-range order can be explained in terms of so called "dilution approximation" for the bulk block copolymer phases[51, 52, 53]. In this approximation the phase diagram of a block copolymer solution is obtained by rescaling χ_{AB} to $\phi_{pol} \chi_{AB}$ according to $\chi_{eff} \sim (\phi_P/T) N^{1/2}$, [54] where ϕ_{pol} is the polymer volume fraction or polymer concentration. Dilution of the film lowers χ_{eff} and shifts the ODT. Therefore, the microphase separated structures in swollen films can be used as a qualitative measure of the degree of swelling in block copolymer films. [36, 55]

Along the same line of argument, the difference in the microdomain morphology of SB1 and SB2 in swollen films can be explained by the two times higher χN parameter of SB2 as compared to that of SB1 (2.1). The essential differences in χN makes it difficult to maintain equal preparation conditions and thermodynamic parameters for comparing molecular architecture

or molecular weight effects on the phase behavior of block copolymers in films. Typically, diblock copolymers with a molecular weight of around 100 kg/mol show very limited mobility under elevated temperatures and even in strongly swollen films, while diblock copolymers of half the length show fast microdomain dynamics under the same conditions.

2.4.4 Mesoscale Swelling Inhomogeneity in Block Copolymer Films

2.13 shows an example of surface structures in SB1 film which has been equilibrated at $p/p_0=78\%$, i.e. slightly below the transition to the disordered cylinder pattern (2.12b). Depending on the local film thickness, terraces with one, two or three layers of cylinders are formed within one sample. The equilibrium heights of the terraces in quenched samples after annealing at $p/p_0=78\%$ are shown in 2.14a.

The degree of order of cylinder domains shows clear dependence on the terrace thickness. In the lowest terrace T1 with a thickness of 10 ± 2 nm, a disordered microphase separated pattern is formed (2.13). This kind of structure points to the vicinity to the ODT, similar to the result shown in 2.12b. Interestingly, the cylinder pattern within the same sample however at the region with a larger thickness of 44 ± 1 nm(terrace T3) exhibits a well equilibrated, cylindrical morphology with a long range order. This kind of well ordered stripped structure is formed in all thicker films at this annealing conditions. Accordingly, regions with a thickness of 27 ± 2 nm (terraces T2) show a cylinder pattern with a persistence length which is intermediate between that in terrace T1 and terrace T3. The 2D power spectral density profiles of the structures in each indicated terrace (2.14b) quantify the amount of segregation in the films and the characteristic dimensions of the microphase-separated patterns. In terrace T3 the spectrum exhibits a sharp first order peaks and also higher order peaks, while the spectrum for the first terrace shows a very broad first order peak, corresponding to a much weaker segregated system. The above observations suggest that the polymer volume fraction ϕ_{pol} is not uniform throughout the lateral dimension of the film, and

that the observed ϕ_i increases as the film becomes thicker.

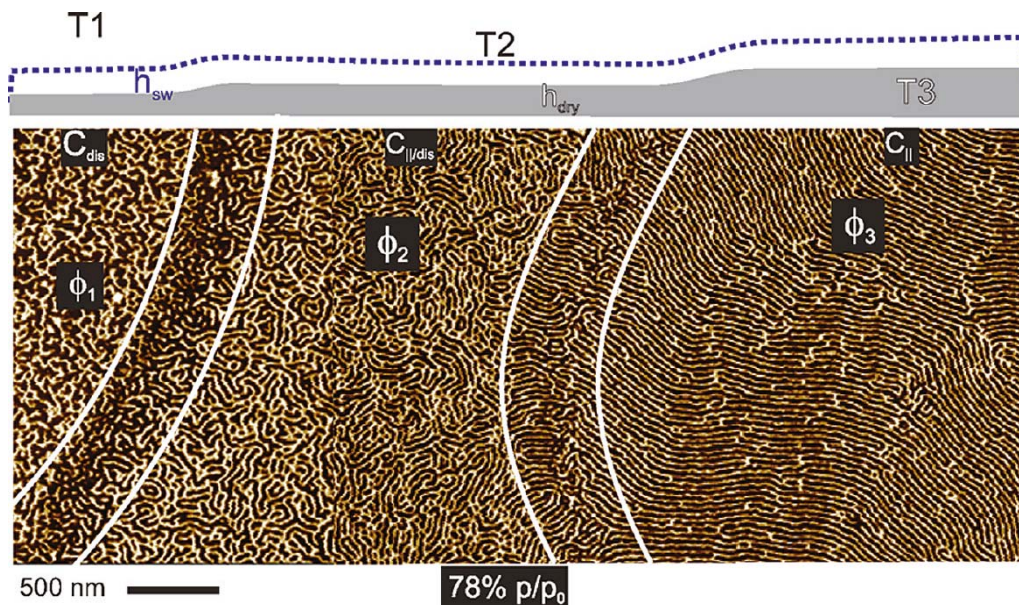


Figure 2.13: SFM phase images of SB1 films annealed at a chloroform partial vapor pressure of 78%. The sketch above the images illustrate the relative height distribution in the sample. The images present differences in the degree of long range order in the lower terrace (left part of the SFM images) and in the neighboring higher terraces.

It is important for the present discussion that the confinement effects on the swelling rates and on the absolute solvent uptake can not be attributed to the specific block copolymer molecular architecture. Similar results have been reported before for homopolymer films.[5, 9, 10, 6] Moreover, the diffusivity of solvent molecules into block copolymer films is described using the same theoretical approaches as it has been done for homopolymer systems.[5, 9] However, the analysis of the microphase separated structures in the annealed films provides new insights into the effect of confinement on the properties of polymers and other types of soft matter. In particular, the thickness-dependent swelling of structured block copolymer films can be understood in terms of the confinement-induced stretching of a cylinder cell perpendicular to the film plane. [45] In thin SB1 films at moderate concentrations, the lateral distances between next-nearest cylinders in the first layer have been

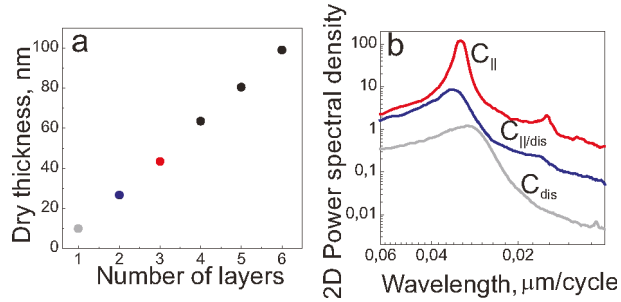


Figure 2.14: (a) Equilibrium thicknesses (terrace heights) in quenched SB1 films after annealing at a chloroform partial vapor pressure of 78%. (b) 2D power spectral density profiles of the SFM images from 2.13 representing terraces (from bottom to top) T1 (gray), T2 (blue) and T3 (red). The position and broadness of the picks, as well as the presence of the secondary picks quantify the characteristic dimensions and the long-range order of the microphase-separated patterns.

found to be 6% smaller than those in the bulk. The elastic energy of the distorted structures likely affects the polymer-solvent interactions and the resulting swelling behavior.

2.5 Conclusions

The swelling and the corresponding morphological behavior of cylinder-forming polystyrene-*b*-polybutadiene diblock copolymers in thin films have been studied by combined *in-situ* spectroscopic ellipsometry and SFM measurements. The confinement of the film and the presence of the interfaces leads to a more than 10% increase of the solvent up-take with decreasing film thickness. The sensitivity of the phase separated pattern towards the solvent concentration in a film has been used to diagnose the non-homogenous swelling of the block copolymer films on a mesoscopic scale. The cylinder domains within the first layer exhibit a low degree of a long-range order due to the vicinity to the order-disorder transition (ODT), in contrast to the cylinder domains in the neighboring terrace with two or three layers of structures. These results disclose newly observed nanoscale effects of the structure confinement on the

polymer-solvent interactions in thin films.

Acknowledgement. This work was carried out in the framework of the "Sonderforschungsbereich 481" (TP B7) funded by the German Science Foundation (DFG).

Bibliography

- [1] R. L. Jones, S. K. Kumar, D. L. Ho, R. M. Briber, and T. P. Russell, *Nature*, 1999, **400**(6740), 146.
- [2] G. Gauglitz, *Analytical and Bioanalytical Chemistry*, 2005, **381**(1), 141.
- [3] Y. Tang, J. R. Lu, A. L. Lewis, T. A. Vick, and P. W. Stratford, *Macromolecules*, 2002, **35**(10), 3955–3964.
- [4] K. Spaeth and G. Gauglitz, *Materials Science & Engineering, C: Biomimetic Materials, Sensors and Systems*, 1998, **C5**(3,4), 187.
- [5] B. D. Vogt, C. L. Soles, R. L. Jones, C.-Y. Wang, E. K. Lin, W.-l. Wu, S. K. Satija, D. L. Goldfarb, and M. Angelopoulos, *Langmuir*, 2004, **20**(13), 5285.
- [6] M. Mukherjee, A. Singh, J. Daillant, A. Menelle, and F. Cousin, *Macromolecules*, 2007, **40**(4), 1073–1080.
- [7] W.-L. Wu, W. J. Orts, C. J. Majkrzak, and D. L. Hunston, *Polymer Engineering & Science*, 1995, **35**(17), 1000–4.
- [8] W. Wang, K. Troll, G. Kaune, E. Metwalli, M. Ruderer, K. Skrabanja, A. Laschewsky, S. V. Roth, C. M. Papadakis, and P. Mueller-Buschbaum, *Macromolecules*, 2008, **41**(9), 3209–3218.
- [9] B. D. Vogt, C. L. Soles, H. J. Lee, E. K. Lin, and W. Wu, *Polymer*, 2005, **46**(5), 1635.
- [10] M. H. Mondal, M. Mukherjee, K. Kawashima, K. Nishida, and T. Kanaya, *Macromolecules*, 2009, **42**(3), 732.

- [11] K. Manoli, D. Goustouridis, S. Chatzandroulis, I. Raptis, E. S. Valamontes, and M. Sanopoulou, *Polymer*, 2006, **47**(17), 6117.
- [12] B. D. Vogt, C. L. Soles, H. J. Lee, E. K. Lin, and W. Wu, *Langmuir*, 2004, **20**(4), 1453.
- [13] A. Karul, K. T. Tan, C. C. White, D. L. Hunston, S. T. Marshall, B. Akgun, S. K. Satija, C. L. Soles, and B. D. Vogt, *Polymer*, 2009, **50**, 3234.
- [14] V. B. D., P. V. M., S. C. L., S. S. K., L. E. K., and W. W.-L., *Langmuir*, 2005, **21**, 2460.
- [15] R. L. Thompson, M. T. McDonald, J. T. Lenthall, and L. R. Hutchings, *Macromolecules*, 2005, **38**(10), 4339.
- [16] R. Levicky, N. Koneripalli, M. Tirrell, J. F. Ankner, H. Kaiser, and S. K. Satija, *Macromolecules*, 1998, **31**(15), 4908–4914.
- [17] D. R. Barbero and U. Steiner, *Physical Review Letters*, 2009, **102**(24), 248303.
- [18] J. Perlich, V. Koerstgens, E. Metwalli, L. Schulz, R. Georgii, and P. Mueller-Buschbaum, *Macromolecules*, 2009, **42**(1), 337.
- [19] I. W. Hamley, J. P. A. Fairclough, A. J. Ryan, C. Y. Ryu, T. P. Lodge, A. J. Gleeson, and J. S. Pedersen, *Macromolecules*, 1998, **31**(4), 1188.
- [20] P. Alexandridis and R. J. Spontak, *Current Opinion in Colloid & Interface Science*, 1999, **4**(2), 130.
- [21] L. C., R. W. B., and R. R. A., *Macromolecules*, 2002, **35**, 4044.
- [22] K. S. H., M. M. J., and R. T. P., *Adv. Mater.*, 2004, **16**, 2119.
- [23] K. A., T. L., and K. G., *Nano Lett.*, 2007, **7**, 843.
- [24] J. Y. S. and R. C. A., *Adv. Mater.*, 2009, **21**, 2540.

- [25] E. H., F. K., S. R., S. G., M. R., and K. G., *Macromolecules*, 1999, **32**, 1204.
- [26] K. A., M. R., and K. G., *J. Chem. Phys.*, 2004, **120**, 1105.
- [27] T. I., K. R., B. Y., S. D., S. A., M. S., and S. M., *Macromolecules*, 2005, **38**, 507.
- [28] C. K. A., B. K. J., and R. T. P., *Polymer*, 2005, **46**, 11635.
- [29] B. P., P. D., S. D.-M., R. B., K. F., and P. C. M., *Macromolecules*, 2003, **36**, 8717.
- [30] K. S., M. M., X. T., K. M., and R. T., *Adv. Mater.*, 2004, **16**, 226.
- [31] D. R. C., P. C., T. E. L., and L. B., *Nature*, 2000, **405**, 433.
- [32] F. K., E. H., M. R., and K. G., *Macromolecules*, 2000, **33**, 947.
- [33] J. Yoon, W. Lee, and E. L. Thomas, *Advanced Materials*, 2006, **18**(20), 2691.
- [34] B. J., K. B. J., S. G. E., R. T. P., L. X., W. J., K. E. J., and H. C. J., *Macromolecules*, 2007, **40**, 7019.
- [35] L. Tsarkova, A. Knoll, G. Krausch, and R. Magerle, *Macromolecules*, 2006, **39**, 3608.
- [36] A. Knoll, R. Magerle, and G. Krausch, *Journal of Chemical Physics*, 2004, **120**(2), 1105.
- [37] L. Tsarkova in *Nanostructured Soft Matter: Experiment, Theory, Simulation and Perspectives*, ed. A. V. Zvelindovsky; Springer, Heidelberg, 2007; p. 231.
- [38] H. Elbs and G. Krausch, *Polymer*, 2004, **45**(23), 7935–7942.
- [39] O. V., T. L., and B. A., *Soft Matter*, 2009, **5**, 812.
- [40] O. V., H. M., K. V., S. S., T. L., and B. A., *ACS Nano*, 2009, **3**, 1091.

- [41] H. S., S. M., C. A., K. G., S. U., and T. M., *Soft Matter*, 2009, **5**, 4206.
- [42] C. M. Papadakis, Z. Di, D. Posselt, and D. M. Smilgies, *Langmuir*, 2008, **24**(24), 13815.
- [43] J. Gensel, C. Liedel, H. G. Schoberth, and L. Tsarkova, *Soft Matter*, 2009.
- [44] ed. J. Brandrup, E. H. Immergut, and E. A. Grulke, *Polymer handbook*, 4th ed., J. Willey & Sons, New York, 1999.
- [45] A. Knoll, L. Tsarkova, and G. Krausch, *Nano Letters*, 2007, **7**(3), 843.
- [46] J. Crank, *The Mathematics of Diffusion*, Oxford Univ. Press, Oxford, 2005.
- [47] C. S., S. P., I. N., H. C., and J. B., *Thin Solid Films*, 2004, **455**, 645.
- [48] A. Knoll, A. Horvat, K. S. Lyakhova, G. Krausch, G. J. A. Sevink, A. V. Zvelindovsky, and R. Magerle, *Physical Review Letters*, 2002, **89**(3), 035501.
- [49] H. A., S. G. J. A., Z. A. V., K. A., and T. L., *ACS Nano*, 2008, **2**, 1143.
- [50] Y. H., M. T. E., and K. E. J., *Macromolecules*, 2000, **33**, 1888.
- [51] E. Helfand and Y. Tangami, *J. Phys. Chem.*, 1972, **56**, 3592.
- [52] G. H. Fredrickson and L. Leibler, *Macromolecules*, 1989, **22**, 1238.
- [53] T. P. Lodge, K. J. Hanley, B. Pudil, and V. Alahapperuma, *Macromolecules*, 2003, **36**(3), 816.
- [54] K. Mori, H. Hasegawa, and T. Hashimoto, *Polymer*, 2001, **42**, 3009.
- [55] L. Tsarkova, G. J. A. Sevink, and G. Krausch, *Adv. Polym. Sci.*, 2010.

Chapter 3

Selfdiffusion and Cooperative Diffusion in Semidilute Polymer Solutions as measured by Fluorescence Correlation Spectroscopy

Ute Zettl¹, Sebastian T. Hoffmann¹, Felix Koberling², Georg Krausch³,
Joerg Enderlein⁴, Ludger Harnau⁵ and Matthias Ballauff¹ *

¹Physikalische Chemie I, University of Bayreuth, D-95440 Bayreuth,
Germany

²Picoquant GmbH, D-12489 Berlin, Germany

³University of Mainz, Germany

⁴3. Institute of Physics, Georg August University, D-37077 Goettingen,
Germany

⁵Max-Planck-Institut fuer Metallforschung, Heisenbergstr. 3, D-70569
Stuttgart, Germany,

and Institut fuer Theoretische und Angewandte Physik, Universitaet
Stuttgart, Pfaffenwaldring 57, D-70569 Stuttgart, Germany

Published in *Macromolecules*, **2009**, *42* (24), pp 9537–9547.

3.1 Abstract

We present a comprehensive investigation of polymer diffusion in the semidilute regime by fluorescence correlation spectroscopy (FCS) and dynamic light scattering (DLS). Using single-labeled polystyrene chains, FCS leads to the selfdiffusion coefficient while DLS gives the cooperative diffusion coefficient for exactly the same molecular weights and concentrations. Using FCS we observe a new fast mode in the semidilute entangled concentration regime beyond the slower mode which is due to selfdiffusion. Comparison of FCS data with data obtained by DLS on the same polymers shows that the second mode observed in FCS is identical to the cooperative diffusion coefficient measured with DLS. An in-depth analysis and a comparison with current theoretical models demonstrates that the new cooperative mode observed in FCS is due to the effective long-range interaction of the chains through the transient entanglement network.

3.2 Introduction

Diffusion in polymer solutions is among the oldest subjects of polymer physics. [1, 2] In general, transport by diffusion can be characterized by two diffusion coefficients: the selfdiffusion coefficient D_s and the cooperative diffusion coefficient D_c . D_s describes the motion of one molecule relative to the surrounding molecules due to thermal motions while D_c describes the motion of a number of molecules in a density gradient. [3, 4, 5, 6, 7] The obvious importance of diffusion in polymer physics has led to a rather large number of studies of D_c by dynamic light scattering (DLS), [3, 4, 8, 6, 7, 8, 5] while D_s can be obtained by pulsed-field gradient nuclear magnetic resonance [4, 7, 5] and label techniques like forced Rayleigh scattering [9] or fluorescence correlation spectroscopy (FCS). [10, 11, 12] However, in many cases D_s and D_c could not be obtained for the same homopolymer using the same technique. Such measurements would be very interesting since a central problem in the dynamics of semidilute entangled polymer solutions is the quantitative understanding of the interplay of selfdiffusion and cooperative diffusion. Very

recently it has been found theoretically that the coupling of self- and cooperative motion due to topological constraints is also important for rather stiff macromolecules. [13]

At present, DLS is certainly among the most accurate methods to measure D_c and there is a number of careful studies conducted on polymer solutions. In principle, FCS is the method of choice for studying diffusion of single macromolecules in a matrix of same molecular weight giving D_s or in a solution of polymers of different molecular weight (tracer diffusion [14, 15, 16]). In opposite to DLS, FCS requires chains labeled by a stable fluorescing molecule. Moreover, the number of labels per macromolecules should be constant to arrive at results that can be directly compared to theory. Given these problems, the use of FCS for measurements of D_s on synthetic polymers has been scarce so far. [10, 11, 12, 17] Moreover, the full potential of this method has not yet fully been exploited yet since FCS should also allow one to obtain D_c . [18, 19]

Recently, a well-defined polymeric model system has been presented and used for quantitative FCS-measurements in dilute solution [10, 12]: Nearly monodisperse polystyrene chains have been prepared by anionic polymerization and subsequently labeled by single fluorescent dye. Since the molecular weight of the different samples span a wide range, these polymers provide a nearly ideal model system for exploring the chain dynamics over a wide range of molecular weights and concentrations. Using these labeled chains we recently presented an in-depth study of the experimental FCS set-up [10] as well as of the dynamics in dilute solution. [12]

Here we pursue these studies further by presenting an investigation of polymer diffusion in the semi-concentrated regime by FCS. In order to obtain accurate data of cooperative diffusion, these studies are combine with DLS-measurements on exactly the same molecular weights and concentrations. Thus, D_c and D_s can now be obtained from identical systems and directly be compared. In the course of these studies we found that a second cooperative mode becomes visible in the FCS-experiments if the concentration exceeds a given value. This surprising finding prompted us to conduct a full theoretical analysis of both the FCS- as well of the DLS-data throughout the entire time

scale and range of concentrations available by these experiments. In doing so we extend the theoretical modeling beyond the usual scaling laws. The entire study is devoted to a comprehensive understanding of polymer dynamics in solution ranging from the dilute state up to the onset of glassy dynamics.

The paper is organized as follows: After the Section Experimental we first present the FCS-data together with the finding of the new cooperative diffusion. In the subsequent section a quantitative modeling of the data in terms of an analytical theory will be given. In the last section special attention will be paid to possible practical applications of these findings to the spinning of nanofibers. A Conclusion will wrap up the entire discussion.

3.3 Experimental Section

3.3.1 Dye Labeled Polystyrene

All experiments reported here were carried out with linear polystyrenes having a narrow molecular weight distribution. For details of the synthesis see ref [10]. The molecular weight and polydispersity of the polymers are summarized in Table 3.1. The solutions for the FCS experiments were prepared in toluene p. a. grade by blending a constant concentration of 10^{-8} M Rhodamine B labeled polystyrene with varying amounts of unlabeled polystyrene from the same synthesis batch. Each labeled polymer carries only one dye molecule at one of its ends. To verify our results, additional solutions were prepared with varying labeled polystyrene and a constant amount of unlabeled polystyrene. We have used preparative gel permeation chromatography to separate labeled polymer and free dye molecules. [10, 12] Therefore, the resulting dye-labeled polymer does not contain any measurable amount of free dye molecules.

3.3.2 Methods

For FCS measurements we modified the commercial ConfoCor2 setup (Carl Zeiss, Jena, Germany) [21] with a $40\times$ Plan Neofluar objective (numerical

Table 3.1: Molecular weight M_w , polydispersity index $\text{PDI}=M_w/M_n$ and hydrodynamic radius R_h at infinite dilution of the polystyrenes used in the present study. The second and the third virial coefficients A_2 and A_3 , respectively, have been calculated using scaling laws taken from the literature (A_2 : ref [20] and A_3 : ref [8]). c^+ is the concentration at which the second diffusion time appears in the FCS measurements.

$M_w[\frac{kg}{Mol}]$	PDI	$R_h[nm]$	$A_2[\frac{cm^3 Mol}{g^2}]$	$A_3[\frac{cm^6 Mol}{g^3}]$	$c^+[\text{wt}\%]$
11.5	1.03	1.(4)	$7.4 \cdot 10^{-4}$	$2.1 \cdot 10^{-3}$	-
17.3	1.03	1.(6)	$6.8 \cdot 10^{-4}$	$2.6 \cdot 10^{-3}$	-
67.0	1.05	3.(9)	$5.1 \cdot 10^{-4}$	$5.8 \cdot 10^{-3}$	20
264	1.02	7.(3)	$3.8 \cdot 10^{-4}$	$1.3 \cdot 10^{-2}$	6.5
515	1.09	9.(8)	$3.3 \cdot 10^{-4}$	$1.9 \cdot 10^{-2}$	4.8

aperture $\text{NA}=0.9$). The Rhodamine B labeled PS-chains were excited by a HeNe-Ion laser at 543 nm. The intensity for all measurements was $4\mu\text{W}$ in sample space. As second setup we used a MicroTime200 (PicoQuant, Berlin, Germany) [22] with a $100\times$ oil immersion objective ($\text{NA}=1.45$). Here the detection beam path was divided by a 50/50 beam splitter on two detectors to crosscorrelate the signals. This crosscorrelation is necessary to prevent distortion of the fluorescence correlation function by detector afterpulsing. [23] For details of the FCS-measurements see refs [21, 10, 12].

Cooperative diffusion coefficients D_c were measured by DLS using an ALV 4000 light scattering goniometer (Peter, Germany).

3.3.3 Evaluation of Data

In FCS [24, 21] a laser beam is focused by an objective with high numerical aperture (typically ≥ 0.9) and excites fluorescent molecules entering the illuminated observation volume. The emitted fluorescent light is collected by the same optics and separated from scattered light by a dichroic mirror. The emitted light is detected by an avalanche photo diode. The time dependent intensity fluctuations $\delta I(\tau) = I(\tau) - \langle I(\tau) \rangle$ are analyzed by an autocorrelation function, where $\langle \rangle$ denotes an ensemble average. This autocorrelation

function can be written as [18]

$$G(\tau) = \frac{1}{N} \int d\mathbf{q} \Omega(\mathbf{q}) C(\mathbf{q}, \tau) \quad (3.1)$$

where $\Omega(\mathbf{q}) = \pi^{-\frac{3}{2}} w_{x,y}^2 w_z \exp(-w_{x,y}^2 (q_x^2 + q_y^2)/4 - w_z^2 q_z^2/4)$ is a Gaussian filter function characterizing the observation volume in Fourier space with $\int d\mathbf{q} \Omega(\mathbf{q}) = 1$, N is the average number of fluorescently labeled molecules in the observation volume, and $\mathbf{q} = (q_x, q_y, q_z)$. Here $w_{x,y} = 296$ nm is the dimension of the observation volume perpendicular to the optical axis and $w_z = 8w_{x,y}$ is the dimension along the optical axis. [10, 12] For an ideal gas consisting of non-interacting molecules the initial amplitude reduces to the familiar relationship $G(0) = 1/N$. [21]

The time-dependent fluorescence density-density autocorrelation function $C(\mathbf{q}, \tau)$ is expressed in terms of a coupled-mode model [25, 26] as

$$C(\mathbf{q}, \tau) = \frac{C_c(q, 0) e^{-q^2 \phi_c(\tau)/6} + C_s(q, 0) e^{-q^2 \phi_s(\tau)/6}}{C_c(q, 0) + C_s(q, 0)} \quad (3.2)$$

where $q = |\mathbf{q}|$. Here the mean square displacements $\phi_c(\tau)$ and $\phi_s(\tau)$ are given by

$$\phi_c(\tau) = 6D_c\tau, \quad (3.3)$$

$$\phi_s(\tau) = 6D_s\tau + B_s(\tau). \quad (3.4)$$

The term $B_s(\tau)$ allows one to take into account the contributions from internal polymer chain motions. [2] If only a few of the molecules are fluorescently labeled, the selfdiffusion coefficient D_s can be measured in the FCS experiment. [12] If all of the molecules are fluorescently labeled, the cooperative diffusion coefficient D_c can be obtained. [19] In the case that neither of these limits applies, both the self mode and the cooperative mode will be present in the spectrum of the autocorrelation function. The diffusion coefficients

can be extracted by fitting

$$G(\tau) = \sum_{i \in \{s,c\}} G_i(0) \left(1 + \frac{2\phi_i(\tau)}{3w_{x,y}^2}\right)^{-1} \left(1 + \frac{2\phi_i(\tau)}{3w_z^2}\right)^{-1/2} \quad (3.5)$$

to the experimental data. FCS is not only sensitive to intensity fluctuations due to the motion of labeled molecules but also due to photokinetic processes of the fluorescent dyes which occur for short times $\tau \lesssim 5 \times 10^{-3}$ ms. This additional relaxation has been taken into account as discussed in ref [10, 27, 12].

DLS allows one to measure the time dependent autocorrelation function of the scattered electric field which can be expressed in terms of the elements of the fluid polarizability tensor. [8] For an incident light wave traveling in the x direction with a polarization vector in the z direction the intensity of the scattered electric field can be written as

$$I_{VV}(\mathbf{q}, \tau) \sim \int d\mathbf{r} d\mathbf{r}' \langle \alpha_{zz}(\mathbf{r} + \mathbf{r}', \tau) \alpha_{zz}(\mathbf{r}', 0) \rangle e^{i\mathbf{q}\cdot\mathbf{r}}, \quad (3.6)$$

where the absolute value of the scattering vector \mathbf{q} is given by $q = |\mathbf{q}| = (4\pi n/\lambda) \sin(\theta/2)$ in which n is the refractive index of the medium. λ is the incident wavelength and θ is the scattering angle. The zz element of the fluid polarizability tensor is denoted as $\alpha_{zz}(\mathbf{r}, \tau)$. The experimentally accessible quantity is the intensity autocorrelation function $g_{VV}^{(2)}(\mathbf{q}, \tau)$. For photon counts obeying Gaussian statistics, the intensity autocorrelation function is related to the electric field autocorrelation function $g_{VV}^{(1)}(\mathbf{q}, \tau)$ according to

$$g_{VV}^{(2)}(\mathbf{q}, \tau) = 1 + f_{VV} \left(g_{VV}^{(1)}(\mathbf{q}, \tau) \right)^2, \quad (3.7)$$

where f_{VV} is dependent on the scattering geometry. The electric field correlation function can be calculated for various systems. For a solution contain-

ing purely diffusing particles the electric field correlation function is given by $g_{VV}^{(1)}(q, \tau) = \exp(-q^2 D_c \tau) / \sqrt{f_{VV}}$.

3.4 Diffusion Coefficients Measured by FCS

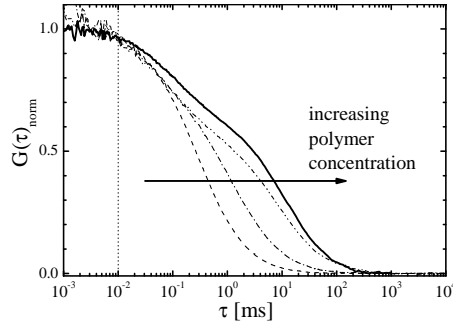


Figure 3.1: Normalized autocorrelation function obtained from FCS for polystyrene of molecular weight $M_w = 67$ kg/Mol in toluene for various polymer concentrations: 0.03 wt% (---), 9.1 wt% (- ·), 20 wt% (- · ·) and 28 wt% (—). A second diffusion time appears at 20 wt% on a shorter timescale compared to selfdiffusion. The thick solid line is the normalized crosscorrelation curve without detector afterpulsing for the 28 wt% polymer solution. The dotted vertical line marks the time scale above which this artefact becomes negligible, i.e., the solid thin and thick lines coincide for $\tau > 0.01$ ms.

Figure 3.1 shows normalized autocorrelation functions measured by FCS. The average number of labeled polymers in the observation volume was kept constant to $N \approx 0.8$ whereas the number of unlabeled polymers increases up to $N_u = 3 \times 10^6$ for the 28 wt % polymer solution. The thin broken curves are measured at the ConfoCor2 setup and the thick solid curve is measured at the MicroTime200 setup. The curves obtained at the ConfoCor2 setup have an additional decay on the time scale less than $10 \mu s$. This additional decay belongs to detector afterpulsing. Hence, the evaluation of the correlation curves has been done only for $\tau \geq 10 \mu s$ as indicated by the dotted line in Figure 3.1. For low polymer concentrations we obtained correlation curves with a single diffusion time. With increasing polymer concentration the correlation curves shift to higher diffusion times.

As an entirely new finding, Figure 3.1 presents a new mode related to a second diffusion time measured with FCS at higher polymer concentrations. This second diffusion time appears at shorter time scales than the one related to selfdiffusion. The concentration c^+ at which the second diffusion time is detected depends on the molecular weight: The higher the molecular weight, the lower is c^+ (see Table 3.1). In general c^+ is about $15\times$ the overlap concentration determined in an earlier study. [12] For the concentration c^+ the ratio between these two diffusion times is in the range of 60. From both diffusion times we calculated the diffusion coefficients from the relations given above.

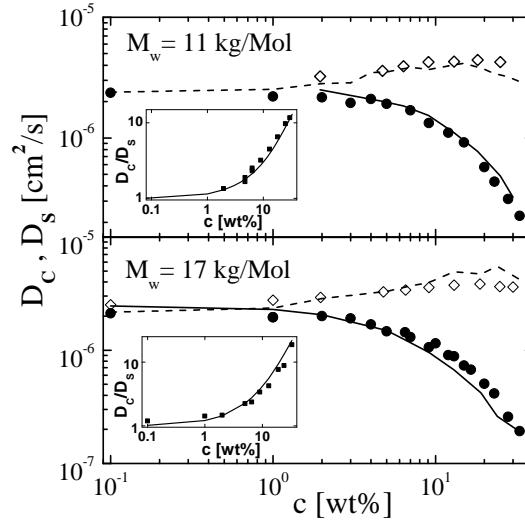


Figure 3.2: Comparison of selfdiffusion coefficients (D_s , ●) with cooperative diffusion coefficients (D_c , ◇) for different molecular weights: $M_w = 11$ and 17 kg/Mol (top and bottom). Open and solid symbols refer to DLS and FCS measurements, respectively. The solid lines represent D_s calculated according to eq 3.8 with D_c as input from DLS measurements. The dashed lines represent D_c calculated vice versa, i.e., with D_s as input from FCS experiments. Insets: Measured ratio D_c/D_s (symbols) together with the corresponding ratio obtained from eqs 3.8 and 3.9 within a third order virial approximation (see Table 3.1).

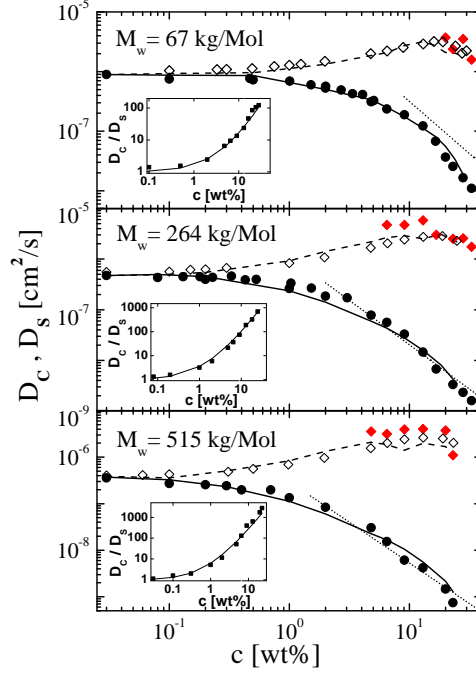


Figure 3.3: Comparison of selfdiffusion coefficients (D_s , ●) with cooperative diffusion coefficients (D_c , ◆, ◇) for different molecular weights: $M_w = 67, 264$ and 515 kg/Mol (from top to bottom). Open and solid symbols refer to DLS and FCS measurements, respectively. The solid lines represent D_s calculated according to eq 3.8 with D_c as input from DLS measurements. The dashed lines represent D_c calculated vice versa, i.e., with D_s as input from FCS experiments. For comparison the dotted lines represents the scaling prediction $D_s \sim M_w^{-2} c^{-7/4}$ for long polymer chains in the semidilute entangled regime (see eq 3.12). Insets: Measured ratio D_c/D_s (symbols) together with the corresponding ratio obtained from eqs 3.8 and 3.9 within a third order virial approximation (see Table 3.1).

In Figures 3.2 and 3.3 all diffusion coefficients measured with FCS and DLS are compared at identical conditions. At infinite dilution both diffusion coefficients D_s and D_c have the same value. In dilute solutions D_s and D_c show a linear dependency on the concentration as expected according to the Kirkwood-Riseman theory. [28] But D_s decreases whereas D_c increases with increasing polymer concentration. The decrease of D_s is due to the friction between the chains and the increase of D_c is due to the increasing osmotic pressure. [3, 29] At high concentrations D_c exhibits a maximum.

The insets in Figure 3.2 and Figure 3.3 show the ratio D_c/D_s of measured values. The lines are theoretical values calculated according to [5, 7]

$$\frac{D_c}{D_s} = (1 - \bar{v}c) \frac{d\Pi}{dc} \quad (3.8)$$

with the partial specific volume of the polymer \bar{v} and the polymer concentration c . The dependence of the osmotic pressure on c can be approximated by a virial expansion

$$\frac{d\Pi}{dc} = 1 + 2A_2M_w c + 3A_3M_w c^2 + \dots, \quad (3.9)$$

where A_2 and A_3 are the second and third virial coefficients, respectively, and M_w is the molecular weight. For the calculation of $d\Pi/dc$ we used the corresponding values from the literature gathered in Table 3.1 and $\bar{v} = 0.916 \text{ cm}^3/\text{g}$. [30] The measured and the calculated ratio are well described as demonstrated by the inset of Figures 3.2 and 3.3. The selfdiffusion coefficients D_s can be determined from the cooperative diffusion coefficient D_c obtained by DLS measurements and vice versa. D_s and D_c can be measured with high accuracy by FCS and DLS using the same polymers. Their relation is fully understood in terms of eq 3.8. For comparison we note that both the molecular dye diffusion coefficient and the macromolecular tracer diffusion coefficient decrease with increasing concentration of the matrix polymer. [16]

Figure 3.4 displays the amplitudes $G_i(0)$ (see eq 3.5) as a function of N for polystyrene with $M_w = 67 \text{ kg/Mol}$ at 20 wt%. The amplitude of the selfdiffusion mode $G_s(0)$ is proportional to $1/N$. In the presence of non-

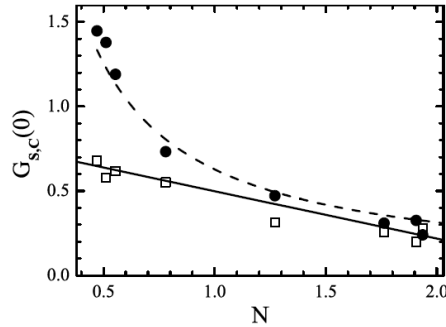


Figure 3.4: Amplitudes $G_s(0)$ (●) and $G_c(0)$ (□) extrapolated from the measured FCS-autocorrelation function $G(\tau)$ as a function of labeled molecules N for polystyrene with $M_w = 67$ kg/Mol at 20 wt%. For the selfdiffusion $G_s(0) \propto 1/N$ (---), while $G_c(0)$ exhibits a linear dependence on N (—) for the cooperative diffusion.

correlated background signal (scattering, afterpulsing, electronic noise) this is modified to $1/N - 2b/N^2$. [21] Here b is proportional to the noise intensity, which is assumed to be significantly smaller than the fluorescence signal. For the cooperative mode one finds an amplitude scaling of $1 - 2bN$. For sufficiently small b , this will yield a dependence as shown by Figure 3.4 for the fast correlation component.

The ratio $G_c(0)/G(0)$ is a non-monotonic function of the concentration for a fixed number of labeled molecules N . It increases from 0 to a value below 1 at the concentration c^+ . $G_c(0)/G(0)$ slightly decreases upon further increasing the concentration in the semidilute entangled regime. Finally, it increases upon approaching the glass transition concentration.

3.5 Scaling Theory and Langevin Equation Approach

In the following, the findings presented in the previous sections will be compared to current models of polymer diffusion.

3.5.1 Scaling Theory and Reptation Model

The application of scaling theory and the reptation model to polymer solutions has been presented in various treatises (see, e.g., refs [1, 2, 31, 32]). Hence, we only discuss the equations necessary for this study. Three concentration regimes can be distinguished: dilute, semidilute unentangled, and semidilute entangled solutions. Scaling arguments and the reptation model lead to following relations for the selfdiffusion coefficient D_s and the cooperative diffusion coefficient D_c :

$$D_s = D_c \sim M_w^{-3/5} c^0, \quad c \ll c^*, \quad (3.10)$$

$$D_c \sim M_w^0 c^{3/4}, \quad c > c^*, \quad (3.11)$$

$$D_s \sim M_w^{-2} c^{-7/4}, \quad c > c^{**}. \quad (3.12)$$

Here the overlap concentration c^* is the boundary concentration between the dilute and semidilute regimes. This concentration depends on molecular weight as

$$c^* \sim M_w^{1-3\nu} = M_w^{-4/5}, \quad (3.13)$$

where the Flory exponent $\nu = 3/5$ for a good solvent has been used. The crossover concentration from the semidilute unentangled to the semidilute entangled regime is denoted as c^{**} .

For very low concentrations in the dilute regime, the selfdiffusion coefficient is indistinguishable from the cooperative diffusion coefficient as is apparent from Figures 3.2 and 3.3. In Figure 3.5 the selfdiffusion coefficient is plotted as a function of the molecular weight M_w for a fixed concentration $c = 9.1$ wt %. The experimental data (solid squares) follow the scaling laws given by eq 3.10 (dashed line) and eq 3.12 (solid line) for $M_w \leq 20$ kg/Mol and $M_w \geq 264$ kg/Mol, respectively. Moreover, D_s is rather independent of concentration for $c \lesssim 10$ wt % in the case of the low molecular weight solution (see Figure 3.2 and eq 3.10). The concentration dependence of D_s of the higher molecular weight solutions ($M_w \geq 264$ kg/Mol) is in accord with the scaling prediction for the reptation model (eq 3.12) which is represented in Figure 3.3 by the dotted lines. Hence the FCS measurements verify the ba-

sic scaling and reptation theory for semidilute entangled polymer solutions similar to earlier forced Rayleigh scattering experiments of polystyrene in benzene. [9, 33]

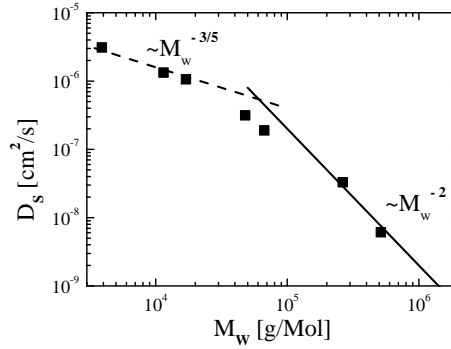


Figure 3.5: The selfdiffusion coefficient D_s (\bullet) measured by FCS at the fixed concentration $c = 9.1$ wt % as a function of the molecular weight M_w . The dashed and solid lines of slope $M_w^{-3/5}$ (see eq 3.10) and M_w^{-2} (see eq 3.12), respectively, represent two asymptotic scaling regimes.

In the limit $c \rightarrow 0$ the experimental data follow the scaling law given by eq 3.10 irrespective of the molecular weight, [12] i.e., also the higher molecular weight PS solutions obey the scaling relation $D_s \sim M_w^{-3/5} c^0$. This result is in agreement with earlier quasi-elastic light scattering experiments for polystyrene in 2-butanone [34] or in benzene. [3]

3.5.2 Internal Motions of Chains

In order to examine the influence of internal chain motions such as bending and stretching on the dynamics (see refs [35, 36, 37, 38] and references therein), one may trace out the internal degrees of freedom of a polymer chain by studying the monomer mean square displacement $B_s(\tau)$ in eq 3.4 in detail. Various theoretical predictions on the time dependence of the monomer mean square displacement of both continuously and single labeled DNA molecules in aqueous solution have been verified using FCS measurements. [39, 40, 41, 42, 43, 44] In these earlier experimental and theoretical studies the Θ condition has been considered. However, for PS in toluene so-

lutions the intramolecular excluded volume interaction has to be taken into account. In this case scaling arguments [45, 46] lead to the following time dependence of the monomer mean square displacement:

$$B_s(\tau) = B_s \tau^{1/(1+1/(2\nu))} = B_s \tau^{6/11}. \quad (3.14)$$

It proves convenient to consider the function $1/G(\tau) - 1$, which amplifies the time dependence of $G(\tau)$ for small times, because $w_z^2 = 64w_{x,y}^2$ in eq 3.5. [43] If the autocorrelation function $G(\tau)$ exhibits a time dependence according to eqs 3.4, 3.5, and 3.14 with $G_c(0) = 0$, a double logarithmic plot will directly yield the exponent $1/(1+1/(2\nu))$ for small times provided the intramolecular dynamics dominates, i.e., $B_s(\tau) \gg 6D_s\tau$.

Figure 3.6 shows such a representation of the autocorrelation function for the 515 kg/Mol PS chains in dilute solution. The experimental data (solid squares) follow the scaling law given by eq 3.14 (dotted line) and the diffusive behavior (lower dashed line) for short and large times, respectively. Hence for short times the decay of the autocorrelation function is dominated by intramolecular chain relaxations, while selfdiffusion dominates for large times. Figure 3.6 demonstrates that the measured autocorrelation function agrees with the calculated results (solid line) obtained from eqs 3.4, 3.5, and 3.14 with D_s and B_s as input. The mean displacements $\sqrt{\phi_s(\tau)}$ as calculated from eq 3.5 with $G_s(0) = 1$ and $G_c(0) = 0$ are given by 131 nm and 598 nm for $\tau = 0.01$ ms and $\tau = 1$ ms, respectively.

It is apparent from Figure 3.6 that the contribution of internal chain motions cannot be observed in the case of the 17 kg/Mol PS chains in dilute solution (solid triangles) because of the dominating diffusive motion (upper dashed line). The selfdiffusion coefficient D_s increases upon decreasing molecular weight according to eq 3.10, while B_s is less dependent on molecular weight. Finally, it is worthwhile to mention the contribution of internal chain motions to the dynamics decreases upon increasing the polymer concentration because of the presence of the surrounding polymer chains. [45, 47]

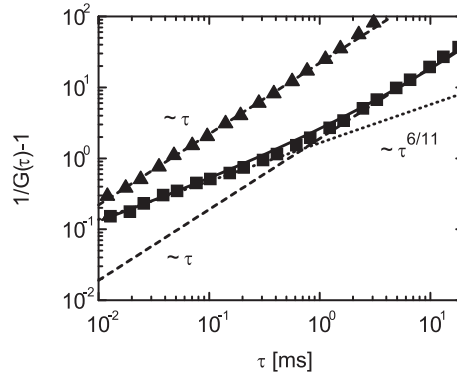


Figure 3.6: The autocorrelation function $1/G(\tau) - 1$ of a 515 kg/Mol (■) and a 17 kg/Mol (▲) polystyrene solution measured by FCS in the limit $c \rightarrow 0$ as a function of the time τ . The dotted and dashed lines of slope $\tau^{6/11}$ (see eq 3.14) and τ (see eq 3.4), respectively, represent two asymptotic scaling regimes. The solid line displays the result for the 515 kg/Mol polystyrene solution as obtained from eq 3.5 with eqs 3.4 and 3.14 as input. The autocorrelation function of the 17 kg/Mol polystyrene solution (▲ and upper dashed line) is shifted up by a factor of 2.

3.5.3 Cooperative Diffusion

We now turn our attention to the scaling law for the cooperative diffusion coefficient given by eq 3.11. Figure 3.7 displays the cooperative diffusion coefficient D_c of the 515 kg/Mol PS solution (solid squares) together with the scaling law (dashed line) as a function of the concentration. Several experimental measurements have yielded the concentration dependence $D_c \sim c^{0.65}$ instead of the scaling prediction $D_c \sim c^{3/4} = c^{0.75}$. [3, 48, 49, 50, 51] Various possible explanations for these deviations from the scaling law have been discussed, [52, 53] such as the countermotion of the solvent induced by the motion of the polymers. On the basis of our results shown in Figure 3.7 we note that the transition between the dilute regime with $D_c \sim c^0$ (dotted line and eq 3.10) and the semidilute unentangled regime with $D_c \sim c^{3/4}$ (dashed line and eq 3.11) is not so abrupt, as has been assumed by scaling theories, but is a rather smooth crossover that extends over more than one order in magnitude of concentration.

It has been emphasized that it would be desirable to model the dynamics

both in the dilute regime and the semidilute regimes explicitly within one theoretical approach. [31] Successful models should incorporate the transition region between the dilute regime and the semidilute regimes. In the next subsection we provide a quantitative basis for such a modelling of cooperative dynamical properties of polymer chains in good solution.

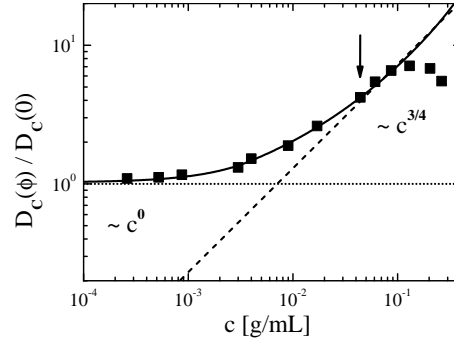


Figure 3.7: The normalized cooperative diffusion coefficient D_c (■; DLS) of a 515 kg/Mol polystyrene solution as a function of the concentration c . The dashed and dotted lines of slope $c^{3/4}$ (see eq 3.11) and c^0 (see eq 3.10), respectively, represent two asymptotic scaling regimes. The solid line displays the results as obtained from the Langevin and generalized Ornstein-Zernike equation according to eqs 3.17 - 3.23. The arrow marks the location of the concentration $c^+ = 0.044$ g/ml at which the cooperative diffusion mode appears in the FCS measurements (see Figure 3.3).

3.5.4 Analytical Theory: Langevin and Generalized Ornstein-Zernike Equation

We consider a monodisperse polymer solution consisting of $N_{tot} = N + N_u$ polymer chains and the solvent. Each polymer chain carries n scattering units. The total dynamic scattering function $S_{tot}(q, \phi, \tau)$ is defined as

$$S_{tot}(q, \phi, \tau) = \frac{1}{N_{tot} n^2} \left\langle \sum_{\alpha, \gamma=1}^{N_{tot}} \sum_{j, k=1}^n e^{i\mathbf{q} \cdot (\mathbf{r}_{\alpha j}(\tau) - \mathbf{r}_{\gamma k}(0))} \right\rangle, \quad (3.15)$$

where $q = |\mathbf{q}|$ is the magnitude of the scattering vector \mathbf{q} and $\langle \rangle_\phi$ denotes an ensemble average for a given polymer volume fraction ϕ . Here $\mathbf{r}_{\alpha j}(\tau)$ is the position vector of the j -th scattering unit ($1 \leq j \leq n$) of the α -th particle ($1 \leq \alpha \leq N_{tot}$) at time τ . The normalized total dynamic scattering function is related to the electric field autocorrelation function measured by DLS according to $S_{tot}(q, \phi, \tau)/S_{tot}(q, \phi, 0) = g_{VV}^{(1)}(q, \tau)\sqrt{f_{VV}}$. (see eq 3.7). The time evolution of the total dynamic scattering function is assumed to be governed by the Langevin equation [2]

$$\frac{d}{d\tau} S_{tot}(q, \phi, \tau) = -\Gamma(q, \phi) S_{tot}(q, \phi, \tau). \quad (3.16)$$

The validity of this equation is not obvious since entanglements have not been taken into account in the derivation of this equation. [2] However, the short time-scale dynamics can be described by eq 3.16 since the topological constraints are not so important in the short time-scale dynamics as is apparent from the fact that the cooperative diffusion coefficient D_c is considerably larger than the selfdiffusion coefficient D_s in the semidilute entangled regime (see Figure 3.3). The decay rate $\Gamma(q, \phi)$ is given by [2]

$$\Gamma(q, \phi) = \frac{k_B T}{4\pi^2 \eta} \int_0^\infty dq_1 q_1^2 \frac{S_{tot}(q_1, \phi, 0)}{S_{tot}(q, \phi, 0)} \left(\frac{q_1^2 + q^2}{2q_1 q} \log \left| \frac{q_1 + q}{q_1 - q} \right| - 1 \right), \quad (3.17)$$

where the temperature T and the viscosity η characterize the solvent. The volume fraction-dependent cooperative diffusion coefficient $D_c(\phi)$ can be calculated according to

$$D_c(\phi) = \lim_{q \rightarrow 0} \frac{\Gamma(q, \phi)}{q^2}. \quad (3.18)$$

Furthermore, the total static scattering function reads

$$S_{tot}(q, \phi, 0) = 1 + \phi h(q, \phi)/(V_p P(q, \phi)), \quad (3.19)$$

where V_p is the volume of a dissolved polymer chain and $h(q, \phi)$ is a particle-averaged total correlation function. The particle-averaged intramolecular correlation function

$$P(q, \phi) = \frac{1}{N_{tot} n^2} \left\langle \sum_{\alpha=1}^{N_{tot}} \sum_{j,k=1}^n e^{i\mathbf{q} \cdot (\mathbf{r}_{\alpha j}(0) - \mathbf{r}_{\alpha k}(0))} \right\rangle, \quad (3.20)$$

characterizes the geometric shape of the polymer chains at a given volume fraction ϕ . While the particle-averaged intramolecular correlation function accounts for the interference of radiation scattered from different parts of the same polymer chain in a scattering experiment, the local order in the fluid is characterized by $h(q, \phi)$. The particle-averaged total correlation function is related to a particle-averaged direct correlation function $c(q, \phi)$ by the generalized Ornstein-Zernike equation of the Polymer Reference Interaction Site Model (PRISM), which reads (see refs [54, 55, 56] and references therein)

$$h(q, \phi) = P^2(q, \phi)c(q, \phi)/(1 - \phi c(q, \phi)P(q, \phi)/V_p). \quad (3.21)$$

This generalized Ornstein-Zernike equation must be supplemented by a closure relation. If the interaction sites are simply the centers of exclusion spheres, to account for steric effects, a convenient closure is the Percus-Yevick approximation. [54] The PRISM integral equation theory has been successfully applied to various experimental systems such as polymers, [54, 57] bottle-brush polymers, [58, 59] rigid dendrimers, [60, 61] and charged colloids. [62, 63, 64, 65, 66, 67, 68, 69]

The overall size of the polymer chains is reduced considerably upon increasing the volume fraction implying a concentration dependence of the particle-averaged intramolecular correlation function $P(q, \phi)$. Therefore, we consider the following particle-averaged intramolecular correlation function [70]

$$P(q, \phi) = (1 + 0.549 q^2 r_g^2(\phi))^{-5/6} \quad (3.22)$$

with the volume fraction dependent radius of gyration

$$r_g^2(\phi) = \begin{cases} r_g^2(0) & , \quad c < c^* \\ r_g^2(0) \left(\frac{c}{c^*}\right)^{-1/8} & , \quad c > c^* \end{cases} . \quad (3.23)$$

Here the relation between the volume fraction ϕ and the concentration c is given by $\phi = \bar{v}c$, where $\bar{v} = 0.916 \text{ cm}^3/\text{g}$ is the specific weight of PS. [30] The scaling law given by eq 3.23 has been confirmed experimentally for PS in a good solvent using small angle neutron scattering. [71]

Figure 3.7 demonstrates that the measured cooperative diffusion coefficients (solid squares) agree with the calculated results (solid line) obtained from eqs 3.17 - 3.23 both in the dilute and semidilute regimes. In particular, the features of the broad crossover region between the dilute and the semidilute regimes are captured correctly by the integral equation theory. In the calculations the model parameter $c^* = 0.0032 \text{ g/ml}$ [12] and $r_g(0) = 32.8 \text{ nm}$ for the 515 kg/Mol PS solution has been used. This radius of gyration is about 6 % larger than corresponding radii of gyration of PS in various good solvents. [20, 72, 8, 73] The deviation between the radius of gyration used in the calculations and the radii of gyration reported in the literature might be due to the fact that the hydrodynamic interaction has been taken into account in terms of the Oseen tensor in order to derive eq 3.17. Using the Rotne-Prager tensor [74, 75] as a first correction to the Oseen tensor will improve the results. Moreover, the size polydispersity $M_w/M_n = 1.09$ of the 515 kg/Mol PS solution leads to a diffusion coefficient which is characteristic for monodisperse polymers of larger radius of gyration. [76]

Finally, we note that the maximum of D_c in the semidilute entangled regime marks the onset of glassy dynamics which is discussed in ref [51]. The friction-controlled dynamics in this concentration regime is not captured by eqs 3.16 and 3.17 and will be discussed in subsection 3.5.6.

3.5.5 Coupling of Cooperative Fluctuations with Single Polymer Chain Motion

In the following we shall discuss the equation of motion which determines the dynamics an individual polymer chain. The PS chains are linear chain molecules which are described by a chain model for macromolecules. [35, 75, 36] We consider a continuous, differentiable space curve $\mathbf{r}(s, \tau)$, where $s \in [-L/2, L/2]$ is a coordinate along the macromolecule and $\mathbf{r}(L/2, \tau)$ is the position vector of the labeled end monomer. The Langevin equation of motion including hydrodynamic interaction is given by [75]

$$3\pi\eta \frac{\partial}{\partial \tau} \mathbf{r}(s, \tau) = \int_{-L/2}^{L/2} ds' (3\pi\eta H(s-s') + \delta(s-s')) \times (O(s')\mathbf{r}(s', \tau) + \mathbf{f}(s', \tau)) + \mathbf{F}(s, \tau), \quad (3.24)$$

with

$$O(s) = 3k_B T p \frac{\partial^2}{\partial s^2} - \frac{3k_B T}{4p} \frac{\partial^4}{\partial s^4}. \quad (3.25)$$

Here $1/(2p)$ is the persistence length, $H(s-s')$ is the hydrodynamic interaction tensor, and $\mathbf{f}(s, \tau)$ is the stochastic force. The force $\mathbf{F}(s, \tau)$ describes the influence of intermolecular forces and is discussed below. The numerical solution of eq 3.24 allows one to calculate the mean square displacement (see eq 3.4) according to

$$\phi_s(\tau) = \langle (\mathbf{r}(L/2, \tau) - \mathbf{r}(L/2, 0))^2 \rangle. \quad (3.26)$$

This chain model has been used in the limit $\mathbf{F}(s, \tau) = 0$ in order to describe FCS measurements of DNA molecules in dilute solution. [41, 42, 43] In particular, the model predicts the observed crossover from subdiffusive motion ($B_s(\tau)$ in eq 3.4) to diffusive motion ($6D_s\tau$ in eq 3.4) upon increasing the time τ . **Moreover, it has been shown that the chain ends are more mobile than the central part of the polymer chain for short times.**

[43] For comparison we note that the quantity $\phi_s(\tau)$ contributes to the so called incoherent dynamic structure factor which is accessible by quasielastic neutron scattering (see ref [77] and references therein).

The key physics determining the dynamics of chain molecules in semidilute entangled solution arises from the intermolecular interaction which are taken into account in terms of the force $\mathbf{F}(s, \tau)$ in eq 3.24. Various expressions for the force $\mathbf{F}(s, \tau)$ have been proposed (see, e.g., refs [78, 79, 80, 81, 82, 83, 84, 85, 86]). These earlier theoretical considerations have demonstrated the coupling of cooperative fluctuations with single polymer chain motion in the semidilute entangled regime. This coupling allows one to measure D_c from the dynamics of individual labeled polymer chains with FCS. Hence, it provides the explanation for the finding of a cooperative mode in the FCS-experiment. The topological interaction in semidilute entangled polymer solutions seriously affects dynamical properties since it imposes constraints on the motion of the polymers. When the motion of a single polymer chain is partly hindered by the presence of other chains the cooperative diffusion becomes highly correlated and can be studied using only a small fraction of labeled molecules. Moreover, the number of molecules statistically involved in the correlated dynamics increases considerably upon approaching the glass transition concentration.

Figures 3.8 (a) and (b) display the function $1/G(\tau) - 1$ for the 17 kg/Mol PS chains and the 515 kg/Mol PS chains in dilute solution (solid squares, $c \rightarrow 0$) and in semidilute solution (solid triangles, $c = 13$ wt %). For the 17 kg/Mol PS chains only selfdiffusion can be measured using FCS irrespective of the concentration (see Figure 3.8 (a)) because of insufficient chain overlap. In the case of the 515 kg/Mol PS chains selfdiffusion dominates for large times as is indicated by the dashed lines in Figure 3.8 (b). The cooperative diffusion observed in the semidilute entangled solution (solid triangles in Figure 3.8 (b)) dominates the autocorrelation function on the same time scale as intramolecular chain relaxations in the case of a dilute solution (solid squares in Figure 3.8 (b)). Hence one may conclude that upon increasing the polymer concentration the contribution of internal chain motions to the single chain dynamics decreases while the contribution of the cooperative

motions increases because of the fluctuations of the surrounding polymer chains. Both types of dynamics are observable on the same time scale but in different concentration regimes for high molecular weight PS chains. In the case of internal chain motions the dynamics is driven by fluctuations of the solvent while fluctuations of the surrounding polymer network induce the cooperative dynamics. The fact that cooperative diffusion and internal chain motions occur on similar time and length scales has already been discussed earlier (see ref [87] and references therein).

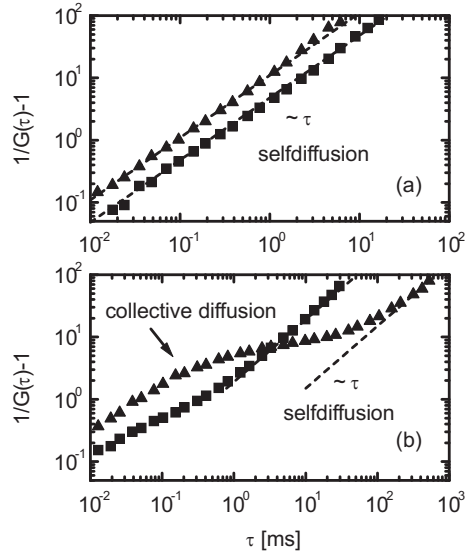


Figure 3.8: The FCS autocorrelation function $1/G(\tau) - 1$ of 17 kg/Mol polystyrene chains (a) and 515 kg/Mol polystyrene chains (b) in dilute solution (■, $c \rightarrow 0$) and in semidilute solution (▲, $c = 13$ wt %). The dashed lines of slope τ characterize selfdiffusion. Intramolecular motions and cooperative diffusion dominate in dilute and semidilute entangled solution, respectively, for short times in the case of the high molecular weight polystyrene chains in (b).

Without entanglements the local concentration fluctuations at low scattering vectors \mathbf{q} are suppressed by the osmotic pressure of the solution, and the total dynamic scattering function $S_{tot}(q, \phi, \tau)$ measured by DLS decays via cooperative diffusion according to eqs 3.16 - 3.18. However, in the presence of entanglements, there is an additional suppression of concentration

fluctuations. Some concentration fluctuations may be frozen in by the entanglements. [88, 89, 90] This fraction of light scattering signal may only decay with the spectrum of relaxation times of the entanglements themselves, leading to a slow relaxation of the total dynamic scattering function as is shown in Figures 3.9 (a) and (b) for the 67 kg/Mol and 515 kg/Mol PS chains in semidilute entangled solution at $c=13$ % wt (solid triangles). The corresponding upper solid lines in Figures 3.9 (a) and (b) have been calculated according to

$$S_{tot}(q, \phi, \tau) = S_c(q, \phi) \exp(-q^2 D_c \tau) + S_{sl}(q, \phi) \exp(-\tau/\tau_{sl}), \quad (3.27)$$

where τ_{sl} is a decay time. For arbitrary values of the magnitude of the scattering vector q and the volume fraction ϕ , the shape of the total dynamic scattering function $S_{tot}(q, \phi, \tau)$ is more complex than the expression given in eq 3.27. For large values of q intramolecular motions lead to a stretched exponential decay of $S_{tot}(q, \phi, \tau)$ for short times (see e.g., refs [75, 76]). Moreover, the contribution of the slow relaxation to $S_{tot}(q, \phi, \tau)$ is in general given by a linear combination of exponentially decaying functions, i.e., $\sum_i \exp(-\tau/\tau_{i,d})$. [91, 92]

Experiments on PS in various solvents have confirmed that the slow relaxation can be measured using DLS. [93, 94, 95, 96, 97, 98, 99, 100, 101] However, the microscopic understanding of the slow relaxation needs to be improved. [102] On the basis of our FCS and DLS measurements shown in Figures 3.8 and 3.9 we note that selfdiffusion (D_s) occurs on an intermediate time scale, i.e., $1/(q^2 D_c) = 0.05$ ms, $1/(q^2 D_s) = 16$ ms, and $\tau_{sl} = 1087$ ms for $q = 157.6 \mu\text{m}^{-1}$ for the 515 kg/Mol PS chains. For comparison Figures 3.9 (a) and (b) also display the measured total dynamic scattering function of the PS chains in semidilute unentangled solution (solid squares). In this case there is no slow relaxation due to insufficient chain overlap. The corresponding lower solid lines in Figures 3.9 (a) and (b) have been calculated according to eq 3.27 with $S_{sl}(q, \phi) = 0$.

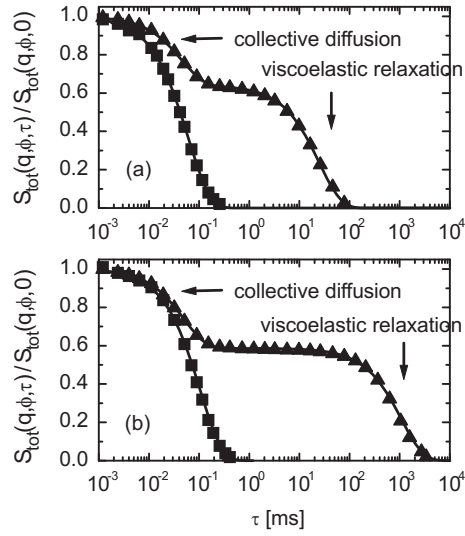


Figure 3.9: The total dynamic scattering function $S_{tot}(q, \phi, \tau)$ of 67 kg/Mol polystyrene chains (a) and 515 kg/Mol polystyrene chains (b) measured by DLS in semidilute unentangled solution (\blacksquare , $c = 1$ wt %) and in semidilute entangled solution (\blacktriangle , $c = 13$ wt %). The solid lines follow from eq 3.27. For short times cooperative diffusion dominates, while the slow relaxation dominates for very large times in semidilute entangled solution. There is no slow relaxation in semidilute unentangled solution, i.e., $S_{sl}(q, \phi) = 0$ in eq 3.27. The absolute value of the scattering vector is given by $q = 157.6 \mu\text{m}^{-1}$.

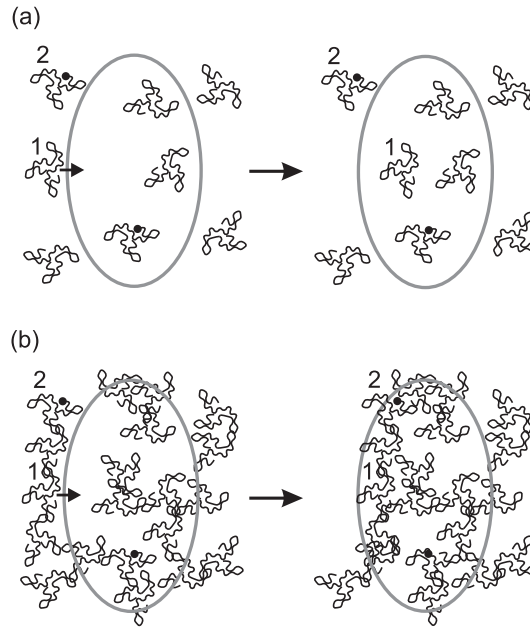


Figure 3.10: Schematic illustration of the cooperative diffusion process which is related to the relaxation of the total polymer number density towards the average total number density. The polymer chain denoted by the index 1 moves in (a) and (b) from left to right into the FCS observation volume enclosed by the grey ellipsoidal lines. The polymer chain diffuses into the observation volume nearly without influencing the locations of the remaining polymer chains in an unentangled solution in (a), while the motion of the polymer chain leads to coherent movement of the surrounding polymer chains in semidilute entangled solution in (b). The size of the polymer chains, the size observation volume, and the number of polymer chains are not drawn to absolute scale. Only the fact that in (b) the motion of the unlabeled polymer chain denoted by the index 1 induces a correlated movement of the labeled polymer chain denoted by the index 2 into the observation volume is relevant. Each labeled polymer chain carries only one dye molecule at one of its ends which is marked by a black dot. As the labeled polymer chain denoted by the index 2 diffuses into the observation volume from left to right in (b), it causes temporal fluctuations of the detected fluorescence intensity which can be measured by FCS even in the case that the number of labeled polymer chains is considerably smaller than the number of unlabeled polymer chains. In addition selfdiffusion can be measured using FCS both in (a) and (b) as discussed in Section IV A. In (b) selfdiffusion of polymer chains corresponds to movements of the polymer chains along their contour through the transient network.

The direct DLS measurement of the slow relaxation confirms our earlier remark that cooperative diffusion becomes highly correlated in the transient entanglement network and can be studied using only a small fraction of labeled polymer chains within FCS. As is illustrated in Figure 3.10 (b) unlabeled polymer chains (see, e.g., the polymer chain denoted by the index 1) and labeled polymer chains (see, e.g., the polymer chain denoted by the index 2) move in a coherent manner due to entanglements into the FCS observation volume enclosed by the grey ellipsoidal lines. The resulting temporal fluctuations of fluorescence light emitted by labeled polymer chains can be detected by FCS in terms of the cooperative diffusion. A spherical volume of mean size equivalent to the radius of gyration of an individual polymer chain contains about 15 polymer chains at the concentration c^+ at which cooperative diffusion is measured with FCS. Consequently, neighbouring chains strongly interpenetrate and entangle with each other leading to highly cooperative motions in this correlated state. Without entanglements cooperative diffusion cannot be detected if only a small fraction of the polymer chains are labeled due to insufficient chain overlap. Hence in dilute and semidilute unentangled solutions the unlabeled polymer chain denoted by 1 in Figure 3.10 (a) moves from left to right into the FCS observation volume nearly without influencing the remaining labeled and unlabeled polymer chains.

3.5.6 Onset of Glassy Dynamics

Upon approaching the glass transition concentration $c_{gl} \approx 80$ wt % of PS in toluene, [51, 103] the dynamics of the polymer chains slows down considerably (see ref [104] and references therein). A first signature of this slowing down is given by the deviations of the measured cooperative diffusion coefficients D_c from the solid line at high concentrations in fig 3.7. The cooperative diffusion coefficient decreases by more than three decades as compared to its maximum value upon further increasing the concentration (see fig 6 in ref [51]). A second signature of the onset of glassy dynamics is given by the shape of the autocorrelation function $G(\tau)$ measured with FCS. Figure 3.11 displays measured functions $1/G(\tau) - 1$ (solid symbols) for the 515 kg/Mol

PS chains at three concentrations $c = 9.1, 13,$ and 20 wt % together with the autocorrelation function for the highest concentration (solid line) calculated according to eq 3.5 with eq 3.3 and

$$\phi_s(\tau) = 6D_s\tau + A_s\tau^\beta, \quad \beta = 0.3. \quad (3.28)$$

Subdiffusive motion characterized by the stretching parameter β is observed as an additional mode on an intermediate time scale between the fast cooperative diffusion (D_c) and the slow selfdiffusion (D_s). The dotted line in fig 3.11 represents the asymptotic shape of $1/G(\tau) - 1$ in the intermediate time regime. Both the exponent $\beta = 0.3$ and the time scale agree with literature values for PS. [51, 105]

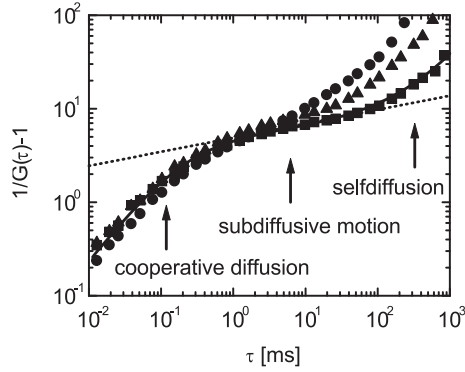


Figure 3.11: The measured FCS autocorrelation function $1/G(\tau) - 1$ of a 515 kg/Mol polystyrene solution at three concentrations: $c = 9.1$ wt %, (\bullet); $c = 13$ wt %, (\blacktriangle); $c = 20$ wt %, (\blacksquare). The solid line displays the result for the highest concentration as obtained from eq 3.5 with eqs 3.4 and 3.28 as input. For short and large times cooperative diffusion and selfdiffusion dominate, respectively. The dotted line represents the asymptotic shape of the autocorrelation function in the intermediate time regime.

3.6 An Application: Comparison with Minimum Concentration Required to Produce Nanofibers

The understanding of dynamical properties of semidilute entangled polymer solutions is also important for various technological relevant applications. As an example we discuss the formation of nanofibers from polymer solutions. Polymer nanofibers are attractive building blocks for functional nanoscale devices. They are promising candidates for various applications, including filtration, protective clothing, polymer batteries, sensors, and tissue engineering. [106, 107] Electrospinning is one of the most established fiber fabrication methods and has attracted much attention due to the ease by which nanofibers can be produced from polymer solutions. [108] Fibers produced by this approach are at least one or two orders of magnitude smaller in diameter than those produced by conventional fiber production methods like melt or solution spinning. In a typical electrospinning process a jet is ejected from the surface of a charged polymer solution when the applied electric field strength overcomes the surface tension. The ejected jet travels rapidly to the collector target located at some distance from the charged polymer solution under the influence of the electric field and becomes collected in the form of a solid polymer nanofiber. However, this method requires a dc voltage in the kV range and high fiber production rates are difficult to achieve because only a single fiber emerges from the nozzle of the pipet holding the polymer solution. [108] In order to overcome these deficiencies an efficient procedure enabling the parallel fabrication of a multitude of polymer fibers with regular morphology and diameters as small as 25 nm has been reported recently. [109] It involves the application of drops of a polymer solution onto a standard spin coater, followed by fast rotation of the chuck, without the need of a mechanical constriction. The fiber formation relies upon the instability of the spin-coated liquid film that arises due to a competition of the centrifugal force and the Laplace force induced by the surface curvature. This Rayleigh-Taylor instability triggers the formation of thin liquid jets emerging from the

outward driven polymer solution, yielding solid nanofibers after evaporation of the solvent.

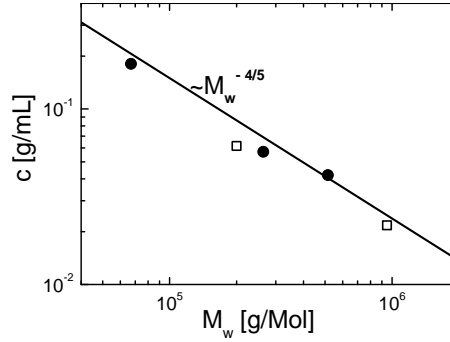


Figure 3.12: The concentration c^+ (●) at which the cooperative diffusion mode appears in the FCS measurements together with the minimum concentration c_{fib} (□) required to produce nanofibers [109] as a function of the molecular weight M_w . The solid line of slope $M_w^{-4/5}$ represents a scaling relation valid for polymers in a good solvent.

The reason why the ejected jets of polymer solution do not further break up into individual droplets, but rather give rise to continuous, solid nanofibers, is related to the dynamic properties of the polymer solutions. In order to elucidate this point in more detail, Figure 3.12 displays the minimum concentration c_{fib} required to produce nanofibers from 200 kg/Mol and 950 kg/Mol poly-(methylmethacrylate) solution (open squares) [109] together with the concentration c^+ at which the cooperative diffusion mode appears in the FCS measurements of the 67 kg/Mol, 264 kg/Mol, and 515 kg/Mol PS solutions (solid circles). Interestingly, the concentrations c_{fib} and c^+ follow approximately the same scaling relationship $c_{fib} = c^+ \sim M_w^{-4/5}$ (c.f., eq 3.13). Hence, the nanofiber formation requires that the polymer concentration exceeds the concentration c^+ where basically all molecules are involved in the correlated cooperative dynamics. Uniform fibers cannot be obtained for lower concentrations due to insufficient chain overlap and the dominating selfdiffusion which leads to a disentanglement under the influence of external forces such as the centrifugal force or the electrostatic force.

3.7 Conclusion

A general analysis of the diffusion in polystyrene solutions obtained by fluorescence correlation spectroscopy and by dynamic light scattering has been presented. Two different diffusion coefficients have been obtained with fluorescence correlation spectroscopy using single-labeled polystyrene in toluene solutions [Figures 3.1 - 3.4]. The selfdiffusion coefficient D_s results from fluorescence correlation spectroscopy in the limit of small concentrations of labeled molecules and for arbitrary concentrations of unlabeled molecules. Moreover, the cooperative diffusion coefficient D_c in the semidilute entangled regime becomes accessible as well which is ascribed to an effective long-range interaction of the labeled chains in the transient entanglement network. The selfdiffusion coefficients D_s can be determined from the cooperative diffusion coefficient D_c obtained by dynamic light scattering measurements and vice versa according to eqs 3.8 and 3.9.

The measurements verify the basic scaling and reptation theory for semidilute entangled polymer solutions [Figures 3.3, 3.5, 3.6 and eqs 3.10, 3.12, 3.14]. A quantitative basis for the modelling of the cooperative diffusion coefficient is given by a Langevin and generalized Ornstein-Zernike equation [eqs 3.15 - 3.23]. The calculated cooperative diffusion coefficients agree with the measured results both in the dilute and semidilute regimes [Figure 3.7]. In particular the features of the crossover region between the dilute and the semidilute regimes are captured correctly by the underlying integral equation theory.

For large times the decay of the fluorescence correlation spectroscopy autocorrelation function is dominated by selfdiffusion, while intramolecular chain relaxations in dilute solution and cooperative diffusion in semidilute entangled solution dominate for short times [Figures 3.6 and 3.8]. An additional slow relaxation in semidilute entangled solution can be observed by dynamic light scattering [Figure 3.9]. Moreover, the fluorescence correlation spectroscopy autocorrelation function exhibits an additional mode on an intermediate time scale upon approaching the glass transition concentration [Figure 3.11].

Finally, it has been shown the minimum concentration required to produce solid nanofibers from a polymer solution follows the same scaling relationship as the concentration at which the cooperative diffusion mode appears in the fluorescence correlation spectroscopy measurements [Figure 3.12]. The nanofiber formation requires that the polymer concentration exceeds the concentration where basically all molecules are involved in the correlated cooperative dynamics. Hence fluorescence correlation spectroscopy is helpful for the understanding of dynamical properties of semidilute entangled polymer solutions in the case of technological relevant applications.

Acknowledgement. We thank A. H. E. Müller and A. Böker for the synthesis of the polymers and the Deutsche Forschungsgemeinschaft, SFB 481 (A11), Bayreuth, for financial support.

Bibliography

- [1] P.-G. De Gennes, *Scaling Concepts in Polymer Physics*, Cornell University Press, 1979.
- [2] M. Doi and S. F. Edwards, *The Theory of Polymer Dynamics*, Clarendon Press, 1986.
- [3] M. Adam and M. Delsanti, *Macromolecules*, 1977, **10**, 1229.
- [4] T. Cosgrove and J. M. Sutherland, *Polymer*, 1983, **24**(5), 534.
- [5] T. Kanematsu, T. Sato, Y. Imai, K. Ute, and T. Kitayama, *Polymer Journal*, 2005, **37**(2), 65.
- [6] W. Brown and P. Zhou, *Macromolecules*, 1991, **24**(18), 5151.
- [7] C. Le Bon, T. Nicolai, M. E. Kuil, and J. G. Hollander, *Journal of Physical Chemistry B*, 1999, **103**(46), 10294.
- [8] G. Min, D. Savin, Z. Gu, G. D. Patterson, S. H. Kim, D. J. Ramsay, D. Fishman, I. Ivanov, E. Sheina, E. Slaby, and J. Oliver, *International*

- Journal of Polymer Analysis and Characterization*, 2003, **8**(3), 187–207.
- [9] H. Hervet, L. Léger, and F. Rondelez, *Physical Review Letters*, 1979, **42**(25), 1681.
- [10] H. Zettl, W. Häfner, A. Böker, H. Schmalz, M. Lanzendörfer, A. H. E. Müller, and G. Krausch, *Macromolecules*, 2004, **37**(5), 1917.
- [11] R. G. Liu, X. Gao, J. Adams, and W. Oppermann, *Macromolecules*, 2005, **38**(21), 8845.
- [12] H. Zettl, U. Zettl, G. Krausch, J. Enderlein, and M. Ballauff, *Physical Review E*, 2007, **75**(6), 061804.
- [13] M. Bier, R. Van Roij, M. Dijkstra, and P. Van der Schoot, *Phys. Rev. Lett.*, 2008, **101**, 215901.
- [14] A. Michelman-Riberiro, H. Boukari, R. Nossal, and F. Horkay, *Macromolecules*, 2004, **37**, 10212.
- [15] M. Gianneli, P. W. Beines, R. F. Roskamp, K. Koynov, G. Fytas, and W. Knoll, *J. Phys. Chem. C*, 2007, **111**, 13205.
- [16] T. Cherdhirankorn, A. Best, K. Koynov, K. Peneva, K. Muellen, and G. Fytas, *J. Phys. Chem. B*, 2009, **113**, 3355.
- [17] G. C. A., *Macromolecules*, 2008, **41**, 6191.
- [18] R. J., *Phys. Rev. A*, 1989, **39**, 2646.
- [19] B. A. Scalettar, J. E. Hearst, and M. P. Klein, *Macromolecules*, 1989, **22**, 4550.
- [20] R. Kniewske and W. M. Kulicke, *Makromolekulare Chemie-Macromolecular Chemistry and Physics*, 1983, **184**(10), 2173.
- [21] R. Rigler and W. Wiegrabe, *Biological Chemistry*, 2001, **382**(3), 353.

- [22] M. Wahl, F. Koberling, M. Patting, H. Rahn, and R. Erdmann, *Curr. Pharm. Biotechnol.*, 2004, **5**, 299.
- [23] J. Enderlein and I. Gregor, *Rev. Sci. Instrum.*, 2005, **76**, 033102.
- [24] D. Magde, E. Elson, and W. W. Webb, *Phys. Rev. Lett.*, 1972, **29**, 705.
- [25] P. N. Pusey, H. M. Fijnaut, and A. Vrij, *J. Chem. Phys.*, 1982, **77**(3), 4270.
- [26] A. Z. Akcasu, G. Nägele, and R. Klein, *Macromolecules*, 1991, **24**, 4408.
- [27] H. Zettl, Y. Portnoy, M. Gottlieb, and G. Krausch, *J. Phys. Chem. B*, 2005, **109**, 13397.
- [28] J. G. Kirkwood and J. Riseman, *Journal of Chemical Physics*, 1948, **16**(6), 565.
- [29] H. D. Kim, T. Y. Chang, J. M. Yohanan, L. Wang, and H. Yu, *Macromolecules*, 1986, **19**(11), 2737–2744.
- [30] G. V. Schulz and M. Hoffmann, *Makromolekulare Chemie*, 1957, **23**(2-3), 220.
- [31] L. T. P., *Adv. Chem. Phys.*, 1990, **79**, 1.
- [32] M. T. C. B., *Adv. Phys.*, 2002, **51**, 1379.
- [33] L. Léger, H. Hervet, and F. Rondelez, *Macromolecules*, 1981, **14**(6), 1732.
- [34] T. A. King, A. Knox, and J. D. G. Mcadam, *Polymer*, 1973, **14**(7), 293.
- [35] L. Harnau, R. G. Winkler, and P. Reineker, *J. Chem. Phys.*, 1995, **102**, 7750.
- [36] L. Harnau, R. G. Winkler, and P. Reineker, *J. Chem. Phys.*, 1998, **109**, 5160.

- [37] L. Harnau, R. G. Winkler, and P. Reineker, *Phys. Rev. Lett.*, 1999, **82**, 2408.
- [38] L. Harnau, R. G. Winkler, and P. Reineker, *Europhys. Lett.*, 1999, **45**, 488.
- [39] D. Lumma, S. Keller, T. Vilgis, and J. O. Rädler, *Phys. Rev. Lett.*, 2003, **90**, 218301.
- [40] R. Shusterman, S. Alon, T. Gavrinov, and O. Krichevsky, *Phys. Rev. Lett.*, 2004, **92**, 048303.
- [41] A. Bernheim-Groswasser, R. Shusterman, and O. Krichevsky, *J. Chem. Phys.*, 2006, **125**, 084903.
- [42] E. P. Petrov, T. Ohrt, R. G. Winkler, and P. Schwille, *Phys. Rev. Lett.*, 2006, **97**, 258101.
- [43] R. G. Winkler, S. Keller, and J. O. Rädler, *Phys. Rev. E*, 2006, **73**, 041919.
- [44] R. Shusterman, T. Gavrinov, and O. Krichevsky, *Phys. Rev. Lett.*, 2008, **100**, 098102.
- [45] K. Kremer and K. Binder, *J. Chem. Phys.*, 1984, **81**, 6381.
- [46] E. P. Petrov, T. Ohrt, R. G. Winkler, and P. Schwille, *Phys. Rev. Lett.*, 2006, **97**, 258101.
- [47] L. Harnau and P. Reineker, *Phys. Rev. E*, 1999, **60**, 4671.
- [48] P. Wiltzius, H. R. Haller, D. S. Cannell, and D. W. Schaeffer, *Phys. Rev. Lett.*, 1984, **53**, 834.
- [49] N. Nemoto, Y. Makita, Y. Tsunashima, and M. Kurata, *Macromolecules*, 1984, **17**, 2629.
- [50] K. J. Zhang, M. E. Briggs, R. W. Gammon, J. V. Sengers, and J. F. Douglas, *J. Chem. Phys.*, 1999, **111**, 2270.

- [51] J. Rauch and W. Köhler, *Journal of Chemical Physics*, 2003, **119**(22), 11977.
- [52] E. Geissler and A. M. Hecht, *J. Phys. (France) Lett.*, 1978, **39**, 631.
- [53] W. Brown and T. Nicolai, *Colloid. Polym. Sci.*, 1990, **268**, 977.
- [54] K. S. Schweizer and J. G. Curro, *Adv. Chem. Phys.*, 1997, **98**, 1.
- [55] L. Harnau, *Molec. Phys.*, 2008, **106**, 1975.
- [56] A. Yethiraj, *J. Phys. Chem. B*, 2009, **113**, 1539.
- [57] L. Harnau, *J. Chem. Phys.*, 2001, **115**, 1943.
- [58] S. Bolisetty, C. Airaud, Y. Xu, A. H. E. Müller, L. Harnau, S. Rosenfeldt, P. Lindner, and M. Ballauff, *Phys. Rev. E*, 2007, **75**, 040803(R).
- [59] S. Bolisetty, S. Rosenfeldt, C. N. Rochette, L. Harnau, P. Lindner, Y. Xu, A. H. E. Müller, and M. Ballauff, *Colloid. Polym. Sci.*, 2009, **287**, 129.
- [60] S. Rosenfeldt, E. Karpuk, M. Lehmann, H. Meier, P. Lindner, L. Harnau, and M. Ballauff, *ChemPhysChem*, 2006, **7**, 2097.
- [61] L. Harnau, S. Rosenfeldt, and M. Ballauff, *J. Chem. Phys.*, 2007, **127**, 014901.
- [62] A. Yethiraj and C.-Y. Shew, *Phys. Rev. Lett.*, 1996, **77**, 3937.
- [63] A. Yethiraj and C.-Y. Shew, *J. Chem. Phys.*, 1997, **106**, 5706.
- [64] C.-Y. Shew and A. Yethiraj, *J. Chem. Phys.*, 1998, **109**, 5162.
- [65] L. Harnau and P. Reineker, *J. Chem. Phys.*, 2000, **112**, 437.
- [66] L. Harnau, D. Costa, and J.-P. Hansen, *Europhys. Lett.*, 2001, **53**, 729.
- [67] L. Harnau and J.-P. Hansen, *J. Chem. Phys.*, 2002, **116**, 9051.

- [68] C. H. M. Weber, A. Chiche, G. Krausch, S. Rosenfeldt, M. Ballauff, L. Harnau, I. Göttker-Schnetmann, Q. Tong, and S. Mecking, *Nano Lett.*, 2007, **7**, 2024.
- [69] K. Henzler, S. Rosenfeldt, A. Wittemann, L. Harnau, T. Narayanan, and M. Ballauff, *Phys. Rev. Lett.*, 2008, **100**, 158301.
- [70] K. S. Fuchs, M.; Schweizer, *J. Chem. Phys.*, 1997, **106**, 347.
- [71] M. Daoud, J. P. Cotton, B. Farnoux, G. Jannink, G. Sarma, H. Benoit, R. Duplessix, C. Picot, and P.-G. De Gennes, *Macromolecules*, 1975, **8**, 804.
- [72] L. J. Fetters, N. Hadjichristidis, J. S. Lindner, and J. W. Mays, *J. Phys. Chem. Ref. Data*, 1994, **23**, 619.
- [73] K. Terao and J. W. Mays, *Eur. Polym. J.*, 2004, **40**, 1623.
- [74] J. Rotne and S. Prager, *J. Chem. Phys.*, 1969, **50**, 4831.
- [75] L. Harnau, R. G. Winkler, and P. Reineker, *J. Chem. Phys.*, 1996, **104**, 6355.
- [76] L. Harnau, R. G. Winkler, and P. Reineker, *Macromolecules*, 1999, **32**, 5956.
- [77] L. Harnau, R. G. Winkler, and P. Reineker, *J. Chem. Phys.*, 1997, **106**, 2469.
- [78] K. S. Schweizer, *J. Chem. Phys.*, 1989, **91**, 5822.
- [79] A. N. Semenov, *Physica A*, 1991, **171**, 517.
- [80] U. Genz, *Macromolecules*, 1994, **27**, 6452.
- [81] K. S. Schweizer, M. Fuchs, G. Szamel, M. Guenza, and H. Tang, *Macromol. Theory Simul.*, 1997, **6**, 1037.
- [82] M. Guenza, *J. Phys. Chem.*, 1999, **110**, 7574.

- [83] A. N. Semenov and M. Rubinstein, *Eur. Phys. J. B.*, 1998, **1**, 87.
- [84] Y. A. Altukhov, V. N. Pokrovskii, and G. V. Pyshnograï, *J. Non-Newtonian Fluid Mech.*, 2004, **121**, 73.
- [85] V. N. Pokrovskii, *Physica A*, 2006, **366**, 88.
- [86] V. N. Pokrovskii, *J. Expt. Theo. Phys.*, 2008, **106**, 604.
- [87] T. Jian, D. Vlassopoulos, G. Fytas, T. Pakula, and W. Brown, *Colloid Polym. Sci.*, 1996, **274**, 1033.
- [88] F. Brochard and P.-G. De Gennes, *Macromolecules*, 1977, **10**, 1157.
- [89] M. Doi and A. Onuki, *J. Phys. II (France)*, 1992, **2**, 1631.
- [90] Y. Einaga and H. Fujita, *Polymer*, 1999, **40**, 565.
- [91] Y. Einaga, A. Itaya, and M. Takaoka, *Polymer*, 2002, **43**, 4869.
- [92] M. Takenaka, S. Nishitsuji, and H. Hasegawa, *J. Phys. Chem.*, 2007, **126**, 064903.
- [93] W. Brown, T. Nicolai, S. Hvidt, and P. Stepanek, *Macromolecules*, 1990, **23**, 357.
- [94] T. Nicolai, W. Brown, R. M. Johnsen, and P. Stepanek, *Macromolecules*, 1990, **23**, 1165.
- [95] T. Nicolai and W. Brown, *Macromolecules*, 1990, **23**, 3150.
- [96] T. Nicolai, W. Brown, S. Hvidt, and K. Heller, *Macromolecules*, 1990, **23**, 5088.
- [97] C. H. Wang and X. Q. Zhang, *Macromolecules*, 1993, **26**, 707.
- [98] W. Brown and P. Stepanek, *Macromolecules*, 1993, **26**, 6884.
- [99] Z. Sun and C. H. Wang, *Macromolecules*, 1994, **27**, 5667.
- [100] C. H. Wang and X. Q. Zhang, *Macromolecules*, 1995, **28**, 2288.

- [101] C.-N. Lin, Y.-M. Song, and T.-L. Yu, *J. Polym. Res.*, 1997, **4**, 107.
- [102] J. Li, W. Li, H. Huo, S. Luo, and C. Wu, *Macromolecules*, 2008, **41**, 901.
- [103] C. Konak and W. Brown, *J. Chem. Phys.*, 1993, **98**, 9014.
- [104] S. Peter, H. Meyer, and J. Baschnagel, *Eur. Phys. J. E.*, 2009, **28**, 147.
- [105] C. Lindsey, G. Patterson, and J. Stevens, *J. Polym. Sci., Polym. Phys. Ed.*, 1979, **17**, 1547.
- [106] S. Ramakrishna, K. Fujihara, W.-E. Teo, T.-C. Lim, and Z. Ma, *Introduction to Electrospinning and Nanofibers*, World Scientific, Singapore, 2005.
- [107] M. Stevens and M. George, *Science*, 2005, **310**, 1135.
- [108] A. Greiner and J. H. Wendorff, *Angew. Chem. Int. Ed.*, 2007, **46**, 5670.
- [109] R. T. Weitz, L. Harnau, S. Rauschenbach, M. Burghard, and K. Kern, *Nano Lett.*, 2008, **8**, 1187.

Chapter 4

A Fluorescence Correlation Spectroscopy Study of Macromolecular Tracer Diffusion in Polymer Solutions

Ute Zettl¹, Matthias Ballauff², Ludger Harnau³ *

¹Physikalische Chemie I, University of Bayreuth, 95440 Bayreuth, Germany

²Soft Matter and Functional Materials, Helmholtz-Zentrum Berlin, 14109 Berlin, Germany

³Max-Planck-Institut fuer Metallforschung, Heisenbergstr. 3, 70569 Stuttgart, Germany, and Institut fuer Theoretische und Angewandte Physik, Universitaet Stuttgart, Pfaffenwaldring 57, 70569 Stuttgart, Germany

Published in *Journal of Physics: Condensed Matter*, **2010**, *22* (49)

4.1 Abstract

We present an identification of the manner in which the dynamics of tracer polystyrene chains varies with the concentration of matrix polystyrene chains dissolved in toluene. Using fluorescence correlation spectroscopy and theory, it is shown that the cooperative diffusion coefficient of the matrix polystyrene chains can be measured by fluorescence correlation spectroscopy in the semidilute entangled concentration regime. In addition the self-diffusion coefficient of the tracer polystyrene chains can be detected for arbitrary concentrations. The measured cooperative diffusion coefficient is independent of the molecular weight of the tracer polystyrene chains because it is a characteristic feature of the transient entanglement network.

4.2 Introduction

The dynamics of solutions composed of high molecular weight polymer chains differs qualitatively from the dynamics of simple fluids due to entanglements. At a microscopic scale, entanglements arise from the fact that linear polymer chains are one-dimensionally connected objects which cannot cross each other. The resulting topological interaction strongly affects dynamical properties since it imposes constraints on the motion of the polymer chains. The common interpretation of the physical origin of entanglement phenomena is that a transient network emerges due to the interactions between the polymer chains. The so-called reptation model is the most developed and widely applied phenomenological theory for the motion of polymer chains (see e.g., ref [2] and references therein). It focusses on the motion of a single polymer chain in an static field due to the surrounding polymer chains. Although widely accepted, there are significant discrepancies between predictions of the reptation model and experiments on polymer solutions because the surrounding polymer chains do not act as a static field but exhibit themselves cooperative fluctuations. Hence there is an important coupling between the single polymer chain motion and the cooperative network fluctuations. As a result of this coupling it should be possible to detect both the single polymer

and the cooperative dynamics using the same experimental technique. Recently it has been demonstrated that two different diffusion coefficients can be obtained with fluorescence correlation spectroscopy (FCS) using single-labeled polystyrene (PS) homopolymer solutions [1]. The self-diffusion coefficient $D_s(c)$ results from FCS in the limit of small concentrations of labeled PS chains and for arbitrary concentrations c of unlabeled PS chains. Moreover, the cooperative diffusion coefficient $D_c(c)$ becomes accessible in the semidilute entangled regime due to an effective long-range interaction in the transient entanglement network. The self-diffusion coefficient describes the motion of one molecule relative to the surrounding molecules due to thermal motions while the cooperative diffusion coefficient describes the motion of a number of molecules in a concentration gradient. It has been pointed out that measurements of both $D_s(c)$ and $D_c(c)$ are very interesting since a central problem in the dynamics of semidilute entangled polymer solutions is the quantitative understanding of the interplay of self-diffusion and cooperative diffusion. Motivated by this prospect, we therefore extend our previous study of homopolymer solutions [1] to the case of macromolecular tracer diffusion as is illustrated in figure 4.1. Hence we study the dynamics of long end-labeled tracer PS chains (black wiggled lines in figure 4.1) immersed in a polymer solution consisting of shorter matrix PS chains (gray wiggled lines in figure 4.1). The study is devoted to an understanding of the coupling of self- and cooperative motion due to topological constraints. Varying the concentration and the molecular weight of the matrix PS chains allows us to modify these topological constraints.

4.3 Dye Labeled Tracer Polystyrene Chains

Linear PS chains with different molecular weights and low polydispersity were prepared as discussed in ref. [2]. Our samples were composed of a small concentration (around 10^{-8} M) of Rhodamine B labeled tracer PS chains of molecular weight $M_w^{(tr)}$ in toluene solutions in which matrix PS chains of molecular weight $M_w^{(ma)}$ were dissolved at various concentrations. The resulting systems are denoted as PS- $M_w^{(tr)}/M_w^{(ma)}$ as is indicated in table 4.1.

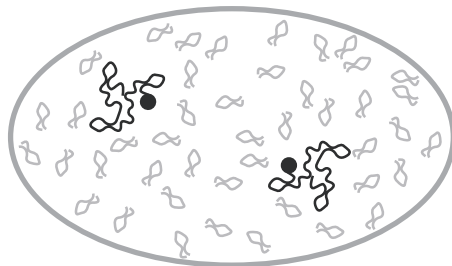


Figure 4.1: Schematic illustration of a polymer solution composed of a small concentration of labeled tracer polymer chains (black wiggled lines) and matrix polymer chains of different molecular weight (gray wiggled lines). Each labeled polymer chain carries only one dye molecule at one of its ends which is marked by a black dot. The FCS observation volume is enclosed by the thick gray ellipsoidal line. The size of the polymer chains, the size observation volume, and the number of polymer chains are not drawn to absolute scale. Only the fact that the molecular weight of the matrix polymer chains can be different from that of the tracer polymer chains is relevant.

Each labeled PS chain carries only one dye molecule at one of its ends. We have used preparative gel permeation chromatography to separate labeled polymer chains and free dye molecules [2, 3]. Therefore, the resulting PS solutions do not contain any measurable amount of free dye molecules.

Table 4.1: Molecular weights $M_w^{(tr)}$ and $M_w^{(ma)}$ of the tracer and matrix PS chains, respectively. The concentration at which the fast diffusion process appears in the FCS measurements is denoted as c^+ . In the main text and the figures the various PS solutions are denoted by the names given in the first column of the table. For comparison the overlap concentration c^* of the matrix PS chains is shown in the last column.

Name	$M_w^{(tr)}$ [kg/mol]	$M_w^{(ma)}$ [kg/mol]	c^+ [wt%]	c^* [wt%]
PS-17/17	17	17		3.5
PS-264/17	264	17		3.5
PS-67/67	67	67	20.0	1.4
PS-264/67	264	67	20.0	1.4
PS-264/264	264	264	6.5	0.54

4.4 Fluorescence Correlation Spectroscopy

FCS is a method relying on the detection and temporal analysis of the fluorescence signal emitted from a small confocal detection volume (see e.g., refs. [24, 4]). A laser beam is focused by an objective with high numerical aperture and excites fluorescent molecules entering the illuminated observation volume. Our FCS setup is based on the commercial ConfoCor2 setup (Carl Zeiss, Jena, Germany) [4] with a 40× Plan Neofluar objective characterized by the numerical aperture NA=0.9. Fluorescence is excited by a He Ne-Ion laser at a wavelength of 543 nm. As a second setup we used a MicroTime200 (PicoQuant, Berlin, Germany) [5] with a 100× oil immersion objective (NA=1.45). Here the detection beam path was divided by a 50/50 beam splitter on two detectors to crosscorrelate the signals. This crosscorrelation is necessary to prevent distortion of the fluorescence correlation function by detector afterpulsing [6]. For details of the FCS-measurements see refs. [4, 2, 7].

The emitted fluorescent light is detected by an avalanche photo diode. The time dependent intensity fluctuations are analyzed by an autocorrelation function $G(\tau, c)$, where τ denotes the time. In order to account for the possibility of the contribution of both self-diffusion and cooperative diffusion, the function

$$G(\tau, c) = \sum_{i \in \{s, c\}} G_i(0, c) \left(1 + \frac{4D_i(c)\tau}{w_{x,y}^2}\right)^{-1} \left(1 + \frac{4D_i(c)\tau}{w_z^2}\right)^{-1/2} \quad (4.1)$$

is used to describe the experimental data [1]. Here $w_{x,y} = 296$ nm is the dimension of the observation volume perpendicular to the optical axis and $w_z = 8w_{x,y}$ is the dimension along the optical axis. $G_i(0, c)$ characterizes the contribution of the i -th component to the total amplitude $G(0, c)$ of the autocorrelation function. In equation (3.1) normal diffusion with mean square displacements $\phi_i(\tau, c) = 6D_i(c)\tau$ has been assumed. Deviations from normal diffusion are due to internal chain motions (see e.g., refs. [1, 8, 9, 10, 43, 44] and references therein) or due to molecular crowding (see e.g., refs. [1, 11, 12, 13, 14, 15, 16] and references therein).

FCS is not only sensitive to intensity fluctuations due to the motion of labeled molecules but also due to photokinetic processes of the fluorescent dyes which occur for short times $\tau < 5 \times 10^{-3}$ ms. This additional relaxation has been taken into account as discussed in refs. [2, 3, 7].

4.5 Autocorrelation Functions Measured by FCS

Two different types of macromolecular tracer diffusion behavior were obtained depending on the concentration and the molecular weight of the matrix polymer chains, as illustrated in figure 4.2. For the PS-264/17 sample containing short matrix PS chains ($M_w^{(ma)} = 17$ kg/mol, see table 4.1), the measured autocorrelation function is characterized by a single self-diffusion process for arbitrary concentrations (open squares in figures 4.2 (a) - (d)). With increasing concentration the decay of the autocorrelation function shifts to longer times. The simple self-diffusion model given by equation (3.1) with $G_s(0, c) = 1$ and $G_c(0, c) = 0$ is successful in describing the autocorrelation data for such systems. This holds also for solutions containing longer matrix PS chains for low concentrations (PS-264/67 in figures 4.2 (a), (b) and PS-264/264 in figure 4.2 (a)). However, for higher concentrations, the simple self-diffusion model no longer describes the data in the case of the longer matrix PS chains. The autocorrelation data exhibit a second decay time on a shorter time scale (solid circles in figures 4.2 (c), (d) and crosses in figures 4.2 (b) - (d)). The experimental data can be described taking into account both self-diffusion and cooperative diffusion in equation (3.1), i.e., $G_c(0, c) \neq 0$. The concentration c^+ at which the second fast diffusion process is detected depends on the molecular weight of the matrix PS chains. Upon decreasing the molecular weight of the matrix PS chains the concentration c^+ decreases (see table 4.1). In the case of the short matrix PS chains of molecular weight $M_w^{(ma)} = 17$ kg/mol no second diffusion process has been observed as already mentioned above. As the entanglement molecular weight of PS is 18 kg/mol, entanglements of matrix polymer chains are not possible

at any concentration of the short matrix PS chains of molecular weight 17 kg/mol [17].

An important result of the analysis of the autocorrelation functions for various concentrations is that the concentration c^+ is *independent* of the molecular weight of the tracer PS chains. For example, $c^+ = 20.0\text{ wt}\%$ for both the PS-67/67 and the PS-264/67 sample (see table 4.1). Moreover, only self-diffusion can be observed for both the PS-17/17 and the PS-264/17 sample, i.e., no concentration c^+ can be defined for these samples (see table 4.1). Hence the fast diffusion process is not a characteristic property of the tracer PS chains but is related to the dynamics of the surrounding matrix PS chains as will be discussed in more detail in the next section.

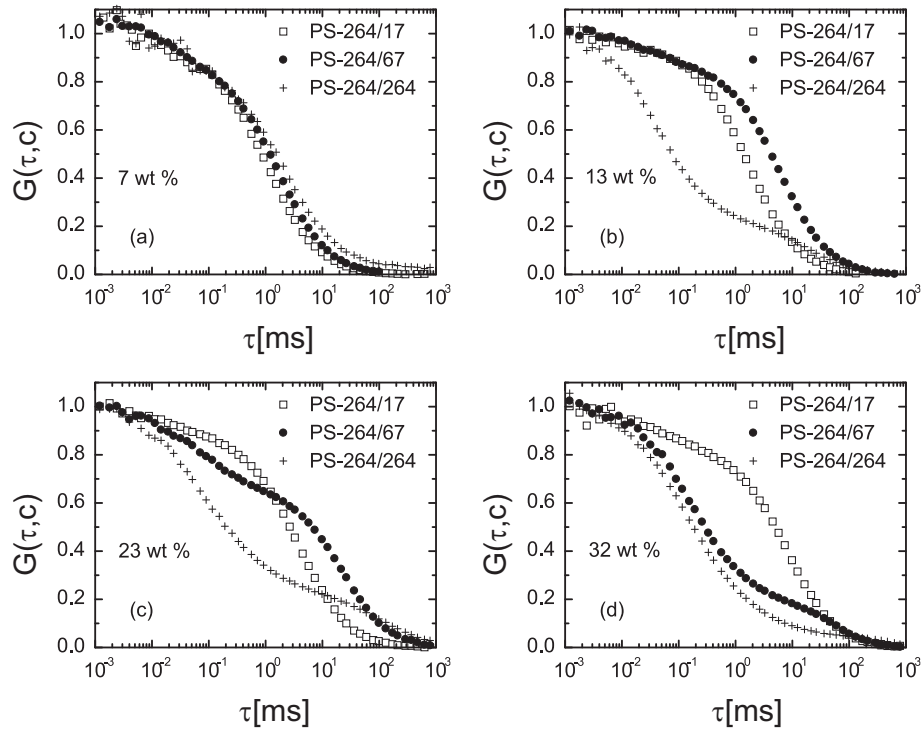


Figure 4.2: Normalized autocorrelation functions obtained from FCS for the three samples PS-264/17, PS-264/67, and PS-264/264 (see table 4.1). The concentration of the matrix PS chains increases from (a) to (d) according to 7, 13, 23, 32 wt%.

4.6 Langevin and Integral Equation Theory

The application of Langevin and integral equation theory to PS chains in solution has been discussed earlier [1, 18, 66]. Therefore, we only present the equations necessary for this study. The time evolution of the total dynamic scattering function $S_{tot}(q, c, \tau)$ is assumed to be governed by a Langevin equation [2], where q is the absolute value of the scattering vector. The total dynamic scattering function can be measured by dynamic light scattering (DLS). The cooperative diffusion coefficient $D_c(c)$ determines the decay rate of the total dynamic scattering function and is given by

$$D_c(c) \stackrel{q \rightarrow 0}{=} \frac{k_B T}{4\pi^2 \eta} \int_0^\infty dq_1 \frac{S_{tot}(q_1, c, 0) q_1^2}{S_{tot}(q, c, 0) q^2} \left(\frac{q_1^2 + q^2}{2q_1 q} \log \left| \frac{q_1 + q}{q_1 - q} \right| - 1 \right), \quad (4.2)$$

where the temperature T and the viscosity η characterize the solvent. Furthermore, the total static scattering function reads

$$S_{tot}(q, c, 0) = 1 + \bar{v} c h(q, c) / (V_p P(q, c)), \quad (4.3)$$

where V_p is the volume of a dissolved polymer chain, $h(q, c)$ is a particle-averaged total correlation function, and $\bar{v} = 0.916 \text{ cm}^3/\text{g}$ is the specific weight of PS [19]. The particle-averaged intramolecular correlation function $P(q, c)$ characterizes the geometric shape of the polymer chains at a given concentration c . The overall size of the polymer chains is reduced considerably upon increasing the concentration implying a concentration dependence of the particle-averaged intramolecular correlation function. Therefore, we consider the following particle-averaged intramolecular correlation function [70]

$$P(q, c) = (1 + 0.549 q^2 r_g^2(c))^{-5/6} \quad (4.4)$$

with the concentration dependent radius of gyration

$$r_g^2(c) = r_g^2(0) \left(\Theta(c^* - c) + \left(\frac{c}{c^*} \right)^{-1/8} \Theta(c - c^*) \right). \quad (4.5)$$

Here $\Theta(x)$ is the Heaviside step function which is 1 for $x > 0$ and zero elsewhere. Moreover, the overlap concentration c^* is the boundary concentration between the dilute and semidilute regimes (see table 4.1). This overlap concentration depends on the molecular weight according to $c^* \sim (M_w^{(ma)})^{-4/5}$, and has been determined for the PS solutions under considerations using FCS [7]. In addition the scaling law given $c^{-1/8}$ in equation (3.5) has been confirmed experimentally for PS in a good solvent using small angle neutron scattering [20]. The particle-averaged total correlation function is related to a particle-averaged direct correlation function $C(q, c)$ by the generalized Ornstein-Zernike equation of the Polymer Reference Interaction Site Model (PRISM), which reads (see e.g., refs [54, 55] and references therein)

$$h(q, c) = P^2(q, c)C(q, c)/(1 - \bar{v}cC(q, c)P(q, c)/V_p). \quad (4.6)$$

This generalized Ornstein-Zernike equation is supplemented by the Percus-Yevick approximation to account for steric effects [54]. The osmotic pressure $p(c)$ is evaluated from equations (3.3) - (3.8) as

$$p(c) = k_B T \bar{v} \int_0^c dc' S_{tot}(q, c', 0)/V_p. \quad (4.7)$$

The PRISM integral equation theory has been successfully applied to various polymer solutions (see e.g., refs [54, 66, 58, 59]).

Figures 4.3 (a), (b), and (c) display the calculated cooperative diffusion coefficients of the 17, 67, and 264 kg/mol matrix PS chains (solid lines) together with the experimental data measured with DLS (open squares) [1] and FCS (solid squares). The figures demonstrate that the measured cooperative diffusion coefficients agree with the calculated results as obtained from equations (3.2) - (3.8). In particular, the crossover region between the dilute and the semidilute regimes is captured correctly by the Langevin and integral equation theory. The maximum of the cooperative diffusion coefficient in the semidilute entangled regime marks the onset of glassy dynamics. This friction controlled dynamics is not captured by equation (3.2). Therefore, deviations

between the solid lines and the symbols are found for high concentrations in figure 4.3. Nevertheless, one can conclude from figures 4.3 (b) and (c) that the diffusion coefficient $D_c(c)$ as obtained by FCS (solid squares) is indeed the cooperative diffusion coefficient of the matrix PS chains. The topological interactions in the semidilute solutions lead to coherent movements of matrix and tracer PS chains characterized by the cooperative diffusion coefficient $D_c(c)$. The resulting temporal fluctuations of the detected fluorescence intensity can be measured by FCS even in the case that the number of labeled tracer PS chains is *considerably* smaller than the number of matrix PS chains.

The self-diffusion coefficient $D_s(c)$ as obtained using FCS measurements (see figure 4.2) and equation (3.1) are also shown in figure 4.3 (solid circles). $D_s(c)$ is found to decrease with increasing concentration of the matrix PS chains due to the friction between the polymer chains. The dashed lines in figure 4.3 are theoretical values calculated according to [21]

$$\frac{D_c(c)}{D_s(c)} = \alpha (1 - \bar{v}c) \frac{dp(c)}{dc} \quad (4.8)$$

with both $D_c(c)$ and $p(c)$ obtained from the Langevin and integral equation theory given by equations (3.2) - (3.8). As a new feature of the present evaluation, we have introduced the parameter α in equation (3.13). This parameter describes the difference of the system under consideration from a homopolymer solution consisting of matrix polymer chains and tracer chains of the same molecular weight, that is, $\alpha = 1$. The dashed line in figure 4.3 (c) demonstrates that the measured self-diffusion coefficient of the homopolymer solution PS-264/264 can be described by equation (3.13) with $\alpha = 1$ and the Langevin and integral equation theory as input. Similarly, $D_s(c)$ can be calculated in agreement with experimental data for the samples PS-17/17 and PS-67/67 using $\alpha = 1$ (data not shown). In order to describe the self-diffusion coefficients of the PS-264/67 and PS-264/17 samples, values of $\alpha = 2.5$ and $\alpha = 7.2$ above unity had to be chosen (dashed lines in figures 4.3 (b) and (a)). The values of α different from unity reflect the fact that the molecular weights of the matrix and tracer polymer chains are different in the case of

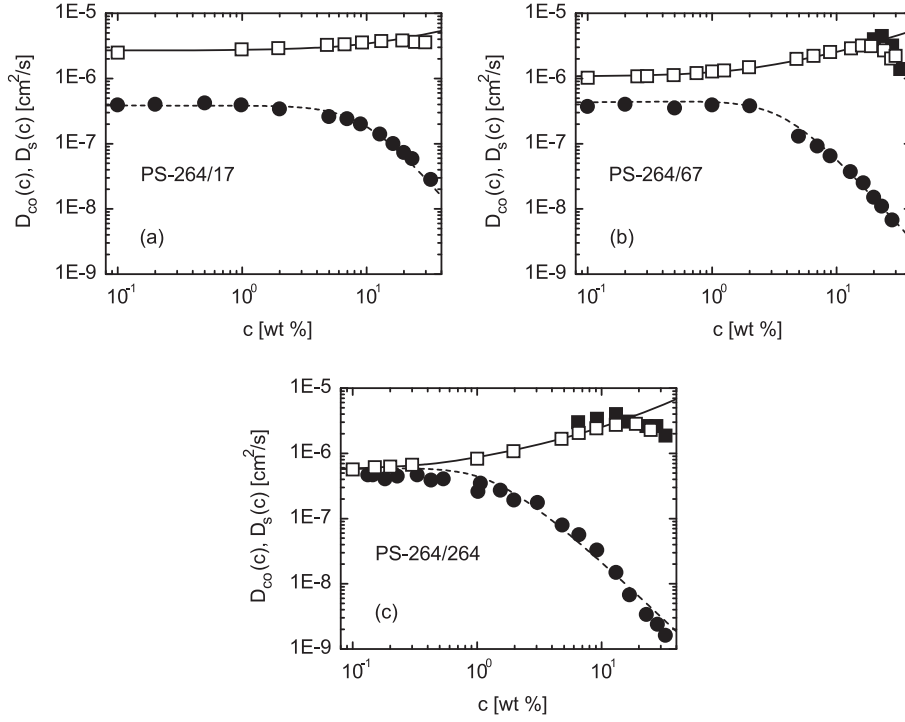


Figure 4.3: Cooperative diffusion coefficients ($D_c(c)$, squares) and self-diffusion coefficients ($D_s(c)$, circles) for the three samples PS-264/17, PS-264/67, and PS-264/264 (see table 4.1) in panel (a), (b), and (c), respectively. Solid and open symbols refer to FCS measurements (see figure 4.2). The open squares denote DLS data obtained from the samples PS-17/17, PS-67/67, and PS-264/264 [1]. The solid lines display the collective diffusion coefficients as obtained from the Langevin and integral equation theory according to equations (3.2) - (3.8). Dashed lines represent the calculated results as obtained from equation (3.13) with equations (3.2) and (3.9) as input and $\alpha = 7.2, 2.5, 1$ in panel (a), (b), and (c), respectively.

the samples PS-264/67 and PS-264/17.

Scaling arguments for self-avoiding random coils lead to the prediction $\alpha = (M_w^{(ma)}/M_w^{(tr)})^{-3/5}$, where the Flory exponent $\nu = 3/5$ for a good solvent has been used. Hence one obtains $\alpha = 2.3$ and $\alpha = 5.2$ for the samples PS-264/67 and PS-264/17, respectively. The predicted value $\alpha = 2.3$ is close to the value $\alpha = 2.5$ used in our analysis in the case of the PS-264/67 sample. This agreement confirms our earlier finding that the self-diffusion coefficients

of both 264 kg/mol PS chains and 67 kg/mol PS chains fulfil scaling relations [1]. However, the 17 kg/mol PS chains are too short to be considered as self-avoiding random coils. Molecular stiffness leads to a more pronounced dependence of dynamical properties on the molecular weight than in the case of self-avoiding random coils [8, 9, 76]. Therefore, the value $\alpha = 7.2$ used in our analysis is larger than $\alpha = 5.2$.

Figure 4.4 demonstrates that the FCS autocorrelation functions for the PS-264/17 and PS-17/17 samples coincide provided the time is multiplied by the factor $\alpha = 7.2$ in the case of the PS-17/17 sample. This scaling is valid for all concentrations under consideration because the 17 kg/mol matrix PS chains do not form an entangled network in semidilute solution as mentioned earlier. Hence the polymeric nature of these short matrix chains does not lead to additional characteristic features of the FCS autocorrelation functions. In the case of a similar comparison of the FCS autocorrelation functions for the PS-264/67 and PS-67/67 samples, scaling can be found only for concentrations lower than c^+ . For higher concentrations deviations from a simple scaling law are found because the self-diffusion coefficient and the cooperative diffusion coefficient exhibit different dependencies on the molecular weight [1].

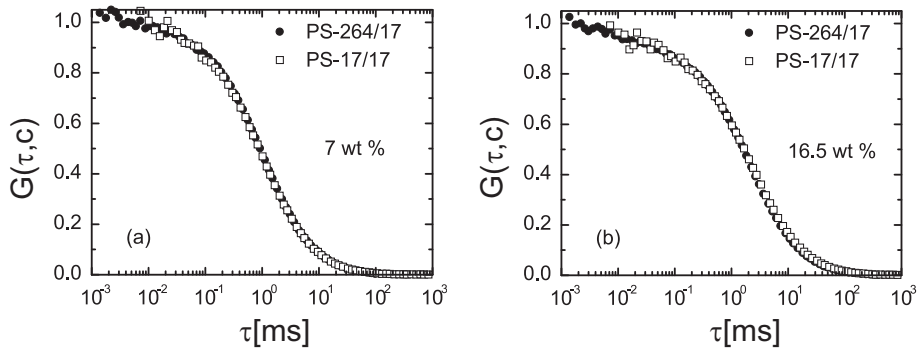


Figure 4.4: Normalized FCS autocorrelation functions for the samples PS-264/17 and PS-17/17 (see table 4.1). The concentration of the 17 kg/mol matrix PS chains is 7 wt % in panel (a) and 16.5 wt % in panel (b). The autocorrelation functions of both samples coincide for a given concentration because the time τ for the PS-17/17 sample has been multiplied by the factor $\alpha = 7.2$ as is discussed in the main text.

4.7 Conclusions

Fluorescence correlation spectroscopy has been used to study the dynamics of labeled tracer polystyrene chains in a system consisting of matrix polystyrene chains dissolved in toluene [figure 4.1]. The self-diffusion coefficient of the tracer polystyrene chains has been measured for arbitrary concentrations of the matrix polystyrene chains. Moreover, the cooperative diffusion coefficient has been determined in the semidilute entangled concentration regime due to the transient entanglement network [figure 4.2]. The minimum concentration of matrix polystyrene chains at which the cooperative diffusion coefficient can be detected by FCS is independent of the molecular weight of the tracer polystyrene chains [table 4.1]. It has been suggested earlier in the context of polymer fiber spinning that a polymer solution is converted to a more stable elastically deformable network at such a concentration [22, 23, 24, 25, 26]. Due to the resulting effective long-range interaction of the polymer chains, the cooperative diffusion coefficient can be detected by FCS even in the case that the number of labeled polymer chains is considerably smaller than the number of unlabeled polymer chains. A theoretical description of the diffusion coefficients is given by a Langevin and integral equation theory [figure 4.3]. Moreover, a single master autocorrelation curve has been found for short unentangled polystyrene matrix chains [figure 4.4].

In summary, the present work gives further support to the recent conclusion that both the self-diffusion coefficient and the cooperative diffusion coefficient can be obtained experimentally using the same technique [1].

Bibliography

- [1] U. Zettl, S. T. Hoffmann, F. Koberling, G. Krausch, J. Enderlein, L. Harnau, and M. Ballauff, *Macromolecules*, 2009, **42**(24), 9537.
- [2] H. Zettl, W. Häfner, A. Böker, H. Schmalz, M. Lanzendörfer, A. H. E. Müller, and G. Krausch, *Macromolecules*, 2004, **37**(5), 1917.

- [3] H. Zettl, Y. Portnoy, M. Gottlieb, and G. Krausch, *J. Phys. Chem. B*, 2005, **109**, 13397.
- [4] ed. R. Rigler and E. S. Elson, *Fluorescence Correlation Spectroscopy*, 2000.
- [5] M. Wahl, F. Koberling, M. Patting, H. Rahn, and R. Erdmann, *Curr. Pharm. Biotechnol.*, 2004, **5**, 299.
- [6] J. Enderlein and I. Gregor, *Rev. Sci. Instrum.*, 2005, **76**, 033102.
- [7] H. Zettl, U. Zettl, G. Krausch, J. Enderlein, and M. Ballauff, *Physical Review E*, 2007, **75**(6), 061804.
- [8] L. Harnau, R. G. Winkler, and P. Reineker, *J. Chem. Phys.*, 1996, **104**, 6355.
- [9] L. Harnau, R. G. Winkler, and P. Reineker, *J. Chem. Phys.*, 1998, **109**, 5160.
- [10] L. Harnau, R. G. Winkler, and P. Reineker, *Phys. Rev. Lett.*, 1999, **82**, 2408.
- [11] M. Wachsmuth, W. Waldeck, and J. Langowski, *J. Mol. Biol.*, 2000, **67**], pages = **298**.
- [12] M. Weiss, M. Elsner, F. Kartberg, and T. Nilsson, *Biophys. J.*, 2004, **87**, 3518.
- [13] A. Masuda, K. Ushida, and T. Okamoto, *Phys. Rev. E*, 2005, **72**, 060101(R).
- [14] D. S. Banks and C. Fradin, *Biophys. J.*, 2005, **89**, 2960.
- [15] N. K. Reitan, A. Juthajan, T. Lindmo, and D. C. de Lange, *J. Biomed. Opt.*, 2008, **13**, 054040.
- [16] T. Cherdhirankorn, A. Best, K. Koynov, K. Peneva, K. Muellen, and G. Fytas, *J. Phys. Chem. B*, 2009, **113**, 3355.

- [17] E. D. von Meerwall, E. J. Amis, and J. D. Ferry, *Macromolecules*, 1985, **18**, 260.
- [18] K. S. Schweizer and J. G. Curro, *Adv. Chem. Phys.*, 1997, **98**, 1.
- [19] G. V. Schulz and M. Hoffmann, *Makromolekulare Chemie*, 1957, **23**(2-3), 220.
- [20] M. Daoud, J. P. Cotton, B. Farnoux, G. Jannink, G. Sarma, H. Benoit, R. Duplessix, C. Picot, and P.-G. De Gennes, *Macromolecules*, 1975, **8**, 804.
- [21] T. Kanematsu, T. Sato, Y. Imai, K. Ute, and T. Kitayama, *Polymer Journal*, 2005, **37**(2), 65.
- [22] H. P. Schreiber, A. Rudin, and E. B. Bagley, *J. Appl. Polym. Sci.*, 1965, **9**, 887.
- [23] T. Hayahara and S. Takao, *J. Appl. Polym. Sci.*, 1967, **11**, 735.
- [24] M. G. McKee, G. L. Wilkes, R. H. Colby, and T. E. Long, *Macromolecules*, 2004, **37**, 1760.
- [25] S. L. Shenoy, W. D. Bates, H. L. Frisch, and G. E. Wnek, *Polymer*, 2005, **46**, 3372.
- [26] R. T. Weitz, L. Harnau, S. Rauschenbach, M. Burghard, and K. Kern, *Nano Lett.*, 2008, **8**, 1187.

Chapter 5

Summary / Zusammenfassung

Summary

This thesis starts with the analysis of the swelling behavior and the microphase separation of block copolymers in thin films. The results of these measurements are diffusion informations of solvent in thin block copolymer films. In-situ ellipsometry measurements showed more than 10 % increase of the relative solvent up-take with decreasing thilm thickness. This solvent up-take was verified by the microphase separation patterns analysed by scanning force microscopy on the quenched films.

For a detailed understanding of the behaviour of blockcopolymers during the microphase separation the diffusion behaviour of polymer molecules has to be investigated. Therefore a model system of homopolymers was used to study the diffusion of single polymer chains in solution. The diffusion coefficients in dilute and semidilute solutions are measured with fluorescence correlation spectroscopy (FCS) and dynamic light scattering (DLS).

The technique of FCS was recently adjusted for synthetic polymer solutions in organic solvents. This new approach led to the measurements of both diffusion coefficients with one technique. In dilute solution the selfdiffusion coefficient is obtained. Whereas in semidilute solutions the cooperative diffusion appears additional in the decay curves of the FCS experiment. The higher the molecular weight the lower is the onset concentration c^+ of the

cooperative diffusion. At molecular weights smaller than the entanglement molecular weight this c^+ is not reachable. c^+ is the same as the minimum concentration required to produce nanofibers by electrospinning and so the lowest concentration for entangled polymers coils in solution. Mixing different molecular weights in the FCS experiment approved the dependency of c^+ on the molecular weight of the matrix.

Zusammenfassung

Zu Beginn dieser Arbeit wurde das Schwellverhalten von Blockcopolymeren sowie deren Mikrophasenseparation in dünnen Filmen untersucht. Die Messungen ergeben Informationen zum Diffusionsverhalten des Lösungsmittels in den dünnen Blockcopolymerfilm. In-situ Ellipsometriemessungen zeigen bei Filmen mit einer Dicke im Bereich einer Monolage eine bis zu ca. 10 % stärkere Aufnahme von Lösungsmittel, als Filme mit mehreren Monolagen Dicke. Dieses stärkere Schwellverhalten wird bestätigt durch die filmdickensensiblen Muster der Mikrophasenseparation, aufgenommen mit Rasterkraftmikroskopie nach dem Einfrieren der Strukturen durch schnellen Entzug des Lösungsmittels.

Für das Verständnis der Mikrophasenseparation ist das Diffusionsverhalten der Polymerketten eine essentielle Information. Für die Untersuchung der Diffusion von Polymeren auf Einzelmolekülbasis wurde ein Modellsystem aus genau definierten Homopolymeren in Lösung untersucht. Die Diffusionskoeffizienten in verdünnten und halb-verdünnten Lösungen wurden mit Dynamischer Lichtstreuung (DLS) sowie auch mit Fluoreszenzkorrelationsspektroskopie (FCS) untersucht. Die Technik der FCS wurde erst vor kurzem für synthetische Polymere in organischen Lösungsmitteln optimal angepasst. Mit dieser Anpassung konnten zum ersten Mal beide Diffusionskoeffizienten zeitgleich mit einer Technik gemessen werden. Im verdünnten Bereich wurde wie erwartet der Selbstdiffusionskoeffizienten erhalten.

Im semiverdünnten Bereich erscheint zusätzlich der kooperative Diffusionskoeffizient in den Abklingkurven der FCS-Messungen. Die Anfangskonzentration c^+ ist kleiner für höhere Molekulargewichte und nur oberhalb des Ver-

schlaufungsmolekulargewichts erreichbar. Ein Vergleich mit der benötigten Konzentration zur Herstellung von Nano-Fäden durch Elektrospinnen zeigt, dass es sich bei c^+ um den Übergang vom unverschlaufenen zum verschlaufenen Konzentrationsbereich handelt.

Mischt man verschiedene Molekulargewichte im FCS-Experiment, so zeigt sich die Abhängigkeit des c^+ vom Molekulargewicht der Matrixmoleküle. Die Länge der Matrixmoleküle bestimmt also die messtechnische Erfassung der kooperativen Diffusion in der Fluoreszenzkorrelationsspektroskopie.

Gleichzeitig wurde die Messung des kooperativen Diffusionskoeffizienten in der Fluoreszenzkorrelationsspektroskopie mit einem theoretischen Modell auf Basis gekoppelter Moden untermauert.

Chapter 6

List of All Publications

- Heiko Zettl, Ute Zettl, Georg Krausch, Joerg Enderlein, Matthias Ballauff: Direct observation of single molecule mobility in semidilute polymer solutions
Physical Review E, **2007**, 75(6), 061804.
- Melanie Pretzl, Alexandra Schweikart, Christoph Hanske, Arnaud Chiche, Ute Zettl, Anne Horn, Alexander Böker, Andreas Fery: A Lithography-Free Pathway for Chemical Microstructuring of Macromolecules from Aqueous Solution Based on Wrinkling
Langmuir, **2008**, 24(22), 12748.
- Ute Zettl, Sebastian Tim Hoffmann, Felix Koberling, Georg Krausch, Joerg Enderlein, Ludger Harnau, Matthias Ballauff: Selfdiffusion and Collective Diffusion measured with Fluorescence Correlation Spectroscopy of Single Dye Labeled Polymers
Macromolecules, **2009**, 42(24), 9537.
- Ute Zettl, Armin Knoll, Larisa Tsakrova: Effect of Confinement on the Macroscopic and Mesoscale Swelling of Thin Block Copolymer Films
Langmuir, **2010**, 26(9), 6610.
- Ute Zettl, Matthias Ballauff, Ludger Harnau: A Fluorescence Correlation Spectroscopy Study of Macromolecular Tracer Diffusion in Polymer Solutions *Journal of Physics: Condensed Matter*, **2010**, 22, p 49.

Appendix A

Direct Calculation of FCS Functions

The derivation follows Elson and Magde [1] including the confocal detection volume (boundary conditions of $\delta C(\mathbf{r}, \tau) = 0$ at all three directions $x, y, z = \pm\infty$) [2]. As guidelines was used the reviews of Schwille and Haustein [3] and Krichevsky and Bonnet [4].

An elegant derivation for the autocorrelation function depend on the root mean square displacement is presented in the appendix to Shusterman, Gavrinov and Krichevsky. [5]

A.1 Autocorrelation Function

The autocorrelation function is defined as (see also equ. (1.12))

$$G(\tau) = \frac{\langle F(t) \cdot F(t + \tau) \rangle}{\langle F \rangle^2}$$

The angle brackets stand for the integral over time $\langle \dots \rangle = \int \dots dt$. The fluorescence intensity $F(t)$ can be expressed as sum of the average fluorescence and the fluorescence fluctuation $F(t) = \langle F \rangle + \delta F(t)$ leading to

$$G(\tau) = \frac{\langle (\delta F(t) + \langle F \rangle) \cdot (\delta F(t + \tau) + \langle F \rangle) \rangle}{\langle F \rangle^2}$$

$$\begin{aligned}
G(\tau) &= \frac{\langle \delta F(t) \delta \cdot F(t + \tau) + \langle F \rangle \cdot \delta F(t + \tau) + \langle F \rangle \cdot \delta F(t) + \langle F \rangle^2 \rangle}{\langle F \rangle^2} \\
G(\tau) &= \frac{\langle \delta F(t) \cdot \delta F(t + \tau) \rangle + \langle F \rangle \overbrace{\langle \delta F(t + \tau) \rangle}^{\stackrel{!}{=}0} + \langle F \rangle \overbrace{\langle \delta F(t) \rangle}^{\stackrel{!}{=}0} + \overbrace{\langle \langle F \rangle^2 \rangle}^{= \langle F \rangle^2}}{\langle F \rangle^2} \\
G(\tau) &= \frac{\langle \delta F(t) \cdot \delta F(t + \tau) \rangle}{\langle F \rangle^2} + 1 \tag{A.1}
\end{aligned}$$

A.2 Number Density Autocorrelation

The so-called number density autocorrelation function (a part of equ. 1.16) in the stationary system is

$$\phi_{jl}(\mathbf{r}, \mathbf{r}', \tau) = \langle \delta C_j(\mathbf{r}, 0) \delta C_l(\mathbf{r}', \tau) \rangle \tag{A.2}$$

For changes due to diffusion, $\delta C_l(\mathbf{r}, \tau)$ is determined by the diffusion equation (2. Fick law):

$$\frac{\partial \delta C_l(\mathbf{r}, \tau)}{\partial \tau} = D_l \nabla^2 \delta C_l(\mathbf{r}, \tau) \tag{A.3}$$

To solve this differential equation it is necessary to define the Fourier transformation.

$$\tilde{C}_l(\nu, \tau) = F_\nu [\delta C_l(\mathbf{r}, \tau)] = \left(\frac{1}{2\pi} \right)^{\frac{3}{2}} \int_{-\infty}^{\infty} dx \int_{-\infty}^{\infty} dy \int_{-\infty}^{\infty} dz e^{i(x\nu_x + y\nu_y + z\nu_z)} \delta C_l(\mathbf{r}, \tau)$$

The inverse transformation is

$$\delta C_l(\mathbf{r}, \tau) = F_r^{-1} [\tilde{C}_l(\nu, \tau)] = \left(\frac{1}{2\pi} \right)^{\frac{3}{2}} \int_{-\infty}^{\infty} d\nu_x \int_{-\infty}^{\infty} d\nu_y \int_{-\infty}^{\infty} d\nu_z e^{-i(x\nu_x + y\nu_y + z\nu_z)} \tilde{C}_l(\nu, \tau)$$

Transformation of equation (A.3) yields

$$\frac{\partial F_\tau^{-1} [\tilde{C}_l(\nu, \tau)]}{\partial \tau} = D_l \nabla^2 \left(\frac{1}{2\pi} \right)^{\frac{3}{2}} \int_{-\infty}^{\infty} d\nu_x \int_{-\infty}^{\infty} d\nu_y \int_{-\infty}^{\infty} d\nu_z e^{-i(x\nu_x + y\nu_y + z\nu_z)} \tilde{C}_l(\nu, \tau) =$$

$$\begin{aligned}
&= D_l \left(\frac{1}{2\pi} \right)^{\frac{3}{2}} \int_{-\infty}^{\infty} d\nu_x \int_{-\infty}^{\infty} d\nu_y \int_{-\infty}^{\infty} d\nu_z \left(\frac{d^2}{dx^2} + \frac{d^2}{dy^2} + \frac{d^2}{dz^2} \right) e^{-i(x\nu_x + y\nu_y + z\nu_z)} \tilde{C}_l(\nu, \tau) = \\
&= -D_l \left(\frac{1}{2\pi} \right)^{\frac{3}{2}} \int_{-\infty}^{\infty} d\nu_x \int_{-\infty}^{\infty} d\nu_y \int_{-\infty}^{\infty} d\nu_z e^{-i(x\nu_x + y\nu_y + z\nu_z)} \underbrace{(\nu_x^2 + \nu_y^2 + \nu_z^2)}_{=\nu^2} \tilde{C}_l(\nu, \tau) \\
&\frac{\partial F_\tau^{-1} [\tilde{C}_l(\nu, \tau)]}{\partial \tau} = -D_l F_r^{-1} [\nu^2 \tilde{C}_l(\nu, \tau)] = F_r^{-1} [-D_l \nu^2 \tilde{C}_l(\nu, \tau)]
\end{aligned}$$

Because the Fourier transform is independent of the time it does not influence the differential equation.

$$\frac{\partial \langle C \rangle(\nu, \tau)}{\partial \tau} = -D_l \nu^2 \langle C \rangle(\nu, \tau)$$

Integration leads to the following solution of the diffusion equation (A.3)

$$\tilde{C}_l(\nu, \tau) = \tilde{C}_l(\nu, 0) e^{-D_l \nu^2 \tau} \quad (\text{A.4})$$

Inserting of the inverse Fourier transformation in equation (A.2) leads to

$$\phi_{jl}(\mathbf{r}, \mathbf{r}', \tau) = \left\langle \delta C_j(\mathbf{r}, 0) F_{r'}^{-1} [\tilde{C}_l(\nu, \tau)] \right\rangle$$

Since ensemble averaging and Fourier transformation are linear operations, their order may be interchanged

$$\phi_{jl}(\mathbf{r}, \mathbf{r}', \tau) = F_{r'}^{-1} \left[\left\langle \delta C_j(\mathbf{r}, 0) \tilde{C}_l(\nu, \tau) \right\rangle \right]$$

Use of equation (A.4) leads to

$$\phi_{jl}(\mathbf{r}, \mathbf{r}', \tau) = F_{r'}^{-1} \left[\left\langle \delta C_j(\mathbf{r}, 0) \tilde{C}_l(\nu, 0) e^{-D_l \nu^2 \tau} \right\rangle \right]$$

τ is independent on the time

$$\phi_{jl}(\mathbf{r}, \mathbf{r}', \tau) = F_{r'}^{-1} \left[\left\langle \delta C_j(\mathbf{r}, 0) \tilde{C}_l(\nu, 0) \right\rangle e^{-D_l \nu^2 \tau} \right]$$

Inserting of the inverse transformation yields

$$\phi_{jl}(\mathbf{r}, \mathbf{r}', \tau) = F_{r'}^{-1} \left[\langle \delta C_j(\mathbf{r}, 0) F_\nu [\delta C_l(\mathbf{r}'', 0)] \rangle e^{-D_l \nu^2 \tau} \right]$$

Interchange of ensemble averaging and Fourier transformation gets

$$\phi_{jl}(\mathbf{r}, \mathbf{r}', \tau) = F_{r'}^{-1} \left[F_\nu \left[\underbrace{\langle \delta C_j(\mathbf{r}, 0) \delta C_l(\mathbf{r}'', 0) \rangle}_{=\phi_{jl}(\mathbf{r}, \mathbf{r}'', 0)} \right] e^{-D_l \nu^2 \tau} \right]$$

Use of equation (A.2) with $\tau = 0$ leads to

$$\phi_{jl}(\mathbf{r}, \mathbf{r}'', \tau) = F_{r'}^{-1} \left[F_\nu [\phi_{jl}(\mathbf{r}, \mathbf{r}'', 0)] e^{-D_l \nu^2 \tau} \right] \quad (\text{A.5})$$

The correlation function $\phi_{jl}(\mathbf{r}, \mathbf{r}'', 0)$ is obtained by taking into account of the fact that the experiments under ideal conditions are in **dilute** solutions. The statistics of solute molecules are independent and the fluctuations of concentrations of different species must be uncorrelated. Having just one kind of particles is expressed in the Kronecker symbol δ_{jl} , which is defined as $\delta_{jl} = 1$ for $j = l$ and $\delta_{jl} = 0$ for $j \neq l$. The delta function $\delta(\mathbf{r} - \mathbf{r}'')$ symbols that the two correlated particles are at the same place. The delta function is defined as $\delta(\mathbf{r} - \mathbf{r}'') = \infty$ at $(\mathbf{r} - \mathbf{r}'') = 0$ and $\delta(\mathbf{r} - \mathbf{r}'') = 0$ at $(\mathbf{r} - \mathbf{r}'') \neq 0$. This means the intensity comes from the same single particle. Similarly the spatial correlation length of concentration fluctuations of a particular species must be very small.

$$\phi_{jl}(\mathbf{r}, \mathbf{r}'', 0) = \langle \delta C_j(\mathbf{r}, 0) \delta C_l(\mathbf{r}'', 0) \rangle \stackrel{\text{Poisson statistic}}{=} \langle C \rangle \delta_{jl} \delta(\mathbf{r} - \mathbf{r}'') \quad (\text{A.6})$$

Substitution of equation (A.6) into equation (A.5) yields

$$\begin{aligned} \phi_{jl}(\mathbf{r}, \mathbf{r}', \tau) &= F_{r'}^{-1} \left[F_\nu [\langle C \rangle \delta_{jl} \delta(\mathbf{r} - \mathbf{r}'')] e^{-D_l \nu^2 \tau} \right] = \\ &= F_{r'}^{-1} \left[e^{(-D_l \nu^2 \tau)} \left(\frac{1}{2\pi} \right)^{\frac{3}{2}} \int_{-\infty}^{\infty} dx \int_{-\infty}^{\infty} dy \int_{-\infty}^{\infty} dz e^{i(x\nu_x + y\nu_y + z\nu_z)} \langle C \rangle \delta_{jl} \delta(\mathbf{r} - \mathbf{r}'') \right] \end{aligned}$$

The integral of a function multiplied with the delta funktion $\delta(\mathbf{r} - \mathbf{r}')$ is the function at the point $(\mathbf{r} - \mathbf{r}')$.

$$\begin{aligned}\phi_{jl}(\mathbf{r}, \mathbf{r}', \tau) &= F_{r'}^{-1} \left[e^{-D_l \nu^2 \tau} \frac{\langle C \rangle}{(2\pi)^{3/2}} e^{i((x-x')\nu_x + (y-y')\nu_y + (z-z')\nu_z)} \right] \\ \phi_{jl}(\mathbf{r}, \mathbf{r}', \tau) &= \frac{\langle C \rangle}{(2\pi)^{3/2}} F_{r'}^{-1} \left[e^{-D_l \tau (\nu_x^2 + \nu_y^2 + \nu_z^2)} \cdot e^{i((x-x')\nu_x + (y-y')\nu_y + (z-z')\nu_z)} \right] \\ \phi_{jl}(\mathbf{r}, \mathbf{r}', \tau) &= \frac{\langle C \rangle}{8\pi^3} \int_{-\infty}^{\infty} d\nu_x e^{i\nu_x(x-x') - D_l \nu_x^2 \tau} \int_{-\infty}^{\infty} d\nu_y e^{i\nu_y(y-y') - D_l \nu_y^2 \tau} \int_{-\infty}^{\infty} d\nu_z e^{i\nu_z(z-z') - D_l \nu_z^2 \tau}\end{aligned}\tag{A.7}$$

To solve the integral we regard just a part:

$$\begin{aligned}h(\nu_x) &= e^{i\nu_x(x-x') - D_l \nu_x^2 \tau} = e^{-(D_l \tau \nu_x^2 - i\nu_x(x-x'))} \\ h(\nu_x) &= e^{-D_l \tau \left(\nu_x^2 - \frac{i(x-x')}{D_l \tau} \nu_x + \left(\frac{i(x-x')}{2D_l \tau} \right)^2 - \left(\frac{i(x-x')}{2D_l \tau} \right)^2 \right)} = e^{-D_l \tau \left(\nu_x - \frac{i(x-x')}{2D_l \tau} \right)^2 + D_l \tau \left(\frac{i(x-x')}{2D_l \tau} \right)^2} \\ h(\nu_x) &= e^{-D_l \tau \left(\nu_x - \frac{i(x-x')}{2D_l \tau} \right)^2} e^{-\frac{(x-x')^2}{4D_l \tau}}\end{aligned}$$

$h(\nu_x)$ can be integrated via substitution to $u = \nu_x - \frac{i(x-x')}{2D_l \tau}$

$$\int_{-\infty}^{\infty} h(\nu_x) d\nu_x = e^{-\frac{(x-x')^2}{4D_l \tau}} \int_{-\infty}^{\infty} e^{-D_l \tau u^2} du \frac{d\nu_x}{du} = e^{-\frac{(x-x')^2}{4D_l \tau}} \cdot \sqrt{\frac{\pi}{D_l \tau}}$$

Here the following relation was used $\int_0^{\infty} e^{-a^2 u^2} du = \frac{\sqrt{\pi}}{2a}$ with $a = \sqrt{D_l \tau}$. Because $h(\nu_x)$ is symmetric, the result of the integral is twice the relation. The derivation of backsubstitution $\frac{d\nu_x}{du} = \frac{d}{du} \left(u - \frac{(x-x')^2}{2\sqrt{D_l \tau}} \right) = 1$ gives nothing further.

Now equ. (A.7) can be solved to

$$\phi_{jl}(\mathbf{r}, \mathbf{r}', \tau) = \frac{\langle C \rangle}{8\pi^3} \left(\sqrt{\frac{\pi}{D_l \tau}} e^{-\frac{(x-x')^2}{4D_l \tau}} \cdot \sqrt{\frac{\pi}{D_l \tau}} e^{-\frac{(y-y')^2}{4D_l \tau}} \cdot \sqrt{\frac{\pi}{D_l \tau}} e^{-\frac{(z-z')^2}{4D_l \tau}} \right)$$

$$\phi_{jl}(\mathbf{r}, \mathbf{r}', \tau) = \frac{\langle C \rangle}{8\pi^3} \cdot \left(\frac{\pi}{D_l \tau} \right)^{3/2} \cdot e^{-\frac{1}{4D_l \tau} ((x-x')^2 + (y-y')^2 + (z-z')^2)}$$

Finally the correlation of concentration fluctuation is obtained to

$$\phi_{jl}(\mathbf{r}, \mathbf{r}', \tau) = \langle \delta C_j(\mathbf{r}, 0) \delta C_l(\mathbf{r}', \tau) \rangle = \frac{\langle C \rangle}{(4\pi D_l \tau)^{3/2}} \cdot e^{-\frac{(\mathbf{r}-\mathbf{r}')^2}{4D_l \tau}} \quad (\text{A.8})$$

A.3 Derivation of Autocorrelation Function

Insert equ. (1.17) in equ. (1.16) gives

$$G(\tau) = \frac{\langle C \rangle}{(4\pi D \tau)^{3/2}} \cdot \frac{\int \int W(\mathbf{r}) W(\mathbf{r}') \cdot e^{-\frac{(\mathbf{r}-\mathbf{r}')^2}{4D \tau}} d^3 \mathbf{r} d^3 \mathbf{r}'}{\langle C \rangle^2 (\int W(\mathbf{r}) d^3 \mathbf{r})^2} + 1 \quad (\text{A.9})$$

Integration of the molecule detection function

$$\int W(\mathbf{r}) d^3 \mathbf{r} = W_0 \int e^{-\frac{2(x^2+y^2)}{w_{xy}^2}} \cdot e^{-\frac{2z^2}{w_z^2}} d^3 \mathbf{r} = W_0 \cdot \pi^{3/2} w_{xy}^2 w_z = W_0 \cdot V_{\text{eff}}$$

resultes in a three dimensional ellipsoide. This is the effective detection volume V_{eff} scaled with the laser intensity W_0 . Now equ. (A.9) is obtained to

$$G(\tau) = \frac{\langle C \rangle}{(4\pi D \tau)^{3/2}} \cdot \frac{\int \int W(\mathbf{r}) W(\mathbf{r}') \cdot e^{-\frac{(\mathbf{r}-\mathbf{r}')^2}{4D \tau}} d^3 \mathbf{r} d^3 \mathbf{r}'}{W_0^2 \cdot \underbrace{(\langle C \rangle V_{\text{eff}})^2}_{\langle N \rangle}} + 1$$

$$G(\tau) = \frac{\langle C \rangle \cdot W_0^2}{\langle N \rangle^2 (4\pi D \tau)^{3/2} \cdot W_0^2} \cdot \int \int_{-\infty}^{+\infty} e^{-\frac{2x^2+y^2}{w_{xy}^2} - 2\frac{z^2}{w_z^2}} \cdot e^{-\frac{2x'^2+y'^2}{w_{xy}^2} - 2\frac{z'^2}{w_z^2}} \cdot e^{-\frac{(\mathbf{r}-\mathbf{r}')^2}{4D \tau}} d^3 \mathbf{r} d^3 \mathbf{r}' + 1 \quad (\text{A.10})$$

The integral can be expanded to

$$\begin{aligned} \text{Int} &= \int \int_{-\infty}^{+\infty} e^{-\frac{2x^2+y^2}{w_{xy}^2} - 2\frac{z^2}{w_z^2}} \cdot e^{-\frac{2x'^2+y'^2}{w_{xy}^2} - 2\frac{z'^2}{w_z^2}} \cdot e^{-\frac{(\mathbf{r}-\mathbf{r}')^2}{4D \tau}} d^3 \mathbf{r} d^3 \mathbf{r}' \\ \text{Int} &= \int \int_{-\infty}^{+\infty} e^{-\frac{2(x^2+y^2+x'^2+y'^2)}{w_{xy}^2} - 2\frac{z^2+z'^2}{w_z^2} - \frac{(x-x')^2 + (y-y')^2 + (z-z')^2}{4D_l \tau}} d^3 \mathbf{r} d^3 \mathbf{r}' \end{aligned}$$

By separation of the variables we obtain

$$f(x, x') = \int \int_{-\infty}^{+\infty} e^{-\frac{2x^2-2x'^2}{w_{xy}^2} - \frac{(x-x')^2}{4Dl\tau}} dx dx'$$

$$f(y, y') = \int \int_{-\infty}^{+\infty} e^{-\frac{2y^2+2y'^2}{w_{xy}^2} - \frac{(y-y')^2}{4Dl\tau}} dy dy'$$

$$f(z, z') = \int \int_{-\infty}^{+\infty} e^{-\frac{2z^2-2z'^2}{w_z^2} - \frac{(z-z')^2}{4Dl\tau}} dz dz'$$

Now we focus on one variable

$$\begin{aligned} f(x, x') &= \int \int_{-\infty}^{+\infty} e^{-\frac{-8\tau Dx^2 - 8\tau Dx'^2 - w_{xy}^2 x^2 + 2w_{xy}^2 xx' - w_{xy}^2 x'^2}{4\tau Dw_{xy}^2}} dx dx' \\ f(x, x') &= \int \int_{-\infty}^{+\infty} e^{-\frac{-8\tau Dx^2 - w_{xy}^2 x^2 + 2w_{xy}^2 xx'}{4\tau Dw_{xy}^2}} e^{-\frac{-8\tau Dx'^2 - w_{xy}^2 x'^2}{4\tau Dw_{xy}^2}} dx dx' = \\ &= \int \int_{-\infty}^{+\infty} e^{-\frac{8\tau D + w_{xy}^2}{4\tau Dw_{xy}^2} \left(x^2 - \frac{2w_{xy}^2 x'}{8\tau Dx^2 + w_{xy}^2} x + \left(\frac{w_{xy}^2 x'}{8\tau Dx^2 + w_{xy}^2} \right)^2 - \left(\frac{w_{xy}^2 x'}{8\tau Dx^2 + w_{xy}^2} \right)^2 \right)} e^{-\frac{-8\tau Dx'^2 - w_{xy}^2 x'^2}{4\tau Dw_{xy}^2}} dx dx' = \\ &= \int_{-\infty}^{+\infty} e^{-\frac{8\tau D + w_{xy}^2}{4\tau Dw_{xy}^2} \left(x + \left(\frac{w_{xy}^2 x'}{8\tau Dx^2 + w_{xy}^2} \right) \right)^2} dx \int_{-\infty}^{+\infty} e^{-\frac{8\tau D + w_{xy}^2}{4\tau Dw_{xy}^2} \left(-\frac{w_{xy}^2 x'}{8\tau Dx^2 + w_{xy}^2} \right)^2} e^{-\frac{-8\tau Dx'^2 - w_{xy}^2 x'^2}{4\tau Dw_{xy}^2}} dx' \end{aligned}$$

We solve the integral over dx via the relation $\int_0^{\infty} e^{-a^2 u^2} du = \frac{\sqrt{\pi}}{2a}$ and substitution

$$f(x, x') = \sqrt{\frac{\pi 4\tau Dw_{xy}^2}{8\tau D + w_{xy}^2}} \int_{-\infty}^{+\infty} e^{\frac{w_{xy}^4 x'^2}{4\tau Dw_{xy}^2 (8\tau Dx^2 + w_{xy}^2)}} e^{-\frac{-8\tau Dx'^2 - w_{xy}^2 x'^2}{4\tau Dw_{xy}^2}} dx'$$

To solve the integral over dx' we can use the same relation direct.

$$\begin{aligned} f(x, x') &= \sqrt{\frac{\pi 4\tau Dw_{xy}^2}{8\tau D + w_{xy}^2}} \int_{-\infty}^{+\infty} e^{\frac{w_{xy}^4 x'^2}{4\tau Dw_{xy}^2 (8\tau Dx^2 + w_{xy}^2)} - \frac{(8\tau D + w_{xy}^2) x'^2}{4\tau Dw_{xy}^2}} dx' \\ f(x, x') &= \sqrt{\frac{\pi 4\tau Dw_{xy}^2}{8\tau D + w_{xy}^2}} \int_{-\infty}^{+\infty} e^{-\frac{(8\tau D + w_{xy}^2)^2 - w_{xy}^4}{4\tau Dw_{xy}^2 (8\tau Dx^2 + w_{xy}^2)} x'^2} dx' \end{aligned}$$

$$f(x, x') = \sqrt{\frac{\pi 4\tau D w_{xy}^2}{8\tau D + w_{xy}^2}} \sqrt{\frac{\pi 4\tau D w_{xy}^2 (8\tau D x^2 + w_{xy}^2)}{(8\tau D + w_{xy}^2)^2 - w_{xy}^4}}$$

Now we obtain the following solution

$$f(x, x') = \frac{\pi 4\tau D w_{xy}^2}{\sqrt{(8\tau D + w_{xy}^2)^2 - w_{xy}^4}}$$

The solution for $f(y, y')$ und $f(z, z')$ is analogous. With this help we obtain equ. (A.10) to

$$G(\tau) = \frac{\langle C \rangle}{\langle N \rangle^2 (4\pi D \tau)^{3/2}} \cdot \underbrace{\frac{\pi^2 4^2 \tau^2 D^2 w_{xy}^4}{((8\tau D + w_{xy}^2)^2 - w_{xy}^4)}}_{f(x, x') f(y, y')} \underbrace{\frac{\pi 4\tau D w_z^2}{\sqrt{(8\tau D + w_z^2)^2 - w_z^4}}}_{f(z, z')} + 1 \quad (\text{A.11})$$

This Equation can be simplified to

$$G(\tau) = \frac{\langle C \rangle}{\langle N \rangle^2} \cdot \frac{\pi^2 4^2 \tau^2 D^2 w_{xy}^4}{4\pi \tau D (4\tau D + w_{xy}^2)} \frac{\pi 4\tau D w_z^2}{\sqrt{4\pi \tau D} \sqrt{4\tau D + w_z^2}} + 1$$

$$G(\tau) = \frac{\langle C \rangle}{\langle N \rangle^2} \cdot \frac{\pi^{3/2} w_{xy}^4}{(4\tau D + w_{xy}^2)} \frac{w_z^2}{\sqrt{4\tau D + w_z^2}} + 1$$

By taking out w_{xy}^2 and w_z^2 you obtain

$$G(\tau) = \frac{\langle C \rangle}{\langle N \rangle^2} \cdot \frac{\pi^{3/2} w_{xy}^2 w_z}{\left(\frac{4\tau D}{w_{xy}^2} + 1\right) \sqrt{\frac{4\tau D}{w_z^2} + 1}} + 1$$

The counter $\pi^{3/2} w_{xy}^2 w_z$ ist the volume of an ellipsoide an representes the effectife detection volume V_{eff} . Now you get the average number of particles in the detection volume $\langle N \rangle$.

$$G(\tau) = \frac{\overbrace{\langle C \rangle V_{\text{eff}}}^{\langle N \rangle}}{\langle N \rangle^2} \cdot \frac{1}{\left(\frac{4\tau D}{w_{xy}^2} + 1\right) \sqrt{\frac{4\tau D}{w_z^2} + 1}} + 1$$

With the known equation $4D\tau_D = w_{xy}^2$ the final auto correlation function is obtained to

$$G'_{jl}(\tau) = \frac{1}{\langle N \rangle} \cdot \frac{1}{\left(\frac{\tau}{\tau_D} + 1\right) \sqrt{\left(\frac{w_{xy}}{w_z}\right)^2 \frac{\tau}{\tau_D} + 1}} + 1$$

A.4 Autocorrelation Methods

In chapter 3 the two autocorrelation techniques are compared, dynamic light scattering (DLS) and fluorescence correlation spectroscopy (FCS). Both techniques evaluate the dynamics of particles in an undisturbed solution. The setup is similar, monochromatic and polarised light passes the sample. Brownian motion of the particles causes temporal fluctuations of intensity. In both cases the self-similarity analysis of these fluctuations leads to the diffusion coefficient.

The scattering vector q is basis of the scattering technique DLS. Here the samples are evaluated at several different single q values. Whereas FCS measurements collect the information of a range of q values and is most sensitive at $q = 0$. [39] Rica et al. described the theory of FCS dependent on q . Here q -range is calculated to the decay of $\exp(-q^2Dt_d)$ to $1/e^2$ by solving the diffusion equation, comparable to appendix A.2. [6] A rough estimation by Winkler et al. gives the q range to the inverse of the waist radius $1/w_{xy}$. [43] Fig. A.1 compares the q -values of DLS measurements with these two estimations for FCS measurements for the system presented in chapter 3 and 4.

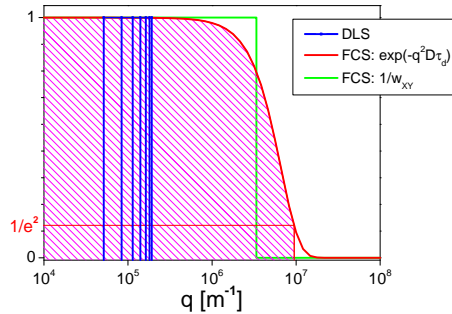


Figure A.1: Comparison of scattering vectors q for dynamic light scattering (vertical blue lines) and the range of q vectors in fluorescence correlation spectroscopy. The latter can be calculated with the decay of $\exp(-q^2Dt_d)$ to $1/e^2$ (red line) [6] or estimated by the inverse of the waist radius $1/w_{xy}$ (green line) [43]. The used values refer to the experiments presented in chapter 3 and 4.

Bibliography

- [1] E. L. Elson and D. Magde, *Biopolymers*, 1974, **13**(1), 1–27.
- [2] R. Rigler, *Journal of Biotechnology*, 1995, **41**(2), 177.
- [3] P. Schwille, *Cell Biochem. Biophys.*, 2001, **34**(3), 383–408.
- [4] O. Krichevsky and G. Bonnet, *Rep. Prog. Phys.*, 2002, **65**(2), 251–297.
- [5] R. Shusterman, T. Gavrinov, and O. Krichevsky, Mar , 2008, **100**.
- [6] J. Ricka and T. Binkert, *Phys. Rev. A*, 1989, **39**(5), 2646.

Danke

Das Gelingen dieser Arbeit wäre ohne das passende Umfeld mit vielen hilfsbereiten Personen nicht möglich gewesen. Mein besonderer Dank gebührt:

Prof. Dr. Andreas Fery für die Bereitschaft mich kurz vor Schluß noch zu übernehmen sowie für Korrekturen und Vorschläge in letzter Minute.

Prof. Dr. Georg Krausch, dass er mir in Forschungs- wie auch in zwischenmenschlichen Angelegenheiten den Blick für's Ganze geweitet hat.

Prof. Dr. Matthias Ballauff, der es mir ermöglicht hat, nach dem Weggang von Prof. Georg Krausch dieses interessante Thema weiter zu bearbeiten.

Prof. Dr. Jörg Enderlein für die Rechnungen der MDF für die verschiedensten Objekte und Lösungsmittel sowie für detaillierte Diskussionen über die theoretischen Grundlagen von FCS.

Prof. Dr. Alexander Böker für die Diskussionsbereitschaft und für einen Messaufenthalt in Grenoble.

Priv.-Doz. Dr. Ludger Harnau für die theoretische Untermauerung und detailverliebtes Korrekturlesen des Papers.

Priv.-Doz. Dr. Larisa Tsarkova für kreative Ideen und Korrekturlesen des Papers.

Dr. Armin Knoll für die gute Einführung in AFM und lustige gemeinsame Zeit.

Dr. Holger Schmalz und Annette Krökel für das Herstellen farbstoff-markierter Polymere.

Dr. Sabine Rosenfeldt für gute Ratschläge im Umgang mit Streuern und deren Eigenheiten.

Dr. Wolfgang Häfner für viele Antworten im Bereich Optik und \LaTeX .

Dr. Frank Schubert, Dr. Kristin Schmidt und Heiko Schoberth für die Hilfe bei diversen Computerangelegenheiten.

Dr. Kerstin Schindler für die Motivation zum Schluss.

Franz Fischer für die große Hilfe bei elektronischen Aufbauten.

Sybille Zimmermann für ihre offene und liebenswerte Art und ihre sofortige Hilfsbereitschaft in allen Notlagen des Lebens. Elisabeth Dünfelder für die Unterstützung in allen administrativen Angelegenheiten.

Sebastian Hoffmann für DLS- und FCS-Messungen während seiner Diplomarbeit.

Sina Rösler, Hanno Röttenbacher und Kathrin Holtzmann für die vielen kleinen Handgriffe im Labor, die es mir ermöglichten, immer noch Zeit für meine Tochter zu finden, sowie der Frauenbeauftragten der Uni Bayreuth für die Finanzierung der HiWis.

Allen hier nicht namentlich genannten aktuellen und ehemaligen Mitglieder der Lehrstühle PCII und PCI für die gute Arbeitsatmosphäre, die Hilfs- und Diskussionsbereitschaft.

Meiner Familie für jegliche Unterstützung, vor allem während der Promotion in Form von Kinderbetreuung und Hilfe im Haushalt.

Versicherungen und Erklärungen

Hiermit erkläre ich, dass keine Tatsachen vorliegen, die mich nach den gesetzlichen Bestimmungen über die Führung akademischer Grade zur Führung eines Doktorgrades unwürdig erscheinen lassen.

Hiermit erkläre ich mich damit einverstanden, dass die elektronische Fassung meiner Dissertation unter Wahrung meiner Urheberrechte und des Datenschutzes einer gesonderten Überprüfung hinsichtlich der eigenständigen Anfertigung der Dissertation unterzogen werden kann.

Hiermit erkläre ich eidesstattlich, dass ich die Dissertation selbständig verfasst und keine anderen als die von mir angegebenen Quellen und Hilfsmittel benutzt habe. Ich habe die Dissertation nicht bereits zur Erlangung eines akademischen Grades anderweitig eingereicht und habe auch nicht bereits diese oder eine gleichartige Doktorprüfung endgültig nicht bestanden.

Hiermit erkläre ich, dass ich keine Hilfe von gewerbliche Promotionsberatern bzw. -vermittlern in Anspruch genommen habe und auch künftig nicht nehmen werde.

Bayreuth, den 1. März 2015

Ute Zettl